Statistical analysis of comparisons between planned and measured dose distributions in photon beam radiotherapy

Šunjić, Svjetlana

Sveučilište u Zagrebu

Faculty of Science

Department of physics

Svjetlana Šunjić

Statistical analysis of comparisons between planned and measured dose distributions in photon beam radiotherapy

DOCTORAL DISSERTATION

Supervisors:

Assist. Prof. Dr. Tomislav Bokulić

Prof. Dr. Crister Ceberg

Zagreb, 2021

University of Zagreb

Prirodoslovno matematički fakultet

Fizički odsjek

Svjetlana Šunjić

Statistička analiza usporedbi planiranih i mjerenih raspodjela doza u radioterapiji fotonskim snopovima

DOKTORSKI RAD

Mentori:

Doc. dr. Tomislav Bokulić

Prof. dr. Crister Ceberg

Zagreb, 2021

Information on supervisors

Tomislav Bokulić is Assistant Professor at the Department of Physics, Faculty of Science, University of Zagreb and Medical Physicist where he is currently employed. He started to work as a junior research assistant, spent over 20 years working as a clinical medical physicist in Sestre milosrdnice University Hospital Center in Zagreb and 5 years in the Dosimetry Laboratory, International Atomic Energy Agency (IAEA) at the position of the dosimetry specialist and quality manager. His major research interests are in physics in nuclear medicine, clinical radiotherapy physics, dosimetry and dosimetry audits, he is an author/co-author of over 25 published papers and contributed to several book chapters, scientific and technical publications.

Crister Ceberg is Professor and Certified Medical Physicist, and serves as Director of the Medical Physics education program and deputy Head of the Division of Medical Radiation Physics at Lund University, Sweden. He is also member of the Royal Physiographic Society of Lund. His research interests in radiotherapy physics concerns the development of new methods and techniques for clinical applications as well as for innovative experimental radiotherapy, and he is an author of 80 published papers and book chapters.

Mojim dragim roditeljima,
za svu njihovu ljubav.

Acknowledgements

The cliché phrase “this thesis would not have been possible if not for the help of …” has never been truer than in reference to my supervisors, Assist. Prof. Tomislav Bokulić and Prof. Crister Ceberg.

Without their enthusiasm, encouragement, support and continuous optimism this dissertation would hardly have been completed. I could not have imagined having a better advisors and mentors for my PhD study.

I cannot begin to express deepest gratitude to Prof. Crister Ceberg for taking me on this research project and for his fantastic guidance and assistance. I am grateful for his helpful comments, valuable suggestions, expert advice and constructive ideas throughout this entire project, provided me with alternative ways to improve my dissertation.

I am extremely grateful to Assist. Prof. Tomislav Bokulić. His patience, friendly guidance, expert advice and dedicated involvement have been invaluable throughout all stages of the work. He provided all support that I needed, was always persistent and direct. He spent endless hours proofreading my work and giving me valuable suggestions and comments, which always resulted in improved version of the dissertation.
My dissertation has benefited substantially from his insightful recommendations.

Thanks a lot, to both of you, for making this possible.

I assure you that all of my efforts are only possible with the loving, unconditional support of my family. My parents have always given me the guidance to make my way through this thing we call life. They were always there during the good times and also when the times were not looking so good.

This is for you.

This thesis would not have been possible without the inspiration and support of a number of wonderful individuals, my friends and my colleagues - my thanks and appreciation to all of them. I could not have done any of this without all of you.

Thank you all.

Abstract

Clinical implementation of intensity-modulated radiotherapy (IMRT) and volumetric modulated arc therapy (VMAT) requires the ability to verify complex radiation dose delivery. The use of new dosimetry tools and procedures for clinical quality assurance (QA) practice is becoming increasingly important, especially when taking into account the necessity of reliable but also time-sparing QA protocols. An effective IMRT QA protocol should verify the accuracy of complex calculated absorbed dose distributions to prevent clinically significant errors that may compromise the treatment safety.

Although many institutions have developed dosimetry modalities for patient specific QA measurements in which typically the evaluated (e.g. calculated) absorbed dose distribution is compared against the reference (e.g. measured) distribution, most of them commonly use gamma (γ) analysis as a comparison metric. The efficacy of the IMRT/VMAT technique asserts the necessity of defining reliable criteria to facilitate the dose distribution comparison process.

In a comparison of a given reference point in a dose distribution and any one of the evaluated dose distribution points, a generalized Euclidean distance may be defined in a k+1 dimensional hyperspace, where k+1 refers to the spatial coordinates plus the dose. The difference between the evaluated and the reference absorbed dose, and the spatial differences are normalized by the maximum the dose and spatial differences criteria in the gamma index expression, respectively. Assuming that the evaluated dose distribution is available with high spatial resolution, the gamma evaluation index is then given by the minimum value of the generalized distance, searching across all available evaluation points.

The γ analysis has nowadays being accepted as an essential tool for the comparison of two absorbed dose distributions, the reference and evaluated distribution. The comparison criteria and failure rate tolerance levels have hitherto normally been based on empirical evidence, rather than the actual uncertainties of absorbed dose measurements and detector positioning. For a proper determination of the acceptable failure rate, a statistical evaluation should be carried out.

The goal of this work was to investigate the gamma analysis method by using a statistical approach to evaluate the relation between the acceptance criteria and the actual uncertainties of the dose measurement. For that purpose, in the initial stage, the gamma analysis program code for 1D and 2D dose distribution comparisons were developed, verified, and validated.

Measured absorbed dose values in cases of 1D and 2D absorbed dose distributions were simulated by assuming that the calculated value at the measurement point represented the expectation value, taking the calculated absorbed dose at a randomly displaced position, and by adding a random measurement noise. The detector displacement and the measurement noise were drawn from normal distributions with standard deviations in the range of interest. Finally, the nearest calculation point was determined according to the gamma evaluation procedure and the smallest gamma index value was calculated.

The acceptance criteria, dose difference, and distance-to-agreement criteria were set equal to the standard deviations of the associated uncertainties. By comparison between absorbed dose calculations and simulated measurements for clinical cases in 1D and 2D, it has been found that the resulting squared gamma index distribution follows a chi-squared (χ^2) distribution with one degree of freedom. This result can be used to verify the statistical significance of measured deviations, and to determine proper failure rate tolerance levels in clinical radiotherapy quality assurance.

The latter simulation results valid only for a single measurement were extended from single detector system to an entire array of detectors, mimicking thus a measurement conditions for verification of calculated absorbed dose distribution.

Simulated dose measurements that were derived from a set of clinical head-and-neck IMRT dose distributions, calculated in a uniform phantom and evaluated by the gamma index analysis, clearly showed that the probability of having a gamma value above unity is not spatially uniform. The gamma evaluation produced relatively more false positives in regions with larger values of the second-order derivative pointing to the feature that the statistical significance of the gamma failure criterion (i.e., $\gamma > 1$) is not uniquely related to a given set of spatial and dose tolerance values. This shortcoming appears (or strongly indicates) to be responsible for the limited ability of the gamma evaluation method to detect errors in clinically relevant situations.

Keywords: gamma analysis, IMRT/VMAT, QA

Sažetak doktorske disertacije

Uvod i motivacija

Nakon razdoblja intenzivne primjene trodimenzijske (3D) konformalne radioterapije (engl. conformal radiotherapy, 3DCRT), pojavom radioterapije moduliranog intenziteta (jakosti) i volumno-modulirane lučne radioterapije (engl. intensity modulated radiotherapy, IMRT, volumetric modulated arc radiotherapy, VMAT), koje se provode linearnim akceleratorima opremljenim višelističnim kolimatorom (engl. multileaf collimator, MLC) čime se dobivaju složeni oblici raspodjela apsorbirane doze, ukazala se potreba za boljim razumijevanjem dozimetrijskih alata i njihovih ograničenja pri mjerenju i usporedbi tih raspodjela kako bi se osigurala sigurna i točna provedba naprednih postupka radioterapije.

Osiguranje kvalitete (eng. quality assurance, QA) terapije zračenjem moduliranog intenziteta od presudnog je značaja i olakšava njegovu uspješnu i pouzdanu kliničku provedbu. Program osiguranja kvalitete uključuje nekoliko dozimetrijskih postupaka koji se provode prije radioterapijskog liječenja pacijenta. Provjerom točnosti izračuna doze, prijenosa plana zračenja s računalnog sustava za planiranje (engl. treatment planning system, TPS) na linearni akcelerator i isporuke doze, osiguranjem kvalitete za pojedinačne pacijente osigurava se točna isporuka propisane doze.

IMRT postupak uključuje predaju apsorbirane doze koja dovodi do velikog gradijenta doze u blizini kritičnih struktura. Moduliranje intenziteta snopa fotona omogućava da se zračenje može usmjeriti izravno kroz kritične organe i strukture, a postupak optimizacije modulacije snopa zračenja ograničava dozu na kritične organe. Takva složenost raspodjela doza znači da se osiguranje kvalitete kod IMRT-a mora više usredotočiti na kumulativnu isporučenu dozu kao i na provjeru doza na više mjesta, a ne na osiguranje kvalitete pojedinih segmenata snopa. Druga važna značajka je podudaranje gradijenta doze s ciljnim volumenom i razmještajem okolnog normalnog tkiva.

Kriteriji prihvatljivosti rezultata osiguranja kvalitete radioterapije moduliranog intenziteta donekle se razlikuju u različitim ustanovama što je posljedica različitih uređaja za zračenje, linearnih akceleratora, algoritama računalnih sustava za planiranja i njihove praktične primjene, kao i mjerne opreme koja se koristi u provođenju programa osiguranja kvalitete. Postoje različiti izvori koji mogu uzrokovati pogreške kako u planiranju IMRT/VMAT raspodjela apsorbirane doze, tako i u njenoj isporuci. To su prije svih, pogreške vezane uz računalni sustav za planiranje, a najvažniji čimbenici koji mogu dovesti do pogrešnog planiranja postupka zračenja

su načini na koji se modelira kraj listića kolimatora kao i učinak jezička i žlijeba (engl. tongue and groove), transmisija kolimatora i višelističnih kolimatora, izlazni faktori malih polja zračenja i izvan osni profili doza. Izbor veličine matrice za izračun doze također može uzrokovati pogreške i artefakte, kao i korištenje modela za popravke heterogenosti sredstva. Pored toga, pogrešku može uzrokovati i ograničenje mjernog sustava koji se koristi u provođenju programa osiguranja kvalitete, kao što je rezolucija matričnog detektora s velikom brojem detektora. Iako ovaj detektor može istovremeno provjeravati doze na više prostornih mjesta, njegov relativno velik razmak detektora ograničava ga u provjeri detaljnih struktura raspodjele doze.

Iako su razne ustanove razvile vlastite modalitete i koriste različite, komercijalne, mjerne sustave, metoda gama analize postala je standard u ocjeni slaganja referentne raspodjele doze (npr. mjerene) i procijenjene (npr. izračunate) u za pacijenta specifičnom postupku osiguranja kvalitete u radioterapiji moduliranog intenziteta i široko je dostupna za uporabu u komercijalnim paketima programske podrške. Konkretno, gotovo sveprisutni kriteriji tolerancije (dopustivosti) razlike u dozi (engl. dose difference, DD) i udaljenosti-do-slaganja (engl. distance-to-agreement, DTA) od 3%/3 mm, prag niskih doza od 10%, globalno normiranje doze i prihvatljiva stopa neuspjeha (engl. failure rate) od 5-10%, koriste se gotovo sa svim novim uređajima i tehnikama zračenja, uz pretpostavku da je visoki postotak gama prolaznosti pokazatelj dobrog podudaranja između mjerenih i izračunatih raspodjela apsorbirane doze.

Zbog nepouzdanosti mjerenja apsorbirane doze i položaja detektora, neke točke u gama analizi neće proći kriterij prihvatljivosti, čak i ako ne postoji stvarno odstupanje, a određeni udio točaka koje ne zadovoljavaju kriterij se mora dopustiti. Iako su se kriteriji prihvatljivosti za stupanj nepostizanja zahtijevane razine tolerancije dosad obično temeljili samo na empirijskim dokazima, odgovarajući podaci trebali bi biti izabrani na temelju statističke analize stvarnih nepouzdanosti i biti povezani s mjerenjem apsorbirane doze i pozicioniranja detektora. U tu svrhu, neki autori su usvojili pristup propagacije nepouzdanosti, koji u analizu uključuje lokalni gradijent apsorbirane doze. U praktičnim izvedbama, međutim, takve metode su općenito ograničene na linearnu aproksimaciju gradijenta, koja može uvesti anomalije u konveksnim ili konkavnim dijelovima raspodjele doze. U slučaju da je poznata raspodjela vjerojatnosti gama indeksa, kriteriji prihvatljivosti bi mogli biti određeni na temelju analize vjerojatnosti. Pod određenim uvjetima, približna raspodjela kvadrata gama indeksa može se izvesti teorijski; aproksimacija raspodjele s tri momenta razvijena je primjenom općih rezultata kvadratnog

oblika normalnih slučajnih varijabli i hi-kvadratne (χ^2) raspodjele. Ova metoda može potencijalno biti izvedena u uobičajenim postupcima gama analize, zahtijeva samo male preinake i nekoliko dodatnih izračuna.

Predmet ove disertacije je ispitivanje kriterija prihvatljivosti rezultata gama analize, proučavanjem statističke raspodjele vrijednosti gama indeksa pod uvjetima bez stvarnih odstupanja (pogreške), u pokušaju izdvajanja statistički značajnih odstupanja u općim uvjetima.

U prvom dijelu disertacije, razvijeni su i provjereni računalni alati za gama analizu u slučajevima 1D i 2D raspodjela doza. Jednodimenzionalne raspodjele apsorbirane doze opisane analitičkom funkcijom odgovarajućeg oblika i 2D raspodjele apsorbirane doze IMRT polja zračenja, izračunate u fantomima za provođenje kontrole kvalitete pripremljene su za simulacije. To su bili skupovi izračunatih raspodjela apsorbirane doze. Mjerene vrijednosti apsorbirane doze simulirane su na način da su pomak idealnog detektora i nepouzdanost mjerenja na slučajan način odabrani prema normalnoj raspodjeli i dodani izračunatim raspodjelama doza. Simulirana mjerenja su zatim uspoređena s izvornim proračunom, a vrijednost gama indeksa je izračunata korištenjem kriterija tolerancije za razlike u dozi i udaljenosti-do-slaganja jednakim simuliranim nepouzdanostima. Na ta način dobivena je i analizirana rezultirajuća raspodjela vrijednosti kvadrata gama indeksa. Uz istraživanja za jednu točku mjerenja, istražen je i klinički važniji slučaj matričnog detektora koji može imati i nekoliko stotina detektora, a koristi se za usporedbu raspodjela apsorbirane doze. Pretpostavljeno je da će ukoliko su detektori u matrici statistički neovisni (ishod mjerenja, odnosno rezultat jednog detektora ne utječe na drugi), vrijednosti stope neuspjeha dobivene u simulacijama, slijediti binomnu raspodjelu. Zbog uočenog odstupanja simuliranih rezultata, od očekivane teorijske raspodjele na ograničenom broju simulacija temeljenih na kliničkim IMRT raspodjelama apsorbirane doze na određenoj dubini u homogenom fantomu, predložen je izračun odgovarajućih empirijskih kumulativnih funkcija raspodjele vjerojatnosti stope neuspjeha. Potom se za željenu vrijednost empirijske kumulativne funkcije raspodjele vjerojatnosti (npr. 0.95) može izračunati odgovarajuća najveća očekivana stopa neuspjeha. Ako je opažena stopa neuspjeha veća od ove vrijednosti, za pretpostaviti je, uz značajnost 0.05, da odstupanja nisu samo slučajna.

Nadalje, veći skup kliničkih IMRT raspodjela apsorbirane doze korišten je ponovno u simuliranju mjerenja doze uz pretpostavku da izračunata doza predstavlja očekivanu vrijednost i uz dodavanje slučajnog prostornog pomaka u širem opsegu i nepouzdanosti doze. I u ovom slučaju, metoda gama analize korištena je za povezivanje simuliranih mjerenja na više položaja

detektora s računatim raspodjelama doze. Raspodjela rezultirajućeg gama indeksa analizirana je za različite razine nepouzdanosti položaja detektora i apsorbirane doze.

Materijali i metode

U uvodnom dijelu istraživanja, razvijeni su i analizirani računalni programi za standardnu usporedbu raspodjela doza metodom gama analize u 1D i 2D slučajevima.

Ovi računalni programi omogućavaju pretraživanje čitave procijenjene (npr. izračunate) raspodjele doze, za svaku pojedinačnu točku referentne raspodjele doze, u svrhu pronalaženja najmanje vrijednosti gama indeksa ili ograničavanje pretraživanja procijenjene raspodjele na korisnički određeni opseg pretraživanja. Pored toga, moguće je odabrati lokalni ili globalni izračun gama indeksa s izborom normalizacije, postavljanje kriterija tolerancije za razlike u dozi i udaljenosti-do-slaganja kao i različite razine interpolacije referentne i procijenjene raspodjele doza definirane parametrom razlučivosti. U ispitivanju razvijenih programa, prvo je analiziran slučaj 1D raspodjele doze. Matematički dobiven referentni profil koji predstavlja područje polusjene (engl. penumbra) 6 MV fotonskog snopa, polja veličine 10 cm × 10 cm, na dvije različite dubine, d_{max} i 10 cm, nastao je superpozicijom funkcija normalnih kumulativnih funkcija raspodjele s određenim vrijednostima srednje vrijednosti i standardne devijacije, te dopuštenim podešavanjem pomaka položaja, dozimetrijskog odstupanja i faktora normalizacije raspodjele, čime se iz referentne raspodjele mogla dobiti željena procijenjena raspodjela doze.

U cilju analize razvijenog računalnog koda u slučaju 2D raspodjela doza, referentna raspodjela simulirana je najprije kao jednolika s vrijednošću apsorbirane doze od 100 cGy u središnjem dijelu postavljenom na pozadinu vrijednosti doze nula. Procijenjena raspodjela doza modificirana je povećanjem doze središnjeg dijela referentne raspodjele i prostornim pomakom referentne raspodjele u x i y smjeru. U ovom skupu usporedbi raspodjela i u svrhu statističke analize, izračunate su vrijednosti srednje (γ_{mean},) i maksimalne (γ_{max}) vrijednosti γ indeksa, 99-tog postotka ($\gamma_{1\%}$) γ indeksa i očekivanim stupnjem prolaznosti gama analize ($P_{\gamma<1}(\%)$) uz globalnu normalizaciju. Drugi skup 2D raspodjela doze, uspoređuje 2D referentnu raspodjelu dobivenu iz mjerenog profila doze na dubini u vodi s procijenjenom raspodjelom doze dobivenom izmjenom dozne i prostorne ovisnosti u četiri kvadranta raspodjele. U konstrukciji procijenjene raspodjele doze, ova 2D raspodjela doze izmijenjena je u pokušaju da se istaknu odstupanja korištenjem kriterija prihvatljivosti od 3% razlike u dozi i 3 mm razlike u udaljenosti -do- slaganja. Ona je izmijenjena na različit način u tri od četiri kvadranta kako bi se provjerio utjecaj samo prostornog pomaka, samo pomaka doze ili oba pomaka istovremeno, na parametre

od interesa, poput razlike u dozi i gama indeksa. Slična provjera je načinjena usporedbama prilagođene 2D raspodjele doze dobivene zračenjem radiokromskog filma malim poljem snopa X-zraka od 6 MV.

Nadalje, da bi se istražila svojstva raspodjele kvadrata gama indeksa (γ^2) u kliničkim situacijama kontrole kvaliteta (eng. quality control), provedene su simulacije za različite 1D i 2D slučajeve raspodjela doze. U 1D slučaju su profili doze fotonskog snopa nominalnog ubrzavajućeg potencijala 6 MV, mjereni u vodenom fantomu na dubini od 1.5 cm, gdje je doza maksimalna, te na 10 cm dubine. Mjereni profili su prilagođeni teorijskim funkcijama, čime je dobivena početna izračunata raspodjela. Iz nje je dodavanjem slučajne nepouzdanosti, dobivene iz normalne raspodjele vrijednosti doze i položaja detektora, simulirano mjerenje. Simulacija je ponovljena veliki broj puta, uspoređena je s izračunatom raspodjelom, te je kvadrat gama indeksa izračunat uz uporabu kriterija razlika doze i udaljenosti-do-slaganja jednak simuliranim nepouzdanostima. Dobivena je raspodjela uspoređena s χ^2 raspodjelom. Ona je usko povezana s kvadratnim oblicima normalno raspodijeljenih varijabli. Kvadrat standardne normalne slučajne varijable je χ^2 slučajna varijabla. Ako su X_1 i X_2 slučajne neovisne χ^2 varijable, tada njihova suma ima χ^2 raspodjelu s $n_1 + n_2$ stupnja slobode što se može poopćiti na zbroj više od dvije slučajne neovisne χ^2 varijable. Iz toga slijedi da je zbroj kvadrata n neovisnih standardnih normalnih slučajnih varijabli, slučajna χ^2 varijabla s n stupnjeva slobode. Ako pretpostavimo da je pozicioniranje pojedinog detektora normalno raspodijeljeno i da su koordinatne osi neovisne jedna o drugoj, kao i da se izmjerena apsorbirana doza također smatra normalno raspodijeljenom i neovisnom o položaju detektora, u skladu s definicijom bi kvadrat γ indeksa trebao slijediti χ^2 raspodjelu s dva stupnja slobode. S druge strane, budući da apsorbirana doza i položaj detektora nisu u potpunosti neovisne varijable (odnos između njih je nepoznat), to više nije slučaj. Daljnje proširenje prethodnih istraživanja, gdje je pokazano da rezultirajuća raspodjela kvadratnih gama vrijednosti slijedi χ^2 raspodjelu s jednim stupnjem slobode, uključuje slučaj matričnog detektora koji može imati i nekoliko stotina detektora. Ova vrsta detektora obično se susreće u praktičnoj procjeni slaganja referentne (npr. mjerene) i procijenjene (npr. izračunate) raspodjele apsorbirane doze u postupcima provođenja kontrole kvalitete s nizom detektora, dioda ili ionizacijskih komora. Ispitano je kako se rezultat, koji vrijedi za jednu točku mjerenja, može primijeniti u slučaju većeg broja detektora koji se upotrebljavaju u postupcima kontrole kvalitete. Iz tog razloga, simulacije su rađene za matrične detektore s 100 i 400 detektora, i dvije skupine raspodjela doza s prostornom razlučivosti od 1 mm i 3 mm. U simulacijama su upotrijebljene raspodjele doze fotonskih snopova moduliranog

intenziteta korištenih u terapiji karcinoma glave i vrata, izračunate na dubini od 5 cm u homogenom fantomu. Razmak između detektora bio je 1 cm za matrične detektore razmještene u pravilne matrice veličine 10×10 ili 20×20. Parametri simulacije bili su: 1, 2 i 3 % za nepouzdanost u raspodjeli doze i 1, 2, 3 mm za prostornu nepouzdanost kombinirani u tri para vrijednosti 1% / 1 mm, 2% / 2 mm i 3 % / 3 mm. Kao i u slučaju mjerenja za jednu točku, ponovno je slučajna nepouzdanost dobivena pri svakom mjerenju doze, ali ovaj put su svi detektori imali iste slučajne prostorne pomake. Dobiven je relativni broj točaka detektora izvan granice tolerancije od 3.841 (tj. stope neuspjeha), a postupak je ponovljen 10^4 puta.

U sljedećem poglavlju teze istraženo je neriješeno pitanje u vezi odabira odgovarajućih kriterija prihvatljivosti za metodu gama analize za usporedbu raspodjela doza. Ovo razmatranje temelji se na prethodno objavljenim istraživanjima. U jednom od tih istraživanja se pretpostavlja da ne-prostorne nepouzdanosti doze ne ovise o prostornim nepouzdanostima, bez obzira na činjenicu da na ne-prostornu nepouzdanost može utjecati pomak jer je nepouzdanost doze funkcija položaja. Ispitivanja su rađena s 1D simulacijama raspodjela doze. U bilo kojoj točki, nepouzdanost doze ovisi o nekoliko vrijednosti doze i gradijentima iz više segmenata snopa, a ne od cijelog profila doze. Nepouzdanost za ukupni profil određena je iz dostupnih informacija o vrijednostima apsorbirane doze i gradijentima za svaki mali doprinos-mali segment.

U drugom radu je korištenjem matematičkog modela, standardni izraz za izračunavanje gama indeksa oblikovan u skup povezanih diferenciranih jednadžbi koje se mogu riješiti do proizvoljnog reda, postižući time općenitu metodu koja ne ovisi o linearnoj interpolaciji doze između elemenata volumena ili plohe u slučaju 2D raspodjela. Rješenja nultog, prvog i drugog reda su razvijena i provjerena. Stopa neuspjeha gama analize, izračunate unutar razvijenog okvira za predstavljene IMRT raspodjele doze i za skenirane raspodjele doze uskog protonskog snopa, pokazale su da su numeričke metode prvog reda točne unutar 1% i bile su najbolji izbor za raspodjele za koje se zna da imaju male vrijednosti derivacije drugog reda. Na temelju tih pretpostavki postavljena je hipotezu da bi se proučavanjem statističke raspodjele gama vrijednosti u uvjetima bez odstupanja/pogrešaka, moglo odrediti koji bi se kriterija prihvatljivosti metode gama analize mogli koristiti za izdvajanje statistički značajnih odstupanja u općim uvjetima.

U tu svrhu, skup od 30 (IMRT) raspodjela apsorbirane doze korištenih za zračenje glave i vrata, izračunatih pomoću računalnog sustava za planiranje u radioterapijskom odjelu Sveučilišne bolnice u Lundu, Švedska (Skåne University Hospital, Lund, Sweden), u homogenom fantomu, korišten je kao ulaz za simulacije mjerenja doza, uzimanjem izračunatih vrijednosti kao

očekivanih vrijednosti, i uz dodavanje slučajne nepouzdanosti mjerenja. U svrhu ispitivanja valjanost aproksimacije u kojoj su vrijednosti derivacija drugog reda (zakrivljenost raspodjele doze) male, ispitani su postojanje, veličina i učinci derivacije drugog reda u raspodjelama doze u homogenim fantomima izračunate uporabom računalnog sustava za izračun i optimizaciju raspodjela apsorbirane doze. Za svaku točku računanja u izabranoj ravnini na nekoj dubini u fantomu, mjerenje detektorom je simulirano dodavanjem slučajnog prostornog pomaka i slučajnog odstupanja u mjerenju apsorbirane doze. Ti brojevi su izabrani na slučajan način iz normalne raspodjele s izabranim standardnim devijacijama za prostorne komponente i dozu. Nova je simulirana točka potom uspoređena s originalnom raspodjelom doze i izračunata je vrijednost gama indeksa. Taj je postupak ponovljen 10^4 puta kako bi se dobila raspodjela gama indeksa. Metoda gama analize korištena je za usporedbu simuliranih mjerenja s izračunatom dozom, a raspodjela dobivenih vrijednosti gama indeksa za 10^4 simulacija analizirana je za različite razine nepouzdanosti položaja i doze.

Rezultati i rasprava

Rezultati analize razvijenog programskog kôda za standardnu usporedbu raspodjela doze metodom gama analize u 1D i 2D slučajevima pokazali su da se on ponaša u skladu s očekivanjima i prethodno objavljenim rezultatima. Kao što su potvrdili naši izračuni, u 1D slučaju, za oba profila fotonskog snopa od 6 MV (dobivenih prilagođavanjem podataka izmjerenim na dubini od 1.5 cm, gdje je doza maksimalna, i na dubini od 10 cm u vodi), γ indeks udovoljava kriterij prihvatljivosti ($\gamma < 1$) u slučaju blago pomaknute raspodjele doze, što je je u skladu s metodom kompozitne analize. Rezultati su pokazali gotovo simetrične raspodjele razlika u dozi, a vrijednosti gama indeksa dostižu plato oko vrijednosti 0.8 što ukazuje na to da sve točke ispitivanog područja prolaze gama analizu. Udaljenosti-do-slaganja ima konstantnu vrijednost, 0.25, kao što se i očekivalo, budući da je procijenjena raspodjela bila pomaknuta za taj iznos u odnosu na referentnu raspodjelu.

Promjena faktora normalizacije procijenjene raspodjele doze, uz primijenjeni prostorni pomak, uzrokovala je asimetričnost razlike u dozi i promjene u ponašanju udaljenosti-do-slaganja i raspodjele γ indeksa. Kod usporedbe raspodjela doze dobivenih iz izmjerenih profila na dubini d_{max}, maksimalna vrijednost γ indeksa postaje bliža vrijednosti 1 na mjestu gdje plato raspodjele prelazi u polusjenu. Vrijednost udaljenosti-do-slaganja smanjuje se s 0.9 cm na lijevom rubu profila, na vrijednost od 0.25 cm u ravnom području profila, i dalje, na vrijednost nula, na desnom rubu profila. U slučaju promjene faktora normalizacije, raspodjela gama indeksa ima

veće vrijednosti na područjima platoa i niske doze. Uvođenjem treće modifikacije, odstupanje doze, dobiveni su slični globalni oblici za raspodjele gama indeksa i udaljenosti-do-slaganja na dubinama d_{max} i 10 cm. Maksimalna vrijednost gama indexa je 1.101 pri usporedbi profila na dubini od 10 cm. Raspodjela vrijednosti udaljenosti-do-slaganja ima "u" oblik sa konstantnom vrijednošću od ~ 0.25 cm u području polusjene, gdje je udaljenost-do-slaganja, u biti, određena prostornim pomakom. Rezultati analize su pokazali da vrijednost razlika u dozi raste brzo u području polusjene, ima vrijednosti ispod 0.3 (samo prostorni pomak) i ima maksimalnu vrijednost, veću od kriterija prolaznosti (za druga dva slučaja modifikacije raspodjele doze).

Kod prvog skupa rezultata ispitivanja kôda u 2D slučaju, pokazalo se da povećavanje faktora razlučivosti u izračunu parametara γ_{mean}, γ_{max} i $\gamma_{1\%}$ vodi ka konvergenciji tih vrijednosti; povećavanjem faktora razlučivosti iznad 50, rezultati su nepromijenjeni. Dobiveni rezultati su u skladu s očekivanim svojstvima γ indeksa. U dijelu proračuna, koji se odnosi na razlučivost, utvrđeno je da rezultati gama analize na prolaznost malo ovise o povećanju parametra razlučivosti; postotak prolaznosti je uvijek 100%, osim za parametra razlučivosti s vrijednošću 1 (bez interpolacije), gdje imamo veće vrijednosti za γ_{mean}, γ_{max} i $\gamma_{1\%}$, i niži postotak prolaznosti. Zadržavajući iste parametre prostornog pomaka i razlučivosti kao u posljednjem proračunu, ali sada i za tri različite razlike u dozi (1%, 3% i 5%) u procijenjenoj raspodjeli doze, rezultat je pokazao da to uzrokuje značajnu stopu neuspjeha gama analize za veću razliku doze između dvije raspodjele.

Rezultati ispitivanja razvijenog programskog kôda za drugi skup 2D raspodjela, prikazuju apsolutnu i relativnu razliku referentne i procijenjene raspodjele doze. U prvom kvadrantu razlika doze ima konstantnu vrijednost nula, jer je ovaj kvadrant nepromijenjen, dok se u drugom (pomak doze) čini konstantnim, ali samo zbog grube razlučivosti skale boja. U kvadrantu 3 (prostorni pomak) blizu ruba snopa, razlika u dozi postaje velika zbog velikih gradijenta doze, čak i samo s relativno malim prostornim pomakom između dviju raspodjela doze. Ova značajka razlika u dozi tipična je za male prostorne pomake u područjima s velikim gradijentom doze. Sličan rezultat kao u kvadrantu 3, je u kvadrantu 4 (dozni i prostorni pomak) gdje opet, u strmim gradijentima doze, i mali prostorni pomak uzrokuje vrlo velike razlike u dozi.

Kao što je istaknuto, dopunskim programima omogućena je usporedba izračunatih i simuliranih izmjerenih raspodjela doza, u smislu njihove apsolutne razlike izračunate na osnovi piksel po piksel. To se koristilo u ovom slučaju za prikaz razlika u dozi uspoređenih raspodjela doza. Uz

to, integralni histogrami različitih veličina poput raspodjela razlika doze i γ indeksa, pokazali su se korisnim u prikazivanju značajki i razumijevanju tih veličina.

Prema tome, na osnovu ovih provjera, može se zaključiti da naši računalni programi za standardnu usporedbu raspodjele doza metodom gama analize rade pravilno.

Rezultati istraživanja raspodjele vrijednosti γ^2 u kliničkim situacijama, u 1D slučaju, pokazuju dobro slaganje; raspodjela γ^2 vrlo dobro slijedi χ^2 raspodjelu s jednim stupnjem slobode. Važno je naglasiti da sličan rezultat, tj. očekivani stupanj tolerancije odstupanja, ostaje blizu 0.05, duž svih položaja na osi x, bez obzira na oblik raspodjele doze i gradijent apsorbirane doze. Ovi rezultati su vrlo korisni jer omogućuju jednostavnu implementaciju statističke interpretacije metode gama analize u trenutne procedure gama analiza, bez izmjena.

U slučaju 2D raspodjele, γ^2-raspodjela dobro slijedi χ^2 raspodjelu s jednim stupnjem slobode, ali ovaj put samo za točke u području s malim gradijentima doze. Razlog tome je jedan od poznatih nedostatka metode gama analize, koja nije osjetljiva na gradijent doze.

Ovo je pokazatelj da aproksimacija nije dovoljno dobra za točke u kojima je gradijent doze velik. Istraživanje je prošireno na ispitivanje druge derivacije u raspodjelama apsorbirane doze, obzirom da sve dok nema velikih vrijednosti derivacije drugog reda raspodjela apsorbirane doze, može se očekivati da će gama indeks imati svojstva u skladu sa statističkim modelom koji pretpostavlja da dvije kategorije nepouzdanosti doze, položajne odnosno prostorno orijentirane i one koje to nisu (dozimetrijske nepouzdanosti), slijede normalnu raspodjelu i da su nekorelirane. Tada je doprinos pomaka položaja ne-prostornoj komponenti nepouzdanosti doze zanemariv.

Rezultati proširenog istraživanja, koje uključuje slučaj matričnog detektora no uz ograničeni broj razmatranih kliničkih raspodjela, pokazali su da simulirani rezultati ne slijede očekivanu binomnu raspodjelu što je vjerojatno rezultat činjenice da položaji detektora nisu neovisni. Iako se rezultati binomne raspodjele ne mogu direktno upotrijebiti, predloženim izračunavanjem empirijske kumulativne raspodjele vjerojatnosti moguće je utvrditi vjerojatnost (npr. 0.05) da će stopa neuspjeha, u uvjetima bez pogreške u raspodjeli doze, premašivati određenu vrijednost.

Kako je dodatno potvrđeno ovim istraživanjem, fiksni skup kriterija gama analize može se koristiti za izdvajanje statistički značajnih odstupanja pri očekivanoj stopi neuspjeha (tj. 0.05), sve dok je derivacija drugog reda apsorbirane raspodjele doze mala. To je slučaj za više od 50% točaka kliničkih IMRT raspodjela apsorbirane doze koja smo istražili. Međutim, za druge točke, derivacija drugog reda je veća, što rezultira stopom neuspjeha koja je znatno veća od 0.05. To

znači da ako se gama analiza koristi s fiksnim kriterijima na temelju standardnih odstupanja nepouzdanosti pozicioniranja detektora i mjerenja doze, dolazi do lažnih neuspjeha u točkama u područjima s velikim vrijednostima derivacije drugog reda. Treba napomenuti da je ovo pitanje svojstveno metodi gama analize, bez obzira na aproksimaciju u kojoj su vrijednosti derivacija drugog reda male (mala zakrivljenost raspodjele doze). Za raspon kriterija koji su odabrani za prostorno i dozimetrijsko slaganje u gama analizi, vjerojatnost gama-vrijednosti iznad jedinice nije ujednačena za raspodjelu doze u prisutnosti velikih vrijednosti derivacije drugog reda, čak i ako postoje samo slučajna odstupanja u mjerenju položaja i doze.

Međutim, u slučajevima kada je prostorna nepouzdanost jednaka ili veća od prostornog razlučivanja matrice raspodjele doza, širina raspodjele stope neuspjeha postaje mnogo manja, a njena srednja vrijednost blizu očekivane vrijednosti 0.05, osim kod najniže vrijednosti nepouzdanosti doze (1%). Za veće nepouzdanosti doze, pokazuje se da se srednja vrijednost raspodjele stope neuspjeha opet približava vrijednosti 0.05. Ako se ta ograničenja prepoznaju, rezultati ovog istraživanja mogu se upotrijebiti za postavljanje statistički značajnih prihvatnih kriterija za metodu gama analize.

Ključne riječi: gama analiza, IMRT/VMAT, QA

List of abbreviations

Abbreviation	Definition
2D	Two dimensional
3D	Three dimensional
3DCRT	Three-dimensional conformal radiotherapy
AAPM	American Association of Physicists in Medicine
BEV	Beam's eye view
BT	Brachytherapy
CC	Collapsed cone
CT	Computed Tomography
DD	Dose difference
DICOM	Digital Imaging and Communication in Medicine
dMLC	Dynamic MLC delivery
DTA	Distance-to-Agreement
DVH	Dose Volume Histograms
EBRT	External beam radiotherapy
ECDF	Empirical Cumulative Distribution Function
EDT	Euclidean distance transform
EPID	Electronic Portal Imaging Device
ESTRO	The European Society for Therapeutic Radiology and Oncology
FMO	Fluence map optimization
FR	Failure rate
gEUD	Equivalent Uniform Dose
IMAT	Intensity Modulated Arc Radiotherapy
IMRT	Intensity Modulated Radiotherapy
Linac	Linear Accelerator

LSI	Leaf step index
MLC	Multi-Leaf Collimator
MR	Magnetic resonance
MU	Monitor unit
NAT	Normalised agreement test
NTCP	Normal tissue complication probability
OAR	Organ at Risk
PACS	Picture archiving and communication systems
PDD	Percentage depth dose
PDF	Probability Distribution Function
PMMA	Polymethyl methacrylate
PTV	Planning Target Volume
QA	Quality Assurance
QC	Quality Control
RDF	The relative dose factor
RF	Radiofrequency
sMLC	Segmented MLC delivery
SOD	Second order derivatives
SSD	Source to Surface Distance
TCP	Tumour control probability
TERMA	Total energy released per unit mass
TI	Therapeutic index
TLD	Thermoluminescent dosimeter
TPR	Tissue Phantom Ratio
TPS	Treatment Planning System
VMAT	Volumetric Modulated Arc Radiotherapy

TABLE OF CONTENTS

Chapter 1
INTRODUCTION

1.1 Overview of radiotherapy

Radiotherapy (radiation oncology or radiation therapy) is a medical speciality that is an essential part of a multidisciplinary approach to cancer treatment that uses directly ionizing radiation (charged particles such as electrons, protons, α particles and heavy charged particles) or indirectly ionizing radiation (photons and neutrons) to kill cancer cells by damaging their deoxyribonucleic acid (DNA). Roughly, half of all cancer patients worldwide receive some form of radiotherapy over the course of their treatment, either alone or in combination with other treatment modalities like surgery and chemotherapy.

Radiotherapy is a complex process and consists of several steps including the diagnosis of cancer, localization of a target volume, treatment planning, determination of dose distribution, delivery of a prescribed dose to a target volume, patient dose verification and the patient follow-up. In external beam radiotherapy (EBRT) the dose is delivered to a target volume from outside the body by irradiating it with high-energy photon, electron, proton or ion beams. This is the most common approach in a clinical setting and medical linear accelerators (linacs) are used for dose delivery. Brachytherapy (BT) is another type of radiotherapy in which sealed radioactive sources in various forms, using different applicators, are inserted directly into the tumour tissue or brought into the close vicinity of the tumour site to irradiate it.

The main difficulty in treating cancers with radiotherapy is a position of the tumour. It is usually situated either within or on the surface of a particular tissue or organ and it is inevitable that healthy tissues will also receive part of prescribed absorbed dose. Radiotherapy treatments aim to deliver the highest possible absorbed dose to the tumour in order to maximise the probability of complete tumour regression whilst minimize as much as possible absorbed dose to the surrounding normal tissue to maintain its function after the treatment.

For many years it has been known that delivering a high absorbed dose to the tumour is critical for tumour control and that probability of complications increases with the absorbed dose and volume of organs and tissues irradiated. Successfully treating the tumour with a high dose while minimizing the dose to normal tissues sets high requirements on both geometrical and dosimetric accuracy and precision.

The key to successful radiotherapy treatment lies in the sensitivity of different tissues to ionizing radiation; tumours often being more sensitive to radiation than the nearby healthy tissues. The dose response or dose effect can be described by the tumour control probability (TCP) and normal tissue complication probability (NTCP) curves as a function of the dose (Figure 1.1).

TCP curves are typically sigmoidal in shape, with minimal likelihood of cure at low doses, a rapid rise in the cure rate once a particular dose is received, and an asymptotic approach to the maximum effect. The NTCP curve follows a similar shape, radiotherapy being most successful in anatomical regions that show the greatest lateral displacement between the TCP and NTCP curves. The ratio of tumour control probability to normal tissue complications probability for a particular dose is called the therapeutic index (TI). Also, radiotherapy treatments are usually fractionated, i.e., the delivered dose is divided into small portion of the total prescribed dose. Fractionated radiotherapy enables normal tissues to partly repair themselves during the time between successive fractions (normal tissues preferentially repair over tumour cells), therefore enlarging the therapeutic index.

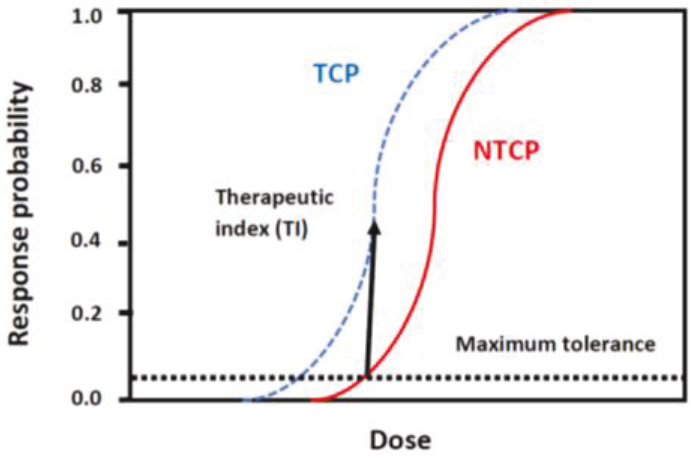

Figure 1.1. Sigmoidal shape dose response curves for tumour control probability (TCP) and normal tissue complication probability (NTCP). The therapeutic index (TI) is the ratio of expected TCP to NTCP at a clinically mandated maximum tolerance (5% in this example).

1.2 3D Conformal and intensity modulated radiotherapy

Treatment planning based on three-dimensional (3D) anatomical information of the tumour and surrounding healthy tissues available from computed tomography (CT) facilitates the establishment of three-dimensional conformal radiotherapy (3DCRT). The development of more accurate treatment planning calculation algorithms, beam's eye view (BEV), helpful in

the design of treatment fields, plan evaluation capabilities enhanced through visualised dose distributions in relation to the anatomy and dose volume histograms, as well as advances in image processing made 3DCRT very effective.

However, there are situations for which 3DCRT cannot produce a satisfactory treatment plan because of the complex target volume shapes or the close proximity of critical normal tissues. Intensity modulated radiotherapy (IMRT) addresses this shortcoming of 3DCRT in that IMRT offers great flexibility in sculpting the dose to complex-shaped targets, achieving better target dose conformity and normal tissue sparing. IMRT is an advanced form of 3DCRT in which the radiation beam is shaped to fit the tumour volume, thus effectively reducing the dose to adjacent normal tissues. The IMRT technique modulates the fluence of a beam during irradiation in a way that the computer controls the motion of the leaves of a multileaf collimator (MLC), all intending to increase the dose adaptation to the tumour volume and improved homogeneity of the dose distribution.

Several diverse techniques have been developed to deliver IMRT. The two most common methods of segmental IMRT and dynamic IMRT use MLCs. In the segmental method, for each beam orientation, several different MLC-shaped fields (segments) are created. Modulated field fluence is achieved by summing all the segments. The beam is turned on only when the segments are in an appropriate position determined through the dose distribution optimisation process. In contrast, with dynamic MLC-IMRT the MLC leaves are in continuous motion during the treatment of each field. The dosimetric advantage of IMRT over conventional radiotherapy techniques has been well documented in the literature [1, 2].

The invention of IMRT was based on analogies to image reconstruction in computed tomography (CT). The concept [3] formulated the task to compute the fluence profile of the beam necessary to produce a required dose distribution in one complete gantry rotation. As opposed to the conventional approach where the dose distribution of the predefined beams is "forward" calculated, this formulation posed treatment planning as an "inverse" problem. For the inverse problem there is no exact solution because there are no fluence modulated profiles that would deliver the full dose to the tumour without delivering the dose to the critical organs surrounding it.

Thus, a reverse approach is taken to find the best possible solution for a given target volume and critical organs. Therefore, it is necessary to produce an IMRT plan to be as close to the ideal dose prescription to the tumour volume and dose avoidance in surrounding critical organs. This has become the basis of the optimisation solutions used in modern IMRT planning.

1.2.1 The concept of IMRT

The concept of IMRT is to modulate the intensity of radiation beam fluence in such a way to achieve a higher degree of spatial conformity of the resulting dose distribution with the planning target volume. The modulation of a single beam only would lead to an undesired, inhomogeneous spatial dose distribution in the target volume. However, when more beams are applied, the resulting ’hot’ and ’cold’ areas are compensated by the ’cold’ and ’hot’ areas produced by the modulated beams from other directions resulting in a uniform dose distribution tightly conformed to the planning target volume (PTV) [4].

Increased sparing of organs at risk (OAR) close to the tumour reduces toxicity to these organs and also gives the potential for dose escalation, achieving better tumour control. IMRT has replaced conventional 3DCRT as a routine technique in the treatment of several cancer types and anatomical sites. The advantage of IMRT over 3DCRT is obvious in terms of sparing of critical organs, dose coverage and homogeneity of PTV [5, 6].

A more detailed discussion on IMRT treatment delivery modalities, properties of treatment planning and verification are given in the Chapter 2.

1.3 Rotational IMRT

Rotational IMRT is the common name for different techniques in which the radiation beam remains on throughout the irradiation while the linear accelerator gantry is moved around the patient at a variable speed and the MLC simultaneously varies the shape of the beam. These techniques commonly include tomotherapy [7], Intensity Modulated Arc Radiotherapy (IMAT) [8], and Volumetric Modulated Arc Radiotherapy (VMAT) [9].

1.3.1 Tomotherapy

In tomotherapy, intensity modulated rotational radiotherapy is delivered by using a fan-beam delivery system. Sequential (serial) tomotherapy uses a fast-moving, actuator-driven MLC attached to a conventional C-arm gantry to modulate the beam fluence. Helical tomotherapy, involves the continuous patient translation through a ring gantry during the fan beam rotation.

A gantry provides a platform to perform tomographic verification using an unmodulated megavoltage beam. The resulting tomograms have adequate tissue contrast and resolution to provide a patient setup verification. Assuming only translational and rotational offset errors, it is also possible to determine the offsets directly from tomographic projections, avoiding the time-consuming image reconstruction operation. The offsets can be used to modify the leaf

delivery pattern to match the beam to the patient's anatomy on each day of the course of the treatment. If tomographic representations of the patient are generated, this information can also be used to perform the dose reconstruction. In this way, the actual dose distribution delivered can be superimposed onto the tomographic representation of a patient obtained at the time of the treatment. The results can be compared with the calculated isodose on the planning CT images. This comparison may be used as an accurate basis for adaptive radiotherapy whereby the optimized treatment delivery is modified before subsequent fractions. The verification afforded with tomotherapy allows for more accurate conformal therapy. It also enables conformal avoidance radiotherapy, a complement to conformal therapy, for the cases in which the tumour volume is ill-defined, but the locations of sensitive structures are adequately determined.

1.3.2 Volumetric modulated arc therapy

As for IMRT, the target conformity in volumetric modulated arc therapy (VMAT) is achieved by modulating the fluence of the radiation beam. In VMAT the entire linear accelerator gantry is rotated during the delivery in addition to the dynamically moving MLC jaws. Moreover, the rotational speed of the gantry and the dose rate may be varied continuously during the beam delivery.

The target conformity and dose sparing of the healthy tissue of VMAT are comparable to that of IMRT, but since the treatment can be delivered faster it generally requires fewer monitor units (MUs) [8], [10], [11].Compared to IMRT, VMAT delivery is more complex and poses higher demands on the accuracy of the gantry angle as well as on the dose rate. The quality assurance (QA) of VMAT is also more demanding as it requires a non–angular dependent detector or a reliable method to correct for the dependence.

1.4 Advanced radiotherapy techniques quality assurance and verification

3DCRT is characterised by the use of multiple static MLC shaped photon beams that irradiate the target volume from different directions. Beam properties are determined during the commissioning of the irradiation unit and periodically checked in a frame of an institution's QA programme. This machine-specific programme typically checks the beam output constancy, flatness, symmetry, beam quality factor, etc. [12, 13]. Furthermore, treatment planning system acceptance testing and commissioning are closely related to the machine QA and important for

the overall accuracy and reliability of radiotherapy treatment. Patient specific QA is limited to the simple independent dose and monitor unit verification calculations.

IMRT treatments involve the delivery of complex dose distributions with steep dose gradients near critical structures. The fluence modulation allows that radiation beams can be directed through the critical organs and structures and the fluence modulation optimization process limits the critical structure doses. Such complexity of achieving the dose means that the QA of IMRT dose distributions needs to concentrate more on the delivered cumulative absorbed dose rather than on the QA of individual beam segments, as well as checking the dose at multiple locations. Another important feature is the match of the dose gradients with the patient's target and surrounding critical organ geometry.

The review [14] of IMRT dose measurement systems discusses in detail the use of the most relevant dosimetry systems (dosimeters, phantoms) and dose comparison tools. It highlights the influence of IMRT features on dosimetry system use. The simplest, early measurement for patient specific plan verification in terms of the absolute dose verification was a point-dose measurement. The measurement with a cylindrical chamber and a simple QA phantom provided a single number that was a small volume measurement (signal averaging) over the volume of the chamber. The measured dose was compared to the dose obtained from the TPS calculation. Since only a point measurement was carried out, the reasonable localisation choice is either the planning target volume (PTV) or organ at risk (OAR) region. This approach is impractical and has very limited value to the IMRT verification process.

Developments in patient specific IMRT QA verification measurements proved to be able to detect clinically relevant errors [15] and able to ensure reliable and accurate radiotherapy and safety of the patient. Once the IMRT absorbed dose distribution for a patient is completed, the so-called verification or hybrid plan in the same geometry can be made for the subsequent measurements. The patient's plan is recomputed onto a homogeneous phantom. Further discussion is provided in Section 3.3.

Today, there are many other devices commercially available for this type of verifications: linear or matrix detector arrays consisting of a large number of diodes or ionization chambers in 2D or 3D arrangements [16-18].

The verification of an IMRT plan is commonly very time-consuming compared to the verification of 3DCRT plans. For the assessment of dose comparisons, the most direct way is to analyse the percentage difference between the measured and calculated absorbed dose.

However, this approach is complicated by the fact that there is a geometric uncertainty associated with the positioning of the detector, which can have a large impact in areas with large dose gradients. The percentage dose differences between measured and calculated doses in these areas can be large but without a clinical significance.

In such situations, another measure of the agreement between the reference (e.g. measured) and evaluated (e.g. calculated) values is the so-called distance-to-agreement (DTA), which is the metric that gives the distance between a point under consideration in one dose distribution (reference) to the point in another (evaluated) for which the absorbed dose is the same. It is the composite of these two measures, i.e., the gamma-evaluation test method, which has become the standard method for quality control (QC) of fluence modulated radiotherapy beams [19, 20].

Due to the unavoidable uncertainties of absorbed dose measurements and detector positioning, some points in the gamma evaluation will always fail the test criteria even if there is no true deviation, and a certain failure rate has to be tolerated. Although test criteria and failure rate tolerance levels have hitherto normally been based only on empirical evidence [21], proper figures should preferably be chosen based on a statistical analysis of the actual uncertainty associated with the absorbed dose measurement and the positioning of the detector. For this purpose, some authors have adopted an error propagation approach, incorporating the local absorbed dose gradient into the analysis [22-25]. In practical implementations, however, such methods are generally limited to a linear gradient approximation, which may introduce anomalies in convex or concave parts of the dose distribution.

If the complete probability distribution of the gamma (γ)-index is known, the test criteria could be determined based on the probability analysis [26]. Under certain conditions, an approximate gamma distribution can be derived theoretically, and a three-moment approximation of the squared gamma distribution has been developed by applying general results about quadratic forms of normal random variables and the chi (χ)-squared distribution [26]. This method could potentially be implemented in conventional gamma evaluation procedures, requiring only slight modifications and few extra calculations.

A more thorough discussion on the dose comparison tools and techniques, methodologies for absolute dose verification, and overview of clinical results, tolerances, and action limits is given in Chapter 3 of this work.

1.5 Aim and scope of this research

The reliability of advanced radiotherapy techniques, such as IMRT and VMAT crucially depend on the ability of the established procedures for QA verification to check the accuracy of the treatment plan and to detect clinically relevant errors.

Most radiotherapy institutions perform routinely the measurement-based patient specific IMRT (VMAT) QA. It is a mandatory part of their QA programme. In a short and simplified protocol version, after the treatment plan is finalised and approved by the radiation oncologist, it is computed on a homogenous phantom used for QA; the plan comprises the MLC sequence as a function of a gantry angle and monitor units (MUs). The phantom is irradiated to measure the dose with an appropriate detector (e.g. ionization chamber array). The planned[1] or calculated (*evaluated*) and measured (*reference*) dose distributions are then compared by some established metrics and based on the institution's tolerances (acceptance limits), accepted or rejected. If the discrepancies found are considered acceptable, then provided that good knowledge and understanding of the evaluation tool and metrics used are ensured, the given plan will be accurate to within the clinically acceptable limits.

This work aims at studying the gamma analysis method by using a statistical approach to evaluate the relation between the acceptance criteria and the actual uncertainties of the dose measurement. The gamma analysis has been criticised for using rather arbitrary acceptance criteria and the need for a statistical approach has been pointed out [26]. The test criteria for the percentage dose deviation and the distance-to-agreement are normally based on empirical experience rather than the actual uncertainties of absorbed dose measurements and detector positioning. For a proper determination of the acceptable failure rate, a statistical evaluation should be carried out [26].

To achieve the goals of this research the following steps were undertaken:

1. Gamma analysis (γ-index calculation) programs were developed, tested, and verified for 1D and 2D clinically realistic dose distributions to establish a calculation framework for relevant subsequent investigations. The developed code has the potential to be further extended to 3D dose distribution comparison cases;

[1] The *reference* and *evaluated* dose distributions. as the most general terms relevant for dose distribution comparisons will be used in the thesis. Typically, but not limited to, a *reference* distribution is the one that is *measured* and an *evaluated* is the *planned* or TPS *calculated* one.

2. Calculation acceleration techniques were explored to enable acceptable computational times;
3. Simulations of the dose measurement were conducted by using the calculated dose distributions in 1D and 2D for clinically realistic quality control (QC) situations and by taking into account the statistical uncertainties of the absorbed dose measurements and detector positioning. This was used to investigate the quadratic gamma (γ^2) index distribution and compare it with the chi-square (χ^2) distribution. The results were evaluated to check if and how the results can be used as a basis for the determination of gamma evaluation acceptance criteria;
4. γ-index calculation was studied with regards to the relation between the acceptance criteria and the actual uncertainties of the measurement for a set of clinical head-and-neck IMRT fields calculated in a QC phantom. The simulated measurements were compared to the calculated dose using the gamma evaluation and the distribution of the failure rate was analysed;
5. Previous simulations valid for a single measurement were extended to cover simultaneous measurements with a large number of detectors, a detector array, to investigate how the results can be applied to clinically relevant situation.

The measured dose distribution data necessary to complete these simulations were obtained either from the linear accelerator commissioning and routine QA procedures at the Clinic of Oncology, University Clinical Centre Sarajevo or from the radiotherapy department at Skåne University Hospital, Lund, Sweden, where the treatment planning system Oncentra Master Plan (Nucletron B.V., Veenendaal, the Netherlands) was used to calculate the absorbed dose distributions in a phantom for a set of clinical, head and neck IMRT fields.

Chapter 2

LINEAR ACCELERATOR PHOTON BEAMS AND RADIOTHERAPY DELIVERY TECHNIQUES

2.1 Medical linear accelerator

Although photon beams of different characteristics, and produced by different types of units, are used in EBRT, we will limit our brief discussion here on high energy photon beams produced in medical linear accelerators (linacs) (Figure 2.1).

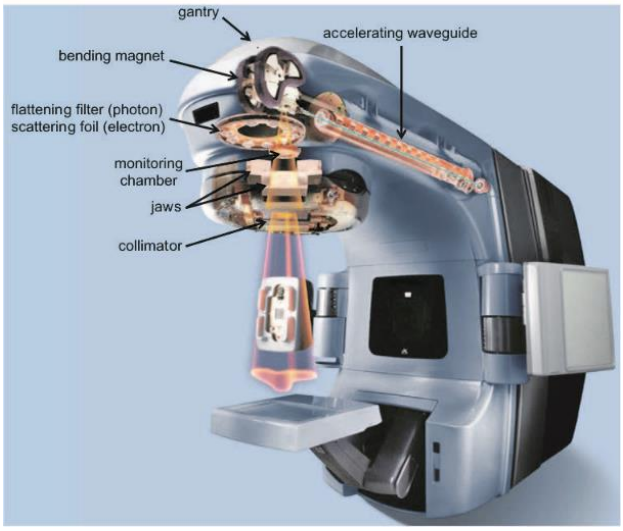

Figure 2.1. Schematic diagram of a medical linear accelerator. Figure from https://oncohemakey.com/intensity-modulated-radiation-treatment-techniques-and-clinical-applications/.

Photons in linear accelerators are produced by irradiating the high-Z target material with a narrow high energy electron beam. Electrons are generated by an electron gun (filament) and accelerated to a given potential, using a radiofrequency (RF) field. Accelerated electrons are directed onto a target using a bending magnet. While the electrons slowdown in the target material, they lose their energy predominately in radiative interactions, and *bremsstrahlung* photons are produced. The resulting high energy photon beam is shaped and modified by the elements mounted in the linear accelerator head, most importantly, the flattening filter(s) and collimators. The photons interacting with the beam modifying elements may be absorbed or scattered. Therefore, the treatment beam contains a spectrum of *primary* photons originating directly from the target, extra focal *head-scattered* photons produced by the primary photons interacting in the accelerator head and the *contaminating charged particles* produced in these interactions. As modern radiotherapy practice now utilizes fluence modifying techniques to

create more conformal dose distributions, the flattening filter becomes unnecessary in the beam production process. Removing the flattening filter increases the dose rate by a factor of 2–4. This increase associated with flattening filter free (FFF) beams is particularly useful for small field stereotactic radiosurgery (SRS), stereotactic body radiotherapy (SBRT) procedures, and can be used for a wide range of fields and treatments.

Linear accelerator calibration

Since in this work the reference is made to the absorbed dose that has been delivered with a linear accelerator to a phantom or dose verification tool such as a matrix of ionization chambers or semiconductor diodes, it is necessary to describe the meaning of linear accelerator beam calibration. The linear accelerator head contains the upper transmission ionization chambers (the monitor chambers). They are responsible for the beam termination when the required absorbed dose has been delivered. The monitor chamber is located above the beam collimating devices. Therefore, it is relatively insensitive to the changes in the field size and does not depend on the patient or phantom geometry under irradiation. To relate a signal from the monitor chamber to the absorbed dose in the treatment geometry, it is necessary to calibrate each beam used for treatment. A unit established to relate the signal and dose is the monitor unit (MU). Prior to its clinical use the linear accelerator beams need to be calibrated for individual energies of electron and photon beams. One approach to calibrate the linear accelerator is conducted so that 100 MU for a 10×10 cm^2 field, delivered with a Source to Surface Distance (SSD) of 100 cm corresponds to 1Gy at the point of maximum dose, d_{max}, along the central axis, in a homogeneous water phantom [27].

Primary and head-scattered photons

The photons, as indirectly ionizing particles, deposit their energy in matter by transferring it to charged particles (electrons and positrons). Due to long mean free paths between their interactions (in the order of 10–50 cm for the typical linear accelerator produced photon beams in water) energy is transferred to the medium in local bursts. As a result of the incident photon interactions, secondary (phantom scattered) photons carrying away the remaining energy may also be produced. The dose deposited by the charged particles launched in the direct photon's first interactions is referred to as the *primary dose*. The dose deposited as a consequence of scattered photons interactions is called the *secondary dose* (or scattered dose). Depending on whether the scattered photon was produced in the accelerator head or in the irradiated medium, the scattered dose is called the head scatter dose or the phantom scatter dose, respectively. The

primary dose amounts to about 85–95% of the total dose, while the scattered dose to approximately 5–15% of the total dose [28].

Contaminant charged particles interact with the matter directly and lose their energy in multiple collisions causing ionizations and excitations of atoms along their track. The range of contaminating charged particles is relatively short and their contribution to the total dose deposited is relevant only within the first 1–2 cm of the matter.

The external radiotherapy photon beams are therefore characterized by a finite size of the radiation source (the focal point on the target), presence of the extra-focal scattered radiation, and charged particle contamination. Their spectra are in general unknown and change across the beam (off-axis softening) and within matter (depth hardening).

2.2 Quantification and measurement of dose

The quantification of the deposition of radiation in the human body is essential for any medical use of radiation. All radiation dosimetry systems are designed to represent the energy deposition to the human body either by directly or indirectly ionizing radiations. Unlike imaging, where the goal is to get maximum image quality with the lowest dose of radiation, radiotherapy searches for the best compromise between a therapeutic dose to a tumour and unwanted dose to the normal tissue. Depending on the specific applications, several quantities and units for describing dosimetric quantities have been introduced. The dosimetric quantities of interest in this work are described in Appendix A.

2.3 Dosimetric properties of photon beams

2.3.1 Characteristics of photon beams

In radiotherapy, photon beams generated by the linear accelerator are polyenergetic and have a wide distribution in energy that ranges from zero to the nominal energy of the accelerated electrons. The shape of the photon beam spectrum depends on the electron beam energy, the thickness of the target (photon) source, the fixed collimators (used for shielding), flattening filter and movable collimators (jaws, MLC). The energy spectrum is the most exhaustive description of the photon beam quality, but it is difficult to measure. Typically, the beam quality is indirectly estimated by measuring the tissue-phantom ratios $TPR_{20,10}$ or percentage dose (PDD) [27] as a function of depth and lateral dose profile in a water phantom. This estimate is incomplete [29], but sufficient for operation of treatment routine.

2.3.2 Dosimetry measurements used to characterize the photon

The attenuation of a photon beam by the air is negligible, and the photon fluence due to divergence can be determined by the inverse square law. On the other hand, when traversing media with varying density, the photon beam undergoes attenuations which are more complicated to calculate. Therefore, different dosimetry quantities and methodologies have been introduced to facilitate dose calculation in radiotherapy situations. Measurement are usually performed in a water phantom due to similar properties of absorption and scattering of muscle and other soft tissues. For practical reasons, the dosimeters are also preferred to be made of water or tissue equivalent material in terms of response to the Compton effect (the most dominant interactions in the energy spectrum of photon therapy). Therefore, this material must have the same electron density as water. With reference to the dosimetry of photon beams in water, additional dosimetry quantities are described in Appendix A.

Relative dose factor (RDF)

The relative dose factor (RDF) is defined as the variation of the absorbed dose at z_{max}, the depth of maximum dose, as a function of the field size in water. Multiple factors were shown to affect the RDF. Namely, the scattered photon from the linear accelerator head structure, backscattered photons, and electrons scattered into the monitor chamber and, at very small filed sizes, the effect of the x-ray source obscured by the collimator [30]. Accordingly, RDF considerably differs from one type of linear accelerator to another. RDF of each representative field size is measured for each available energy, as a necessary procedure in linear accelerator commissioning and periodic QA. The measured RDF is referred to as a selected standard field size (commonly the 10 ×10 cm^2 field) at the distance from the source to the isocentre of the linear accelerator.

Photon beam cross-profiles and off-axis ratio (OAR)

Photon beam cross-profiles consist of three distinct regions: plateau (central region), penumbra and, umbra. The plateau represents the portion of the beam including doses over 80% of the maximum dose. The flatness of the plateau is affected by the fluence and energy distribution of the primary photons (dependent on the primary electron beam properties and details of target and flattening filter design) and their changes with the depth in the phantom/patient.

The penumbra represents the fall-off area at the beam edges. Specifically, the penumbra region is the part of the dose that lies within 20-80% (or sometimes 10-90%) of the maximum dose. The size of the penumbra is geometrically determined by the focal spot of the photon beam (source shape and size) (Figure 2.2a), the field size, the MLC shape (Figure 2.2b), and the lateral

spread of the charged particles at the field edges (dependent on the beam energy and medium density). Technically, the shape of the leaf ends differs from one manufacturer to another. Single-focused leaves (Elekta and Varian) are rounded (non-divergent) while double-focused leaves (Siemens) have flat divergent leaf ends. The rounded leaf ends are designed to reduce a wider penumbra width generated from flat divergent leaf edges. The umbra is the region where doses are below 20% (10%) of the maximum dose. These low dose regions result from radiation transmitted through collimators and scattered radiation from the linear accelerator head shielding.

The off-axis-ratio (OAR) between the dose at an off-axis point, either in the cross-line (x-direction) and in-line (y-direction) directions, and the dose on the central beam axis for any given depth provides a 2D information on the dose distribution inside the phantom. This measurement is performed in QA programs to assess the beam flatness and the beam symmetry, which are relevant also for dose calculations.

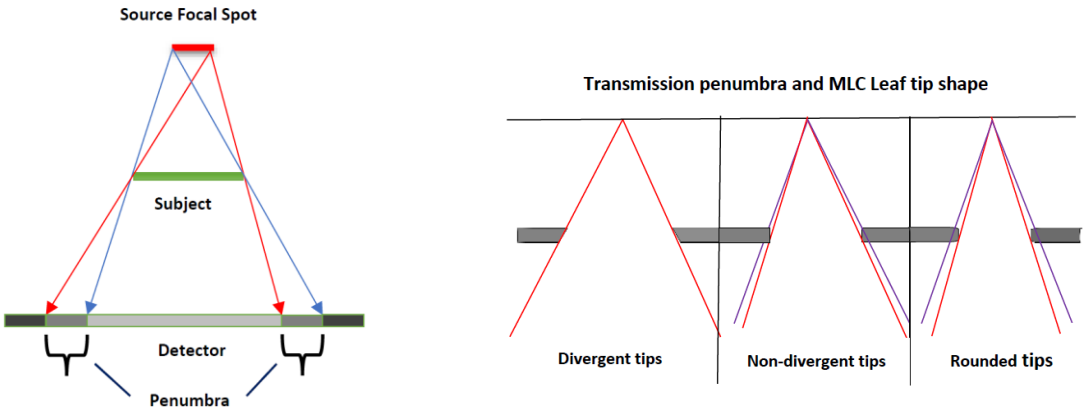

a) b)

Figure 2.2. (a) The penumbra appears as blurring of the field edge and it is directly proportional to the physical size of the source. (b) The penumbra depends also on the MLC tip shape [31].

2.3.3 Dosimetry of photon beams in a patient

Unfortunately, dose calculation in water does not apply to the patient since the patient tissues are not perfectly water equivalent and the patient's surface is not entirely flat. The beam passes inhomogeneities so that high-density tissues (e.g. bone) increase the attenuation whereas low-density tissues (e.g. lung) decrease the attenuation. That is why complex models are needed thus making dose calculation in inhomogeneous media a complicated task. Therefore, dosimetry in water is adequate to characterize the radiation beam but not sufficient to calculate the dose deposited in a patient.

In this subsection, the concept of IMRT treatment planning is further presented, with the emphasis on the role and specific requirements for the dose computation algorithms employed within this scheme.

2.4 IMRT treatment planning

The IMRT approach breaks each beam up into hundreds of tiny constituent-beamlets with an individual fluence level. The resulting IMRT beam has a better resolution than a uniform 3DCRT beam for conforming to the 3D shape of the patient's tumour and avoiding organs at risk (OARs). For example, in IMRT, fluences for certain beamlets that are collinear with critical organs might be set to low or zero values, while other beamlets collinear with the tumour can be set to high values.

Although IMRT has many advantages over the 3DCRT approach, it also complicates treatment planning. Whereas 3DCRT requires the assignment of only a few fluences (one for each beam), IMRT requires thousands (one for each beamlet). The considerable task of planning the IMRT beamlet fluences, such that a desirable treatment is achieved, necessitates extensive use of optimization formulations and techniques.

This task requires the use of computerized planning systems with advanced calculation algorithms. The treatment planning for IMRT means the procedure of determining the physically deliverable fluence patterns that deliver the dose distribution that most closely matches the required one.

The challenge in creating IMRT treatment plans is to determine the fluence modulation for each beam, as the number of free parameters is enormous. The solution to avoid the cumbersome and time-consuming manual treatment plan creation is the algorithmic optimization of the fluence patterns. This so-called inverse planning [32] simplifies the manual iterative decision-making process described above. In inverse planning, the one derives organ dose constraints from the clinical requirements. A fluence map optimization (FMO) algorithm then tries to find the fluence map that matches these requirements best. To take account for the finite width of the MLC leaf's and to reduce algorithmic complexity, the two-dimensional fluence map of each beam is discretized into small quadratic sub-beams - beamlets (illustrated in Figure 2.3).

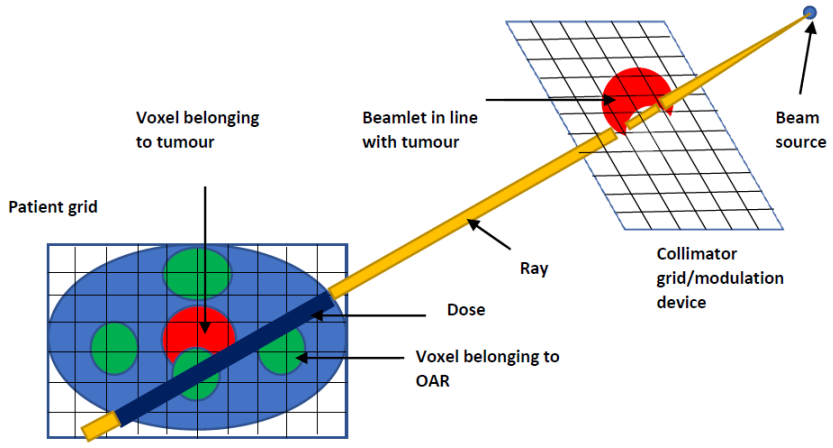

Figure 2.3. Ionising radiation originates from the beam source point and falls onto a collimator. It allows shaping the beam in different forms and fluences and is discretised in beamlets. The longer a beamlet is "open", the higher the fluence through that beamlet, and the higher the resulting dose in the patient. As soon as the pencil-beam enters the patient, the ionising radiation interacts with the tissue, leading to dose. The patient is discretised in voxels.

2.4.1 IMRT delivery techniques

The most widespread method of beam modulation is performed with a computer-driven MLC. Before the advent of MLC, many researchers and investigators of IMRT in the late 1980s/early 1990s assumed that many more than 10 beams were required to simulate a rotational treatment. In another research [33] it was realised that less than 10 radiation fields were often enough to provide clinically acceptable dose conformity and OAR sparing and therefore his work paved the way for motor-driven MLCs to be practically implemented in IMRT.

The MLC enables a more sophisticated use, resulting in beam modulation. The field shape formed by the collimator may be assigned to a fraction of the total prescribed number of monitor units (MUs), thus subjecting any given point in the patient to irradiation for a certain time.

In various implementations of this method, the MLC leaves may move continuously during the irradiation or the beam may be interrupted for the time necessary to change the field shape [34-35]. The first method, referred to as *dynamic MLC delivery* (dMLC) can be realized in two ways: either a variable opening formed by each pair of opposing leaves is swept at changing speed across the irradiation field or the opening formed by the leaves shrinks around the unimodal regions of the fluence modulated field (close-in technique). The leaf motion is under the control of a computer that also monitors the leaf positions. The concept is illustrated in Figure 2.4.

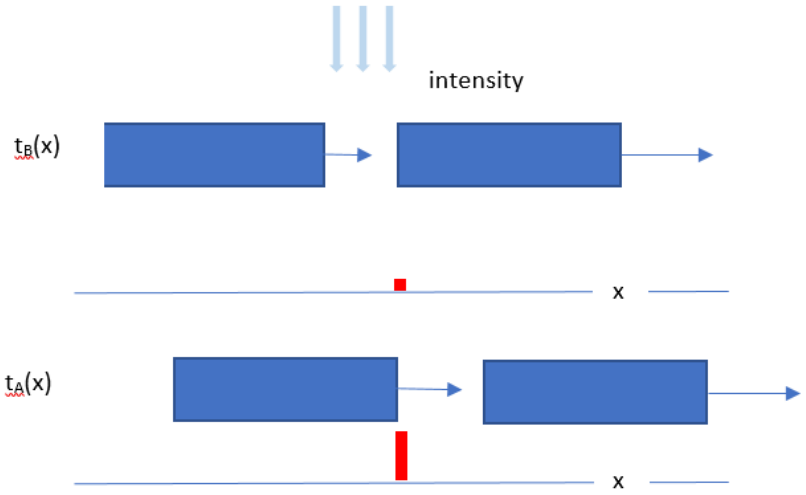

Figure 2.4. Simplified illustration of fluence builds up at just one-point x indicated with the height of the thin red bar. The upper row shows the moment $t_B(x)$ when the leading leaf has just crossed the point x and radiation can reach the point indicated with a tiny red bar. In the moment $t_A(x)$ the trailing leaf reaches point x and irradiation stops. Different velocities of the leading and trailing leaf can shape different shapes and slopes of the fluence profile.

The 1D fluence profile with one pair of MLC leaves is formed with the independent motion of two leaves. Multiple parallel pairs of MLC leaves may then create arbitrary two-dimensional fluence maps. It is assumed that beam output is constant and there is no transmission through the leaves, and the influence of penumbra or scattering is neglected. If the unidirectional sweeping of leaves is considered, the fluence at any point x is proportional to the difference between the time $t_B(x)$ when the leaf edge of the right, leading leaf (B) crosses that point x and starts the irradiation, and time $t_A(x)$ when the left, trailing leaf (A) crosses that same point and stops the irradiation. Therefore, the leaf motion trajectories must be designed such that $t_A(x) - t_B(x)$ equals the desired treatment time, i.e., the desired fluence rate at every point x. There are many possible trajectories that fulfil this constraint. The most desirable is the one that delivers the fluence profile in the shortest time.

An optimization problem with this objective and the above-mentioned constraint on $t_A(x) - t_B(x)$, plus a constraint on the maximum leaf speed was formulated and solved with a linear programming approach [36].

At the beginning of the development of dIMRT, the major concern was the safety of the delivery, i.e., how reliable computer control of the accurate leaf movement can be achieved. The other concern was related to the delivery of a high number of monitor units and respective transmission dose contribution.

In the second approach called *segmented MLC* delivery (sMLC) or *step-and-shoot* delivery, a series of MLC shapes (segments, subfields) is applied with a defined number of MUs assigned to each of them, producing a stair-stepped approximation of the required fluence map.

Figure 2.5 shows the differences between the MLC leaf motion as well as the photon fluence between the step-and-shoot and dynamic IMRT deliveries. The leaf position and corresponding photon fluence at a measurement point are discrete in the step-and-shoot IMRT delivery, while they are continuous in the dynamic IMRT delivery [1].

MLC leaf shape design, different between the linear accelerator vendors is important from the point of view of the dose delivery, QA and dose computation [35]. The leaves have various widths allowing different levels of conformity, different heights assuring the required level of attenuation, rounded or straight ends, can be focused or double focused, and have different shapes of the side walls (so-called tongue and groove arrangement) reducing the interleaf leakage. The 'tongue-and-groove' effect may become a significant issue for achieving dose distributions better conformed to tumour targets, and refers to an underdose that occurs in a junction region between neighbouring leaves if the tongue on one leaf extends beyond its neighbour's groove and later the situation is reversed with the groove extending beyond the tongue.

In one study [37], a maximum dose difference of 5.4% was found between calculations with and without MLC leakage. When the effects of MLC tongue-and-groove effects were evaluated in the same study, a maximum of 5.1% difference was found [37].

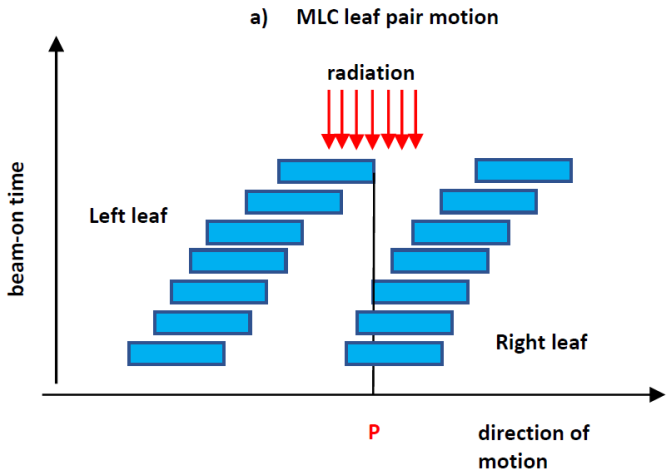

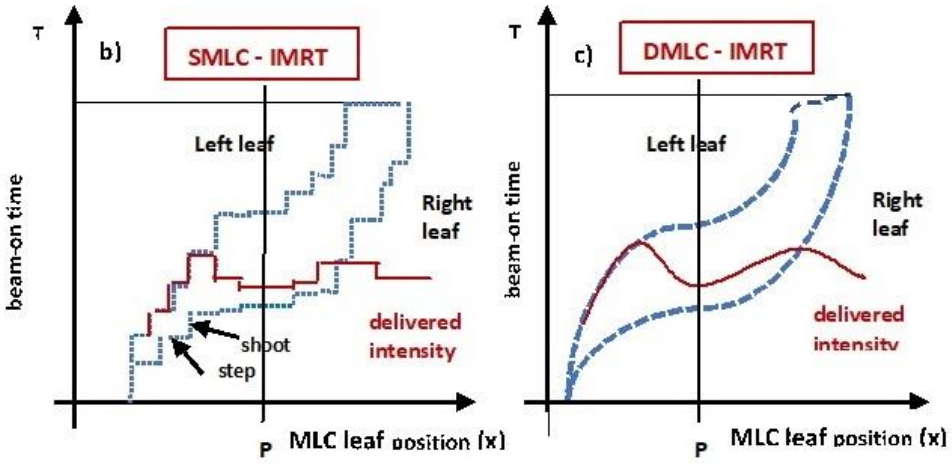

Figure 2.5. (a) Example of MLC leaf pair motion as a function of the beam-on time. The MLC leaf path and the corresponding photon fluence rate at point P defined in figure (a) as a function of the beam-on time: (b) step-and-shoot IMRT and (c) dynamic IMRT.

2.4.2 IMRT verification

One of the crucial issues in the process of radiotherapy is the equivalence between treatment planning and the actual delivery of the treatment. Advanced radiotherapy techniques, such as IMRT, require extensive verification measurements to ensure that treatments are delivered correctly [38].

Differences between the planned (*evaluated, calculated*) dose and delivered (*reference, measured*) dose by the linear accelerator may arise from inaccuracies in the treatment planning systems (TPS) dose calculation algorithm or from an error in IMRT treatment delivery.

The "black-box" nature of IMRT planning has caused the medical physics and radiation oncology communities to place emphasis on pre-treatment verification through dosimetric measurements. The European Society for Therapeutic Radiology and Oncology (ESTRO) state in their Guidelines for the Verification of IMRT that,

> *...patient specific verification was required for IMRT and each plan should be checked prior to delivery. This was different from the conventional approach where checks are generally performed during the commissioning process of a new TPS (treatment planning system) or before the implementation of a new technique...*

These recommendations should not be ignored. An excessive dose of radiation leads to radiation necrosis of healthy tissues, whilst an inadequate dose would fail to kill the cancer

cells, in the time leading to recurrence of the tumour. The importance of accurate and precise dosimetry and radiotherapy treatment planning therefore cannot be overemphasised.

IMRT dose distributions are characterised by numerous steep dose gradients to conform as tightly as possible to the target volume whilst minimising the dose to normal tissue. Conventional 3DCRT treatments are composed of relatively large uniform beams and therefore patient specific QA consists of simple independent dose and monitor unit verification calculations which are supplemented by routine machine-specific QA (e.g. output constancy, energy, beam flatness and symmetry etc.). In IMRT, the complex MLC pattern means that an independent dose calculation alone is not sufficient as these methods estimate a point dose. In IMRT, the dose at any point is delivered by a fraction of the total modulated field. The MLC pattern varies from patient to patient and the number of MUs is heavily linked to the complexity of this pattern. Therefore, it is necessary to perform a patient specific QA measurement to verify the fluence from the IMRT beams to ensure the suitability of the MLC pattern.

Conventional dosimetric methods such as using ionization chamber, diode or thermoluminescent dosimeter (TLD), have limitations for IMRT verification in that they are only able to provide a point by point sampling and so do not comprehensively sample what may be complex distributions with steep dose gradients impacting on both the tumour volume and OAR. Traditional radiographic film dosimetry, which provides very high resolution in 2D, is no longer an option for most centres, with film processors becoming obsolete as radiotherapy centres turn to digital picture archiving and communication systems (PACS).

In recent years, various commercial 2D and 3D ionization chamber or diode detector arrays have become available [39]. These electronic devices have allowed for verification of absolute dose in 2D or 3D with near real-time results. This allows for analysis to be performed in the IMRT QA measurement session and therefore out of tolerance results can be investigated immediately. Conventional methods such as ionization chamber point dose measurements and film dosimetry are gradually being replaced by detector arrays. More details on IMRT verification are given in the next Chapter.

Chapter 3
DOSE DISTRIBUTION COMPARISONS AND EVALUATIONS

3.1 Introduction

The first clinical results obtained with IMRT were published in the mid-nineties of the past century [40, 41]. At about the same time, the description of commissioning and QA programmes of such systems were also published [42, 43].

IMRT techniques (described in Chapter 1) use complex treatment fields that may have a different level of modulation. The dose distribution realised by IMRT have typically more heterogeneous dose distribution than those of 3DCRT, and accordingly, dose delivery becomes more complicated. Unfortunately, this complexity leads to additional sources of errors, so end-to-end patient management is prone to uncertainty.

Continuous and intensive research is ongoing in developing tools and QA methods that can be adapted to new advanced devices and techniques. The necessity for more comprehensive QA programs for the new techniques has been presented in several publications, guidance, recommendations, and reports [14], [44-47].

Patient specific QA of 3DCRT treatments, composed of relatively large uniform beams, comprised simple independent dose and monitor unit verification calculations. In IMRT the patient specific means verification of the fluence from the IMRT beams that may vary considerably from patient to patient, to ensure the suitability of the MLC pattern.

Since the commencement of IMRT, procedures for the delivery system and patient specific IMRT plan QA have emerged based on direct measurement of radiation dose distribution in a phantom [48, 49] or indirect methods that compare the TPS calculation with an independent computer calculation [50, 51]. Both verification methods require a comparison tool to quantify the difference between the two dose distributions. IMRT QA verification is an important process used to check the accuracy of IMRT plan dose calculations and to detect clinically relevant errors in the radiation delivery, thereby ensuring safe patient treatments.

Different approaches have been introduced to qualitatively and quantitatively compare the dose distributions, such as the point-to-point dose difference or the evaluation of the distance between two close points having the same dose value [47]. As progress, radiochromic films and

2D arrays of ionization chambers or diodes have been introduced within tissue-equivalent uniform or anthropomorphic phantoms. Recently, commercial devices embedding a detector configuration for 3D volumetric dosimetry have also been adopted. However, these devices rely on interpolation and extrapolation algorithms from several 2D projections to ensure a 3D dose distribution.

3D chemical dosimeters, such as polymer gel dosimeters and radiochromic 3D detectors [44] are the only dosimeters that actually measure full 3D dose distributions. Their properties and use are out of the scope of this work and therefore not further discussed.

This chapter presents the essential dose distribution comparison tools and metrics, provides an overview of research in developments of their use, and briefly reviews patient specific pre-treatment measurement methods and relevant clinical results when dose distribution comparison tools are used.

3.2 Dosimeters and phantoms for dose distribution comparisons

Due to the complexity of the IMRT technique, dosimetric verification of patient specific IMRT absorbed dose distributions has become necessary. A QA process for IMRT plans is typically carried out through verification of the two-dimensional (2D) isodose distributions.

In IMRT dose verifications, the fluences optimized in a patient geometry are usually applied to a CT scanned phantom geometry made of water-equivalent plastic. A measured absorbed dose distribution is a distribution measured in 2D or 3D for example with an ionization chamber or diode detector arrays, electronic portal imaging device (EPID), radiochromic film or gel. The absorbed dose is recalculated in the phantom geometry and comparison between the measured and calculated phantom dose is performed. Measurements of the IMRT dose distributions and the spatial locations of the dose gradients are critical to the safe implementation of IMRT. The use of IMRT leads to complex dose distributions with steep dose gradients within the target volumes. Consequently, the measurements are challenging due to the absence of a charged particle equilibrium, positioning problems of the detector, spatial resolution of a commercial detector and the effects of the detector size.

Dose verification based on measurements can be performed with a broad variety of detectors. Simple point measurements are insufficient for dose verification of complex dose depositions with high dose gradients such as in IMRT.

2D dosimeters are required to verify the dose distributions of IMRT since they measure the dose in a plane. The most widely utilized 2D dosimeters are radiographic or recently the radiochromic films. Radiochromic films [14], have a high spatial resolution of at least 0.1 mm, they are near tissue equivalent and have a low energy dependency. The films can be inserted in solid and water phantoms, which make them practical in IMRT dose verifications. The problem of film measurements is the measurement noise, which is greater than with the other dosimetry techniques used in radiotherapy dose measurements. The scanning and analysing of the irradiated films are time-consuming and there might be variations in film sensitivity caused by a film batch and due to film scanning artifacts [14].

The two most common 2D detector types available and used for fluence or absorbed dose measurements are the electronic portal imaging device (EPID) and 2D detector arrays composed of a large number of ionization chambers or diodes.

The most common EPID detector consists of an x-ray converter (scintillating screen) that produces light photons when hit by x-rays, followed by detection of these photons in an amorphous silicon plate. The emitted light can then be used to estimate fluence. EPIDs were originally designed as a position verification device, but extensive research has led to the development of sophisticated fluence modelling based on EPID dosimetry [44], [52]. A major advantage of an EPID detector is that it has a high resolution and is incorporated within the treatment machine behind the patient allowing the fluence measurement during patient treatment. However, the disadvantage is that differences in the expected and measured response of the detector can come from either the treatment machine, the patient geometry, or both.

In recent years, various commercial 2D and 3D ionization chamber or diode detector arrays have become available. These electronic devices have allowed for verification of absolute dose in 2D or 3D with near real-time results. This allows for analysis to be performed in the IMRT QA measurement session and therefore out of tolerance results can be investigated immediately. 2D detector arrays or matrixes use multiple point detectors to measure the dose distribution. Hundreds of point detectors, either ionization chambers or diodes, are aligned usually in one plane and in simple geometry. Multiple cumulative readings are taken during the IMRT delivery verification and the results are available instantly after the dose delivery. The detector centre to centre distance of the 2D-arrays is usually between 5 to 10 mm. The spatial resolution is consequently much lower than with the films or EPID dosimeters.

These detector arrays are used to perform patient specific pre-treatment IMRT verification. In all methods currently in clinical practice, the patient's calculated treatment plan is recomputed onto a phantom that exists as an object in TPS. This forms a hybrid plan.

Tools that enable us to directly measure the dose distributions in three-dimensional (3D) space are not commonly available. One such 3D dose measurement device is individually fabricated chemical gel dosimeters. They are made of a continuous uniform medium which polymerizes upon irradiation. Therefore, the intrinsic spatial resolution of those dosimeters is very high, and it is only limited by the method by which one converts the dose information recorded by the medium to the absorbed dose. High-resolution 3D maps can be obtained by magnetic resonance (MR) scanning, optical-CT scanning, or x-ray CT. The gel dosimeters eventually lose the recorded dose distribution with time, as in the case of liquid Fricke dosimeter, so imaging must be performed within about two hours of irradiation to avoid serious degradation of the dosimetric detail [14].

3.3 Absolute dose verification

With a simple phantom and an ionization chamber, the absolute point dose (1D) measurement can be conducted for patient specific treatment plan verification. A point dose measurement is a small volume averaged measurement; the smaller the volume the better the approximation of a point dose measurement. Too small volumes may however lead to inaccurate dose estimation if an error in ionization chamber positioning is done, particularly if it happens in a high dose gradient region. The measured dose should ideally be compared to a planned volume dose, not to the point dose at the centre of a chamber volume observed in the QA irradiation plan. This type of measurement cannot be effectively used to properly validate the treatment plan's accuracy.

In 2D dose measurements, the ionization chamber, or diode arrays, films or electronic portal imaging devices (EPID) can be used. The most common application is to measure the 2D dose distribution obtained by IMRT. The relative dose measured is compared with a QA plan. 2D detector arrays are used for single field measurements and if arrays are inserted into some slab phantoms, they can be used for rotational IMRT QA.

In the film (e.g. EBT2, EBT3 radiochromic film) based dosimetry, attention should be paid to consistent characterisation of each film batch in terms of dose-response, uniformity, and sensitivity. The advantages of films in terms of high spatial resolution are counterbalanced with

the difficulties in accurate dose determination in points and uncertainties arising from densitometry.

The 3D dose measurements involve the use of 3D gels, polyacrylamide and Fricke gels, and radiochromic plastics, such as PRESSAGE dosimeters [53, 54]. These dosimeters are used effectively in true composite measurement techniques in IMRT/VMAT dose delivery procedure. The basis of gel dosimeters is radiation-induced polymerisation of monomers; small monomers join and below saturation, regions of gel exposed to radiation exhibit polymerisation in proportion to the absorbed dose.

3.4 Dose distributions comparison techniques and metrics

A comparison of dose distributions can be done using several different methods. Dose distributions are usually represented as arrays of points, each defined by a location, $\vec{r}$, and the dose value, D.

In further discussions of the dose comparison techniques, it will be assumed that there are two dose distributions that might have been determined in one (1D), two (2D) or three (3D) dimensions, termed a *reference* (e.g. measured) and an *evaluated* (e.g. calculated) dose distribution [19]. The reference distribution is typically the one against which the evaluated distribution is being compared. There are situations in which the roles of the evaluated and reference dose distributions are reversed. In further text it will be shown that some of the comparison techniques are invariant with respect to the selection of the *reference* and *evaluated* dose distribution and some are not.

When practical in the thesis, the general terms, reference and evaluated dose distribution will be replaced with the actual, measured and calculated.

The goal of dose comparison as part of a clinical workflow is to determine if the reference and evaluated dose distributions agree to within certain limits that are clinically relevant. This question of clinical relevance involves more than the dose itself; it also involves the dose gradients as well as dose errors resulting from spatial uncertainties. Therefore, it is essential to understand both the spatial and dosimetric uncertainties when conducting dose distribution comparisons.

In this section the dose difference, the distance-to-agreement, composite evaluation method and the gamma evaluation methods will be presented.

3.4.1 Dose difference method

If the evaluated dose at the point $\vec{r}$ is equal to $D_e(\vec{r})$ and the reference dose at the same point equals to $D_r(\vec{r})$ the (normalised) dose difference at r is equal to:

$$\delta(\vec{r}\,) = \frac{D_e(\vec{r}) - D_r(\vec{r})}{D_r(\vec{r})} \tag{3.1}$$

Dose distributions can be directly compared by the dose-difference test with an acceptance criterion often defined as a percentage of the dose. Direct comparison is straightforward if the resolution of grids for both distributions are the same. If not, interpolation is needed.

The drawback of the dose difference method resides in its high sensitivity to steep dose gradients, where small spatial shifts can lead to high dose differences between the evaluated and reference distributions, without having a clinical significance [55]. The high dose difference may or may not be of clinical significance depending on the location in the patient anatomy. This dilemma prevents the use of a single threshold value to accept or reject the result. Besides, as the dimensionality of dose distribution increases (2D, 3D, 4D), the interpretation of results in the presence of local dose gradients become more complex. To cope with these complications, different approaches have been introduced to compare the dose distributions both qualitatively and quantitatively.

3.4.2 Distance-to-agreement

The concept of a distance-to-agreement (DTA) was introduced to take the spatial discrepancy between two distributions into account [55]. The distance-to-agreement for a given point, $\vec{r}_r$, in the reference dose distribution is specified as the minimal spatial distance of that point to a point, $\vec{r}_e$, in the evaluated distribution where the dose is the same as in the reference distribution.

$$DTA(\vec{r}_r) = min\{|\vec{r}_e - \vec{r}_r|\}\,\forall\{\vec{r}_e\} \tag{3.2}$$

Unlike the dose difference method, this method requires a search in the evaluated dose distribution to identify the closest distance to the point in the *reference* distribution that has the same dose as that point, which is equivalent to finding the closest distance of the *evaluated* distribution isodose line.

DTA is a useful complement to dose difference measurements, especially when it comes to high dose gradient regions. However, as a comparison between dose distributions, it becomes excessively sensitive in low-dose gradient regions, where even a small dose difference causes the relevant isodose line to move far from the reference point. Because of this reason, and

because most dose distributions are dominated by low-dose gradient regions, DTA distributions are difficult to interpret and by themselves not very useful.

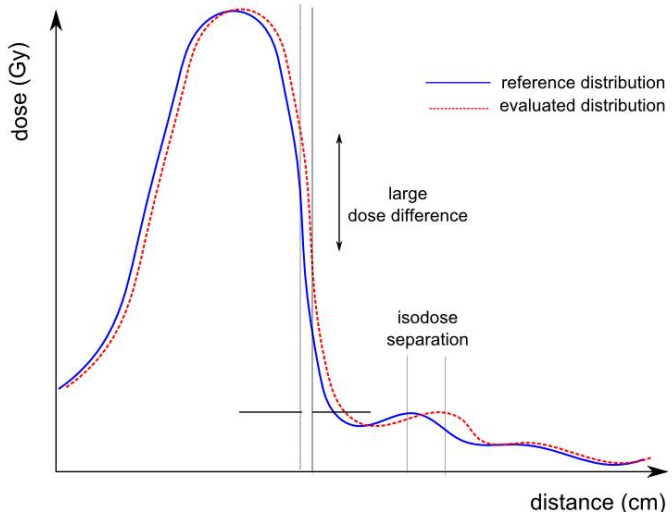

Figure 3.1. Illustration of the dose difference and DTA. Note the large dose difference for two spatially close points in the high-dose gradient region and large DTA in low dose, low-dose gradient region.

It is meaningful to specify DTA for the high-dose gradient region and the dose difference test for the low-dose gradient region [56]. Hence, when used simultaneously, DTA and the dose difference test are complementary to each other in the high-dose gradient and low-dose gradient region, respectively.

A value for the maximum accepted spatial difference, referred to as the DTA criterion, Δr, is often set between 2 to 5 mm. This limit corresponds to the tolerance for misalignment or rotation of the phantom at irradiation.

3.4.3 Composite evaluation method

Considering the dose difference and DTA methods were complementary in their sensitivity to low and steep dose gradient regions, respectively, a composite of these two measures, which shows only regions that fail both criteria, was introduced [56]. The spatial distance between the reference and evaluated dose points is denoted by:

$$r(\vec{r_r}, \vec{r_e}) = [\vec{r_e} - \vec{r_r}] \tag{3.3}$$

and the dose difference between the reference and evaluated point by the expression:

$$\delta(\vec{r_r}, \vec{r_e}) = [D_e(\vec{r_e}) - D_r(\vec{r_r})] \tag{3.4}$$

where $\vec{r_r}$ is the radius vector of the reference point and $\vec{r_e}$ denotes the radius vector of the evaluated point, $D_r(\vec{r_r})$ and $D_e(\vec{r_e})$ are the dose distributions in the reference and evaluated

dose distributions. The composite distribution c ($\vec{r}_r$) is a binary distribution formed by the points that fail both the dose difference and DTA criteria, ΔD and Δr:

$$c(\vec{r}_r) = \delta_f(\vec{r}_r) \cdot r_f(\vec{r}_r) \tag{3.5}$$

$$\delta_f(\vec{r}_r) = \begin{cases} 0 & |\delta(\vec{r}_r)| \leq \Delta D \\ 1 & |\delta(\vec{r}_r)| > \Delta D \end{cases} \tag{3.6}$$

$$r_f(\vec{r}_r) = \begin{cases} 0 & |DTA(\vec{r}_r)| \leq \Delta r \\ 1 & |DTA(\vec{r}_r)| > \Delta r \end{cases} \tag{3.7}$$

In short, two binary distributions are multiplied point by point to form another binary distribution, indicating agreement within the predefined limits or failure. In high-dose gradient regions, the dose difference distribution yields large values for small spatial offsets between the compared dose distributions. The DTA analysis returns the approximate spatial difference between the two distributions. While the composite method automatically manages both steep and low-dose gradient regions, it suffers from being strictly a pass-fail test. If a point fails, the test does not indicate how much it fails.

3.4.4 Gamma evaluation

The composite evaluation method suffers from being just a pass or fail test. It does not provide the magnitude of the failure. Low [19] generalised of the composite method by combining the dose difference and distance difference to a dimensionless metric. This is known as a γ-index.

In the case of a 2D dose distribution, which we consider for simplicity even though it can be generalized to a higher dimension, the acceptance criteria that simultaneously consider the dose difference and DTA outline an ellipsoidal surface. It can be represented by the equation:

$$\sqrt{\frac{\mathrm{r}(\vec{\mathrm{r}}_\mathrm{r},\vec{\mathrm{r}}_\mathrm{e})^2}{\Delta \mathrm{r}^2} + \frac{\delta(\vec{\mathrm{r}}_\mathrm{r},\vec{\mathrm{r}}_\mathrm{e})^2}{\Delta \mathrm{D}^2}} = 1 \tag{3.8}$$

where $\vec{r}$ represents the radius vector of any point, $\vec{r}_r$, $\vec{r}_e$ are the radius vectors of the reference and evaluated dose points, r and δ are defined by the expressions Eq. (3.3) and Eq. (3.4).

For each point in the evaluated dose distribution, the generalised Γ function (Figure 3.2) can be calculated according to the following equation:

$$\Gamma(\vec{r_r}, \vec{r_e}) = \sqrt{\frac{r(\vec{r_r},\vec{r_e})^2}{\Delta r^2} + \frac{\delta(\vec{r_r},\vec{r_e})^2}{\Delta D^2}} \tag{3.9}$$

where Δr and ΔD are the DTA and dose difference criteria. Finally, the γ-index is the minimum value calculated over all evaluated points:

$$\gamma(\vec{r_r}) = \min\{\Gamma(\vec{r_r}, \vec{r_e})\} \forall \{\vec{r_e}\} \tag{3.10}$$

The summary of symbols and expressions used to describe the gamma function is given in Appendix B.

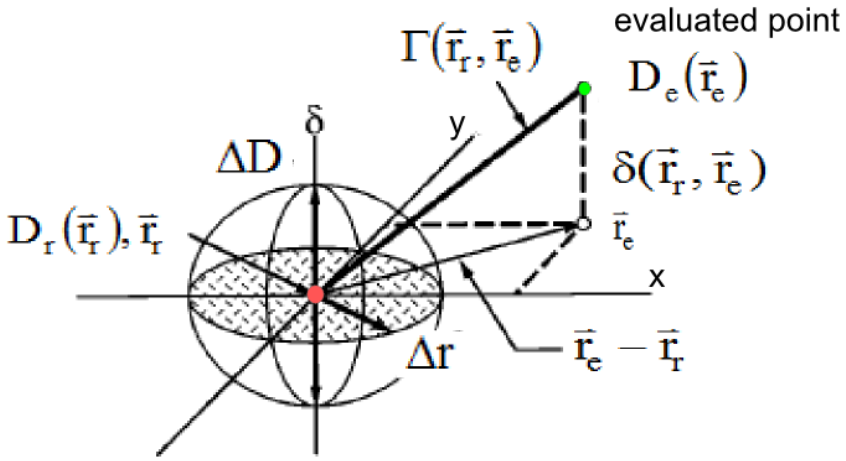

Figure 3.2. Geometric representation of a combined gamma criterion for dose difference and DTA for a 2D dose distribution [19]. The axes x and y represent the spatial plane and the axis δ represents the difference in dose between the evaluated and the reference position.

The dose values and spatial coordinates can be considered as the coordinates of the hyperspace (n+1 dimensions) in which there are, for instance, n=1, 2, or 3 spatial coordinates and 1 dose coordinate. Throughout this document this nomenclature will be used and where appropriate adjusted to the specific dimension under consideration.

A set of γ-index values for all reference dose distribution points can be constructed and the percentage of points passing the test with $\gamma < 1$ is generally reported. This is called the γ-index *passing rate*. The γ-index calculation is usually limited to points that are above 10-20% of the maximum dose value within the dose distribution. This is done to exclude from the analysis out of radiation field regions where a relative dose difference can be calculated and worsen the passing rate without proper justification.

The γ-index values can be calculated following a *local* or *global* normalisation. A local γ-index, Eq. (3.1) defines a local dose difference; the difference is normalised to the e.g. reference dose at the local point. This permits the same relative tolerances in target volumes and critical structures. For global γ-index, the denominator of the Eq. (3.1) is replaced by the D_{norm} which is usually the maximum dose within the reference dose distribution, a point or small region selected in a high-dose and low-dose gradient region. The prescription dose can also be used.

So, in this type of normalisation the difference between any evaluated and reference dose pair is normalised using the same value for all points.

The local γ-index shows failures in high-dose gradient regions and in low-dose regions, whereas the global γ-index will tend to mask these errors but show the errors within the higher dose regions of the dose distribution.

The advantage of local normalisation is that the same relative tolerances are applied to the target volume and critical structure volumes. However, this approach may lead to too strict dose accuracy requirements in regions of low dose; a tiny dose difference normalised to a low local dose easily exceeds the tolerance.

The DTA should ideally be a function of the clinical requirement of placing steep dose gradients; the DTA criterion for critical structures should be different from the criterion for other structures.

Two more helpful dose distribution comparison tools are the gamma histogram and gamma angle. In analogy with the dose-volume histograms (DVH), an indispensable tool in evaluating clinical acceptability of calculated dose distribution, the gamma histograms were proposed [57]. They indicate the percentage of area or volume that is covered by a certain γ-index value. The gamma histograms could be frequency (differential) gamma area/volume histograms, or cumulative (integral) gamma volume histograms. The gamma area histograms can be constructed if the two-dimensional, detector array or films, are used to acquire the dosimetric data.

Another helpful parameter for interpreting the gamma distributions is a gamma angle. The concept is depicted in Figure 3.3.

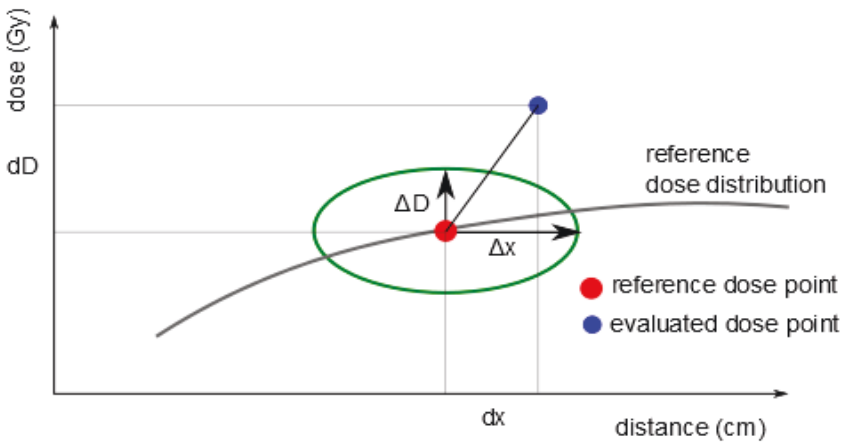

Figure 3.3. Gamma angle definition.

If our consideration of a generalized γ-index method is reduced to just two dimensions denoted with a coordinate x and another coordinate as the dose D, the gamma angle between the dose axis and the vector (gamma (γ) vector) pointing from the reference dose point to the evaluated dose point is given by:

$$\gamma_{angle} = arctg\left(\frac{dx/\Delta x}{dD/\Delta D}\right) \tag{3.11}$$

where dx stands for the spatial difference between the evaluated and reference dose point, dD is their dose difference and Δx and ΔD are spatial (DTA) and dose difference criteria, respectively.

If the discrepancy between the reference and evaluated dose is only due to the dose difference, the vector will be parallel to the dose axis, and conversely, if it is parallel to the distance axis x, the discrepancy will be entirely due to the distance. Furthermore, for the gamma angle defined as zero for the vector parallel to the dose axis, all angle values should be between 0 and 90^0 degrees since only the absolute values of the distance and dose differences are considered. By observing the value of the gamma angle, one may conclude if the mismatch between the evaluated and reference dose distribution at a certain point is dominated by the dose or distance discrepancy.

Gamma analyses in clinical situations are typically made between discretized representations of dose distributions often with the reference and evaluation dose data sampled at different spatial resolutions. The importance of the resolution was first analysed in the assessment of the gamma evaluation [58] and they were particularly concerned with overestimations of gamma values caused by large grid spacing in the discrete dose distributions, particularly in regions of a high-dose gradient. The accuracy of the dose distributions comparison depends on interpolation. If we assume that the DTA criterion is 3 mm, which is most commonly used clinically, the voxel size of the dose distribution is 3×3×3 mm^2 and the dose difference is 0 in the gamma calculation, γ-index values are accurate to within 0.333 provided the spacing resolution ratio is 3:1. The approximate rule given by Low et al. [20] is that the spatial resolution of the evaluated dose shall be at least one-third of the DTA criterion, but they made no recommendations regarding the maximum spatial resolution for comparisons for which there is a resolution disparity (e.g. higher resolution film vs. lower resolution TPS dose grid).

More detailed studies [59, 60] concluded that higher spatial resolution of the evaluated dose distribution, of the order of 0.1 times the spatial difference criterion is necessary. The collimator gantry error was introduced into the two arcs of the VMAT head and neck plan, and in the other

case in a prostate treatment plan, a minor gantry sag to the MLC position in the DICOM plan was introduced. The plans without errors were evaluated dose distributions in γ analysis and then a varying level of interpolation was introduced into the data sets through an integral interpolation factor reducing the original pixel spacing from 2.5 mm to 2.5 mm/2, 2.5 mm/4, etc. to prepare distributions for γ analysis. The calculated mean γ-index value clearly showed the sharp change when the ratio of the distance difference criterion to the modified pixel spacing was around 1, and stabilisation when this ratio approached ~10. This was shown for both groups of plans and for the different distance and dose evaluation criteria, confirming the importance of adequate interpolation to achieve accurate γ-index value.

3.5 An overview of the existing research related to the development and the use of the dose comparison tools

An increase in the clinical usage of IMRT and a novel radiation technique, VMAT, which is an advanced form of IMRT, has spurred the development of tools that can quantitatively compare 2D dose distributions. Since the IMRT deliver complex 3D dose distributions, it is essential to use verification techniques that are more comprehensive than, for instance, single-point ionization chamber measurements, to ensure that the actual dose delivered is similar to the calculated absorbed dose distribution.

Traditionally, dose agreement tests have been completed by manually comparing dose differences and more quantitatively way subdivide the area of interest into regions with various dose gradients and apply different acceptance and tolerance criteria [55]. The authors described the large effects of small spatial shifts on observed dose differences for high-dose gradients and introduced the concept of a distance-to-agreement (DTA) based on them. The DTA is defined in section 3.4.2. They suggested to use a fixed-dose criterion for the analysis of low-gradient regions and complementary, perform a DTA-based analysis for high-gradient regions.

However, these concepts cannot be applied easily for the verification of single fluence modulated beams or composite treatment plans where low-dose gradient and high-dose gradient regions can alternate.

The gamma method, as described above in section 3.4.4, combines both the dose difference and DTA criteria by defining a distance in the dose-space domain and an acceptance ellipsoid around each point of the reference dose [19].

Since being introduced, the gamma analysis has been used by investigators to evaluate dose calculation algorithms and compare dosimetry measurements.

In the case of large spacing between the points in the evaluated dose distribution compared to the distance criterion, and where steep dose gradients are present, the evaluated point with the minimum distance to the reference point may not accurately represent the γ-index, rendering an artefact [58]. That is, interpolation as an obvious solution to supress the calculation artifacts from coarsely sampled dose distribution may not ensure faultless report of the acceptability of the dose distribution. As a solution, a filter cascade of multiple levels was designed in this study to speed up the dose comparison. On the first level, the minimum γ-index value is searched for within a limited search distance to reduce the calculation time. If no point is found for which the γ-index value is smaller than unity, the point under investigation is passed onto the next level. Otherwise, the calculation is stopped, and the reference point is accepted. On the second level, the algorithm searches for at least two evaluated points, close to the reference point, for which the dose differences have opposite signs. The compared (evaluated) distribution must intersect the passing criteria region at some point and the reference point should therefore be accepted. The reference points rejected on the second level are moved to the third level where rare points at the outside boundary of the passing criteria region are taken into account. The algorithm was proven successful in the efficient comparison of calculated versus measured IMRT absorbed dose distributions obtained by IMRT.

Another research examined the behaviour of the gamma distribution in the presence of noise and evaluated the influence of pixel spacing [20]. As noted by the authors [20], γ-index can be affected by normally distributed pseudorandom noise in the evaluated and reference distributions. A thorough analysis of the influence of the noise, introduced in the reference and evaluated dose distribution, on the dose difference comparison metrics such as the dose difference, distance-to-agreement, composite dose and γ-index was conducted. For that purpose, a reference dose distribution was calculated from a projection of a 10×10 cm^2, 6 MV energy photon beams incident on a water phantom. A 2D dose distribution was modified in four 45^0 rotated quadrants to create artificial evaluated dose distributions; one of them was left unmodified, another contained the dose shift, the third had a spatial skew and the fourth both, the spatial skew and dose shift.

The γ-index result is not the same if the evaluated and reference dose distribution are interchanged in the comparison process. This is a result of the definition of a γ-index, in which the search for a minimum is done on one dose distribution coordinate and the user determines

over which coordinates the search is performed. If the noise exists in evaluated distribution it will lead to an artificially reduced gamma, since for each reference point in a "smooth" distribution a closer point in a rapidly oscillating evaluated distribution can be found more readily than if the evaluated distribution would be represented by a smoothed evaluated distribution. In another case, if the reference distribution is oscillating (containing noise) the search for the closest distance in evaluated distribution that is smooth will interchangeably result in larger and smaller gamma; effectively smearing the γ-index values. Specifically, γ-index is underestimated (i.e., better agreement) in the presence of noise in the evaluated distribution, while noise in the reference distribution adds noise to γ -index in proportion to the normalized dose noise.

Furthermore, the authors described by simple reasoning, how gamma automatically accounts for the local gradient to select the proper test when comparing the dose distribution. Namely, as the γ-index calculation is the measurement of the distance between the evaluated and reference dose distribution in the re-normalised space, the vector that gives the shortest distance is orthogonal to the evaluated distribution. The orientation of that vector is of a local dose gradient. For steeper dose gradient the vector is more perpendicular to the dose axis (steepest change of the dose as we move from point to point) and more parallel to the spatial axes. For infinite gradient, the gamma vector is perpendicular to the dose axis and measures the DTA. The opposite applies to zero dose gradients.

Some authors [22], [58, 59], [61, 62] have reported weaknesses of the γ-index. One of them is that in regions of a high-dose gradient, the γ-index may erroneously be larger than one (this may happen when dose difference criteria is small and the dose gradient is steep), as an error is reported on a point of the reference dose although it is valid. This false error detection is called a false positive. The second is the necessity to search for the point of the evaluated dose that is the closest to a given reference point. This task can be time-consuming in the case of 3D dose distributions.

Several approaches aimed to improve the simple "trial and error" technique of searching for the minimum gamma distance in an abstract vector space with one or more spatial coordinates and one dose coordinate. One of them is the definition and use of an evaluation factor χ, defined as a ratio of the dose difference to the locally determined acceptance criterion, which in addition to the maximum tolerated dose difference contained also a misalignment error proportional to the local dose gradient [22]. The evaluation factor is described with the following equation:

$$\chi \equiv \frac{D_e(\vec{r}) - D_r(\vec{r})}{\sqrt{\Delta D^2 + \Delta r^2 \cdot \left\|\vec{\nabla} D_r\right\|^2}} \tag{3.12}$$

where Δr and ΔD are the spatial and dose difference criteria, respectively. The nominator is the dose difference between the evaluated and reference dose and the calculation works when both dose distributions have the same array size. The evaluation test χ effectively extends the dose tolerance based on the gradient and the distance limit at that point. Its advantage is that it indicates over- or underdosing. In dose distribution regions where the second order derivative is large, the extended dose limits change rapidly; the χ values near the "shoulder" part of the evaluated distribution may not be calculated accurately. An improvement of the above-mentioned method, fast and reliable, is known as a δ-envelope method.

As presented in section 3.4.4 one useful tool for interpreting γ results is the γ_{angle} [61].The γ_{angle} is defined relative to the dose difference axis and calculated using the absolute dose and spatial differences in order to be always between 0 and π/2. A γ_{angle} value of <π/4 indicates a higher influence of the dose difference criterion, while a γ_{angle} value >π/4 indicates a higher influence of the DTA criterion. The π/4 value indicates an intermediate influence between the dose difference and DTA criteria. The γ_{angle} can be interpreted as a form of 'influence percentage'; for instance, a γ_{angle} value of 18^0 indicates that the gamma value is 20% influenced by the DTA and 80% by the dose difference. In the study by Stock et al. [61] the IMRT absorbed dose distribution were recalculated with unmodified fluence maps in a verification phantom, forming a hybrid plan. The absorbed dose distributions were measured with films and compared to the TPS calculated ones. The γ analysis algorithm and software were developed in-house. Statistical parameters calculated were: average γ value (γ_{mean}), $\gamma_{1\%}$ where 1% of evaluated points have an equal or higher γ value, and $\gamma_{>1}$ that represents the percentage of points that failed the criterion of γ value less than 1. Based on the γ and γ_{angle} evaluation, a three-step decision filter was created to either accept or conditionally accept the hybrid IMRT plan. For instance, plans with simultaneous γ_{mean} value in the range 0-0.5, $\gamma_{>1}$ within the range 0-5%, and $\gamma_{1\%}$ within 0-1.5 were suggested to be accepted. The conditional acceptance having these parameters outside of ranges indicated above, typically included additional analysis of the gamma angle distributions, dose difference maps, profiles, and the leaf step-index (LSI) to quantify the tongue and groove effect. It is essentially a sum of products of monitor units (MUs) of a field segment *j* in a beam *i* and the sum of lengths of a pair of leaf steps.

However, all these methods have not considered space-specific uncertainty information, i.e., single tolerance criterion is applied to all test points even in case dose uncertainty is

significantly different from the point to point. In another study [23], the authors introduced a novel dose uncertainty model. Here, the total dose uncertainty is separated into two components, positional or space-oriented, and non-space-oriented uncertainties. While the first category covers uncertainties caused by spatial displacements and possible mis-registrations of dose distributions under the comparison, the second category may, for instance, include different dosimetry uncertainties such as uncertainties related to dosimetric input data to TPS. The model assumes that these two types of uncertainties are normally distributed and uncorrelated, or precisely, that the contribution of the positional displacement to the non-spatial dose uncertainty is negligible.

In the revised dose uncertainty model, authors have demonstrated that the dose uncertainty can be a priori predicted during radiotherapy treatment planning [24]. They categorized the dose uncertainties into planning and delivery uncertainty and a convolution method was applied to account for spatial displacements during irradiation. They have shown that there is a strong linear relationship between the dose uncertainty and the dose difference of the QA measurements.

Another research proposed a reinterpretation of the γ-index to avoid the need to interpolate the evaluated distribution to a finer grid, thus reducing the calculation time [62]. This was carried out by subdividing the evaluated distribution into line segments, triangles, and tetrahedral for one, two, and three–dimensional (3D) dose distribution, respectively. The closest distance between any reference point and these simplexes is calculated using matrix multiplication and inversion. The main finding reported in this paper is that this method is as accurate as 16 times finer linear interpolation of the evaluated dose distribution with an order of ~20 times speedup in calculation time.

In a fast calculation algorithm [59] of a γ-index, the evaluated and reference dose distribution under comparison were first resampled on the same uniform grid, not necessarily the same for all dimensions. For each reference point, the γ-index was calculated by searching through the evaluated distribution; the search was seeded at the point defined with the radius vector $\vec{r}_r$ that corresponds to the evaluated dose point determined with the same vector $\vec{r}_e=\vec{r}_r$. The search was limited to the sphere defined by the maximum search radius. The dose values at those points were interpolated "on the fly" at a chosen sample size. When the search distance around each reference point is set, all distances between a reference dose point and evaluated points bound by the search distance can be calculated either for the 2D or 3D dose arrays. Due to the identical grid, the interpolation factors depend only on the spatial location of the interpolation point of

interest and are independent of the reference point. Additional speed of the algorithm was gained by avoiding calculation of the γ-index for those points that did not have a chance to have a smaller γ-index than the one found so far; if for a certain point the spatial part ($r^2(r_e,r_r)/\Delta r^2$) of the testing criterion became larger than the current minimum gamma, the search was stopped.

In an attempt to speed up the computationally expensive process of calculating gamma values, a fast Euclidean distance transform (EDT) to obtain a table of gamma indices evaluated over a range of the spatial-dose space was used [63]. The authors redefined relation between the γ-index and EDT. The distance transform of the binary image finds for every point in the image its distance from the set of feature points. The reference distribution was regarded as a set of feature points in the (k+1)D space and the γ-index becomes the EDT over the range of the (k+1)D space where the Euclidian distance for any two points (x,d) and (y,D) where x and d denote the reference point position and dose, and y and D are evaluated (test) position and dose value. The proposal was successfully tested in 1D and 2D dose distribution cases with a calculation speedup of about 100 times for a 2D test dose distribution. The predicted speedup was of the order of tens of thousands for 3D γ-index calculations.

In their work [64], the accuracy of the geometric technique proposed by Ju et al. [62] was combined with the efficiency of the pre-sorting technique [59] into the modified γ-index calculation algorithm. A sorted table of the normalized geometric distance of all the pixels/voxels in the maximum search range is calculated and the search range is defined based on the radius defined as a quotient of the dose difference and dose difference criterion multiplied by the distance-to-agreement criterion to avoid overestimation of the calculated γ-index. The algorithm is implemented using a graphical processing unit (GPU) composed of many processing cores instead of a standard central processing unit (CPU) calculation. Using GPU provides a parallel calculation for a large number of reference dose points using multiple threads. A calculation time reduction of 45–70 times compared to CPU calculations of the γ-index was achieved.

Another dose comparison parameter proposed was the normalised agreement test (NAT) [65]. It is based on a calculated array of NAT values derived from a comparison of the reference and evaluated dose distribution. The prerequisite for employing this parameter is that the two dose distributions are co-registered and that the local dose differences and spatial DTA distances are calculated for all points. If the percent dose difference is less than ΔD the NAT is equal to zero. If not, the check is made if the contour distance is less than Δr, the spatial tolerance criteria. If

the answer is positive, the NAT equals zero. The algorithm next checks if the evaluated percent dose is less than 75% of the maximum computed dose. The NAT value is again zero if the reference dose is higher than the evaluated in areas out of the PTV; the discrepancy is considered as having no negative biological impact. Otherwise, the NAT value is calculated as $NAT=D_{scale}(\delta-1)$, where δ is lesser value of $|\delta(\vec{r_e}, \vec{r_r})/\Delta D|$ or $|r(\vec{r_e}, \vec{r_r})/\Delta r|$. D_{scale} is the larger value between the normalised evaluated and normalised reference dose at the point of interest. The NAT value represents the percentage deviation of the chosen tolerance criteria scaled by the evaluated dose at that point.

An approach that consists of solving a set of coupled differential equations defining the reformulated γ-index to an arbitrary order has been described and evaluated in relevant clinical test cases [66]. The fraction of gamma values less or equal than 1 within the region of interest was calculated in test cases and small differences of about 1% were obtained when using linear interpolation and spline interpolation. First and semi-second-order numerical methods were also accurate within 1%. The best method found by the authors for the dose distributions that may have large second derivatives was the first-order iteration numerical method.

The standard γ-index analysis was modified by introducing uncertainties into computation in such a way that they can be directly propagated [26]. In developing the new methodology, it was assumed that the reference and evaluated dose distributions (2D case), $D_{ij(kl)}$, and coordinates $X_{ij(kl)}$ and $Y_{ij(kl)}$ are normally distributed random variables with means equal to the reference, $d^r_{i,j}$, or evaluated, $d^e_{k,l}$ dose values at positions *i,j* or *k,l* in arrays. The absorbed dose uncertainties are σ^e_d, σ^r_d, and isotropic spatial coordinate uncertainties σ^e_s, σ^r_s. Furthermore, it was assumed that the dose differences and spatial coordinate differences between the reference and evaluated distributions are normally distributed:

$$D_{ijkl} = D^e_{k,l} - D^r_{i,j} \sim N(d^e_{k,l} - d^r_{i,j}, \sqrt{{\sigma^e_d}^2 + {\sigma^r_d}^2})$$

$$X_{ijkl} = X^e_{k,l} - X^r_{i,j} \sim N(x^e_{k,l} - x^r_{i,j}, \sqrt{{\sigma^e_s}^2 + {\sigma^r_s}^2})$$

$$Y_{ijkl} = Y^e_{k,l} - Y^r_{i,j} \sim N(y^e_{k,l} - y^r_{i,j}, \sqrt{{\sigma^e_s}^2 + {\sigma^r_s}^2}) \quad (3.13)$$

The squared gamma random variable is a weighted sum of normal random variables with different means and standard deviations and with some rearranging:

$$\Gamma_{ijkl}{}^2 = \frac{\sigma_d^{e2}+\sigma_d^{r2}}{\Delta D^2}\frac{D_{ijkl}^2}{\sigma_d^{e2}+\sigma_d^{r2}} + \frac{\sigma_s^{e2}+\sigma_s^{r2}}{\Delta R^2}\left(\frac{X_{ijkl}^2}{\sigma_s^{e2}+\sigma_s^{r2}} + \frac{Y_{ijkl}^2}{\sigma_s^{e2}+\sigma_s^{r2}}\right) = \Sigma_D D_\sigma^2 + \Sigma_R(X_\sigma^2 + Y_\sigma^2) \qquad (3.14)$$

it becomes a weighted sum of *non-central chi squared random variables*. From the equation (3.16) one observes that the variable, D_{ijkl} divided by $\sqrt{\sigma_d^{e2} + \sigma_d^{r2}}$ is distributed according to a normal distribution with the standard deviation equal to 1 and similar applies to the spatial components. The authors further used the property that if some variable U_n represents a finite set of independent normally distributed random variables with mean values μ_n and standard deviation 1, the sum of U_n^2 will have a *non-central chi square distribution* $\chi^2(n,\delta^2)$ with n degrees of freedom and non-centrality parameter $\delta^2=\Sigma\mu_n^2$. Taking this into account, the following is valid:

$$\widetilde{D}_{ijkl}^2 = \frac{D_{ijkl}^2}{\sigma_d^{e2}+\sigma_d^{r2}} \sim \chi^2\left(1, \frac{(d_{kl}^e - d_{ij}^r)^2}{\sigma_d^{e2}+\sigma_d^{r2}}\right)$$

$$\tilde{R}_{ijkl}^2 = \frac{X_{ijkl}^2}{\sigma_s^{e2}+\sigma_s^{r2}} + \frac{Y_{ijkl}^2}{\sigma_s^{e2}+\sigma_s^{r2}} \sim \chi^2\left(2, \frac{(x_{kl}^e - x_{ij}^r)^2 + (y_{kl}^e - y_{ij}^r)^2}{\sigma_s^{e2}+\sigma_s^{r2}}\right) \qquad (3.15)$$

In a gamma test the goal is to evaluate the probability of the event with $\Gamma_{ijkl}{}^2>1$, denoting the failure rate. The normal variables in the expression (3.15) are non-central; their means are differences between the doses or spatial coordinates. In the past, different versions of expansions of the distribution function of a weighted sum of noncentral χ^2 variables were proposed can be found: power series expansion, series of distribution functions of central and non-central χ^2 variables or series with Laguerre polynomials. In one of the approaches to make the expansion of the distribution function as a weighted sum of non-central chi squared variables the following holds when the quadratic form Q is expressed in the form:

$$Q = \sum_{r=1}^{m} \lambda_r \chi_{h_r,\delta_r^2}^2 \qquad (3.16)$$

where λ_r (r=1,2) in this case are equal to Σ_D and Σ_R, and δ_r^2 (r=1,2) to D_σ^2 and $X_\sigma^2 + Y_\sigma^2$. The δ_r^2 is the non-centrality parameter, and the $\chi_{h_r,\delta_r^2}^2$ are independent χ^2 variables with h_r degrees of freedom. In this case, the following holds:

$$P[Q > x] \cong P[\chi_{h'}^2 > y] \qquad (3.17)$$

where: $y = (x - c_1)\cdot\left(\frac{h'}{c_2}\right)^{\frac{1}{2}} + h'$, $c_j = \sum_{r=1}^{m}(h_r + j\delta_r^2)$, j=1,2,3 and $h' = \frac{c_2^3}{c_3^2}$

When this approximation is applied to the problem of finding $P[\Gamma_{ijkl} > g^2]$, the set of parameters c_1, c_2, c_3, h' and y (y_{iijkl}) can be obtained and the relation (3.17) used to calculate the probability of gamma being larger than g^2 for the reference dose points *i,j* and evaluated dose points *k,l* taking into account the dose and spatial uncertainties.

The proposed modified probabilistic γ-index analysis was tested in a practical example with a 2D segmented composite reference field, an irradiated film. The film had 5 segments of different size to which progressively higher doses were delivered. Five modification cases were generated including only large spatial shifts (e.g. 4 mm) in x and/or y direction in selected film segments or combining the dose modifications (from 0.5% to 1.5 % max.) with the spatial shifts (1 or 4 mm). These modified planar dose distributions (evaluated) were compared with the original (reference). The uncertainties used were: 0.2% dose and 0.5 mm spatial, 0.5% and 0.5 mm, and 0.2% and 1 mm. The tests were conducted for tolerances 2%/2 mm and 3%/3 mm. For a standard gamma index test and the modified probabilistic test, the passing rate was set at 98% and 100% respectively.

A standard gamma index test acceptance criteria 3%/3 mm and a pass rate tolerance of 97% accepted all test cases used in the publication, although some of them were deliberately designed with such errors that should have prevented passing the test. Applying tighter 2%/2 mm criteria, only one case was rejected and another one with the same spatial shift unexpectedly passed presenting inconsistency in results.

If the proposed probability-based test does not produce a 100% pass rate it is possible to state that the test failing points couldn't have been caused merely by the measurement but there might have been also a problem with the irradiation.

The incorporation of radiobiological concepts in the plan verification process was done by modifying the standard definition of the γ-index in the following way:

$$\gamma_+(\vec{r}_r, \vec{r}_e) = min\left\{\sqrt{\frac{r^2(\vec{r}_r,\vec{r}_e)}{\Delta r^2} + \frac{\delta_{rb}^2(\vec{r}_r,\vec{r}_e)}{\Delta D^2}}\right\} \tag{3.18}$$

where δ_{rb}^2 represents similarly to the original definition the radiobiologically modified difference between the reference and evaluated physical dose points. This information can be either the Equivalent Uniform Dose, the equivalent to 2Gy per fraction dose (EQD2), or biologically effective uniform dose $\bar{D}$. To use the equation above, the physical dose distributions need to be converted to a corresponding radiobiological distribution. If an equivalent dose to 2 Gy per fraction approach is used, every pixel (voxel) dose value shall be

converted by calculating EQD2, applying accepted α/β values for planning target volumes PTV and OAR-s (e.g. 10 Gy for PTV, 3 Gy for OAR).

A comprehensive review [60] discusses the challenges in calculating the γ-index when attempting to avoid uncertainties in the calculation and doing it at acceptable times. Using the *MATLAB* code developed by them, the authors showed that a significant speed-up of γ-index calculations can be obtained with the use of limited search in the evaluated dose distribution. The spline interpolation algorithm gave results for γ-index closest to non-interpolated data; the highest gamma passing rate and lowest mean gamma value. The calculated mean gamma value varied considerably for pixel spacing in the evaluated dose distribution larger than 1/10 of the distance difference criterion. To ensure more consistent comparison of the γ-index results, the authors proposed that the following should be reported in research publications: the type of normalisation used, absolute or relative analysis, local or global gamma calculation, if and what low dose cut-off was used, gamma passing criteria expressed as x%/y mm and the software used; and whether the tool used was own development or commercial product.

Finally, a recent comprehensive review [67] aimed at providing a reference for dose comparison techniques for treatment plan verification. Over thirty techniques were identified by the authors, although some of them can hardly be considered as conceptually different and new, but rather as an improvement in some respect (e.g. calculation speed) or extension of some of the already existing techniques. As the review shows, the γ-index calculation with different variants has been commonly accepted in verification processes. Despite the ease of implementation, speed, interpretability, and familiarity with the γ-index the search for a better metric that would rely on statistical and clinically relevant parameters should be continued.

3.6 Clinical pre-treatment patient specific IMRT verification

Most frequent clinically used pre-treatment patient specific IMRT verification techniques [68] can be categorised into the:

a) perpendicular field-by-field (PFF);

b) perpendicular composite (PC) and;

c) true composite (TC) techniques.

In the perpendicular field-by-field (PFF) technique, the linear accelerator gantry is fixed at 0^0 degrees for all radiation fields and the collimator is also fixed at the nominal angle. The TPS

calculates the dose to the plane containing the detectors (e.g. array of ionization chambers, electronic portal imaging device (EPID), film). Aligning of the array of detectors dose distribution with the TPS dose distribution is done through their common centre. If the film is used as a detector, the alignment is done by the pinpricks or other fiducials. A comparison between the TPS calculated distribution and the measured dose is performed field by field. This approach has the advantage of being able to discern the discrepancy due to just a single irradiation field. Combined fields may at certain field regions compensate for two opposite dose differences in compared distributions and lead to negligible dose difference in combined fields.

In perpendicular composite (PC) technique, practically the same approach as for perpendicular field by field technique can be used. The dose contribution from all fields is summed and a single integrated dose distribution is analysed. An EPID can be used to acquire individual images (dose distributions) for VMAT and sum them later.

The disadvantage of this technique is that the error from any beam may stay obscured by the superposition of doses from other beams. In VMAT delivery the errors from using a uniform dose rate versus non-uniform dose rate cannot be discovered by the PC technique.

A true composite technique mimics the real treatment delivery to a patient. The radiation fields are delivered to a phantom containing a measuring device and positioned on a treatment couch. All irradiation parameters as for a patient treatment are used: monitor units (MUs), gantry angle, collimator angle, and MLCs. The detector might be a film or a matrix of diodes or ionization chambers. A combination of a film and an ionization chamber may be also used. Most frequently the film is positioned in a coronal plane. When detector arrays are used for measurements, additional scattering material is added to obtain the depth of at least 5 cm around the detector. The diodes typically have considerable angular dependence within +/- 10^0 relative to a horizontal axis. Although in VMAT delivery this dependence is smeared out since beams from many angles superpose to each other, care should be taken in case of IMRT when a substantial amount of irradiation comes from the lateral directions.

3.7 Features and challenges of using γ-index for clinical treatment plan evaluations

A survey [48] was conducted to collect the data on the IMRT QA analysis methods common to different IMRT systems in clinical practice. The goal of the study was to gather information on the adopted QA method: perpendicular field by field (PFF) irradiation or perpendicular composite (PC) technique, absolute versus relative dose analysis, criteria in the analysis of the

percentage difference, DTA and γ-index, acceptance criteria and measures undertaken if the tested fields or plans failed to meet the acceptance criteria.

The results of the survey showed that over 30% of surveyed institutions used a PC method as opposed to a PFF method. Over half of institutions performed absolute dose comparisons and the most frequent acceptance testing criteria was 3%/3 mm. Finally, the acceptance criteria for prostate, head and neck, brain, and breast IMRT treatment plans were not established in a large percentage of surveyed institutions.

The goal of another study [15] was to assess how well the gamma passing rate per treatment field, as a common IMRT QA performance metric, correlates with dose errors in the anatomic region of interest. Clinically approved head and neck IMRT treatment plans were chosen to test the methodology. The Pinnacle TPS was used to prepare the treatment plans for the linear accelerator with 120 MLCs and 6 MV photon beams. In the proposed simulation scheme, errors were simulated with the impact on dose gradients and dose levels in treatment plans. These errors were embedded into the experimental beam models; photon beam penumbra values were increased, and higher and lower MLC transmissions were introduced into the beam models.

New IMRT plans were generated using the altered beam models keeping the same dose objectives and the number of iterations as in the original error-free plan calculations. The error-free beam model was used as the simulated measurements for IMRT QA dose planes and doses.

The *MapCHECK* (Sun Nuclear Corporation, USA) software was then used to compare the simulated measured planes with the planned QA planar doses. γ-index passing rates were calculated for 1%/1 mm, 2%/2 mm, and 3%/3 mm criteria (global gamma, 10% dose threshold). Several anatomy dose metrics were also calculated, such as the maximum dose in the spinal cord, dose to 1 cm of a spinal cord, mean dose in the ipsilateral and contralateral parotid gland, larynx mean dose, and dose to 95% of the CTV volume. This was performed in the planned and simulated measured patient dose distributions. The absolute errors of anatomy dose metrics were plotted against the gamma passing rates to examine the correlations. The dose errors represented the differences between the dose calculated using the error free system and the expected dose i.e., the one calculated with the introduced beam model error. It was found that the gamma passing rates were not sensitive to clinically relevant patient dose errors on a per patient basis; only weak or moderate correlations were observed between the anatomy-based dose metric and gamma passing rates. High IMRT QA passing rates observed in concert with large anatomy based metric errors indicate false negative results while low passing rates

combined with low errors render false positive results. The predictive power of the most common metric (γ-index pass rate) and acceptance criteria and tolerances are according to the results in this study, insufficient; high gamma passing rates do not automatically imply accurate plan dose calculation and/or delivery.

In eight head and neck, IMRT treatment plans with a total of 53 fields, random MLC position errors of up to 2 mm, and systematic errors of 1 and 2 mm were introduced to estimate the sensitivity of patient specific IMRT QA to leaf position errors [69]. 6 MV photon beams in the step and shoot IMRT delivery technique were used with a linear accelerator equipped with 120 MLCs. The perpendicular field-by-field technique of dose comparison was used; planar dose distributions calculated before and after the introduction of errors were compared to dose distributions measured with radiochromic films and 2D *MapCHECK* (Sun Nuclear Corporation) diode detector array. The change in average passing rate and the nonparametric test of significance was used in this study to decide on the error identification. IMRT QA procedures with both film and detector array were able to detect the errors on the order of only 2 mm. Sensitivity to MLC position error when using a 2%/2 mm criterion was significantly larger than for a 3%/ 3 mm criterion. Asymmetry in response to +2 mm (increased opening) MLC positioning error leading to higher passing rates and -2 mm (decreased opening), giving lower passing rates, was noticed. The simulation showed that no systematic MLC calibration error or TPS modelling error was responsible for the observed asymmetry.

The error curve methodology [70] sustained the earlier evidence on the inability of common gamma criteria to detect large patient specific QA errors. In their study, eleven fixed beam dynamic MLC (dMLC) IMRT plans and 10 validation plans including a range of treatment sites, field sizes, standard and hypo-fractionated cases were selected. All dose distributions were originally measured with *ArcCHECK* (Sun Nuclear) and passed standards QA procedure with 3%/3 mm, dose threshold of 10% and at least 90% passing rate). Calculations were performed with the *Eclipse* (Varian Medical Systems, Palo Alto, CA) TPS, utilizing the AAA algorithm and a 1 mm calculation grid to avoid any post-calculation interpolation in SNC Patient software from the *ArcCHECK* device.

To check the sensitivity of different gamma criteria, three types of errors were introduced in plans: a) MU errors- dose calibration errors; b) MLC errors-simulation of potential inaccuracies in MLC trajectories or control point definition and c) changes in the penumbra width in the beam model. Many plan calculations were created each with a different error magnitude; the error-containing plans were created. They were compared with measurements.

Composite *ArcCHECK* measurements and TPS calculations with and without induced errors were compared in terms of the γ-index in SNC Patient software. Thirty-six different criteria were obtained by combining the range of dose difference values and DTA (range from 1% /1 mm to 5%/5 mm, 12 cases) with 3 dose thresholds of 10%, 20% and 50%.

The gamma passing rate for each criterion was recorded as a function of error magnitude expressed in percentage. The curves obtained in this way can be approximated by Gaussian curves and for each passing rate of interest (e.g. 85, 90, 95%), the FWHM in % error magnitude can be automatically extracted.

The work showed that gamma sensitivity to errors can be significantly increased with the use of higher (50%) low dose thresholds. One earlier study [71], in which *ArcCHECK* was used for Tomotherapy, showed that gamma passing rates were independent of the choice of the low dose threshold for both global and local dose normalization, but only for dose thresholds of 5 and 10%.

The study [70], however, had limitations. Firstly, the number of case studies was low and an increased number of cases per treatment site would likely provide stronger evidence on the studied γ-index sensitivity, on what criteria to use for the specific treatment site. Secondly, only global gamma was investigated. Next, the methodology is not meant to identify a particular error, but rather provides insight into the sensitivity of different gamma criteria. Finally, the scope of the study was limited to a specific combination of the detector, software, gamma comparison technique with a detector manufacturer's software solution, TPS and delivery techniques, and machine.

The study [72], comprising randomly selected 30 VMAT treatment plans, 10 per head and neck, brain, and prostate cancer case, was designed to determine the effect of the low-dose threshold in γ-index calculation. Varian Eclipse TPS with AAA calculation algorithm was used to plan the treatment with standardized prescription dose, number of arcs, and range of angles.

For every VMAT plan, a portal dose verification plan was generated utilizing a portal dose calculation algorithm. A dose reconstruction without a patient or phantom was used.

The linear accelerator then irradiated the EPID with the verification dose and portal images were compared with the corresponding calculated portal images. In γ-index analysis three sets of the dose difference and DTA criteria, 1%/1 mm, 2%/2 mm and 3%/3 mm, and four low dose thresholds, 0, 5, 10 and 15%, applying a minimum passing rate of 95%.

When the global γ-index analysis was conducted, the gamma passing rate decreased with the low-dose threshold. For the acceptance criteria of 3%/3 mm and 2%/2 mm, a gamma passing rate stayed above 95% despite the low-dose thresholds applied. Conversely, performing local γ-index, the points excluded by the low-dose threshold of 10% may enlarge the average passing rate by 7-10% compared to that with a 0% low-dose threshold, applying 3%/3 mm criterion in the case of the head and neck, brain, and prostate cases.

3.8 Tolerances and action levels

The result from any quality assurance measurement needs to be checked against some limits of acceptability. There are two types of limits; those that are defined as the amount the quality measures allowed to deviate without risking harm to the patient as well as defining limit values when clinical action is required (action limits) and those that define boundaries (tolerance limits) within which the process is considered to be subject to random fluctuations and therefore still being a normal process. If the system starts to move rapidly towards the tolerance limits or even crosses the limits, the system is not operating normally anymore. This requires investigation of the potential cause.

The difficulty with the γ-index analysis resides in choosing the proper tolerances and interpreting the results. Tolerances and pass rates depend on a type of the test (physical or clinical) and a detector (e.g. ionization chamber, array, etc.). For instance, the test will have a different sensitivity depending on whether the dose distribution comparison is defined locally (a function of the dose at the point to evaluate) or globally (a function of the maximum dose in the evaluated or reference distribution). Also, points in the low-dose region may bias the pass rate if the dose tolerance is too high.

Based on the literature review of IMRT QA results, delivery techniques and evaluation methods, the American Association of Physicists in Medicine (AAPM) Task Group 218 issued recommendations [68] concerning the tolerances, action limits and pass rate thresholds to apply to evaluate the acceptability of IMRT QA verification plans. General recommendations were made for IMRT QA verification of dose distributions, followed by the universal and possible site-specific tolerance and action limits for evaluating IMRT QA analysis, and few vendors aimed recommendations for faster, accurate, reliable, and more practical software tools. A process-based tolerance and action limits given in the report accounts for all characteristics of variation in IMRT QA such as human contribution to QA measurement or modulation complexity differences in different applications.

.

Chapter 4
MATERIALS AND METHODS

4.1 Introduction

Since most of the research done in relation concerning the topics in this thesis are simulation studies with relatively large data arrays that require fast computation capabilities and flexibility, the decision was initially made about the environment that could be used for this purpose, integrating efficient computation, with data visualization, programming and easy-to-use environment.

All calculations, simulations, data analysis and visualisations were ultimately carried out using *MATLAB* (MathWorks Inc., version R2016a) code. The application built-in debugger and profiler were used in routine code testing and optimisation to identify errors and analyse the points where the developed program code spends the most time. To speed up the performance of the code, some standard techniques like the modular programming approach, use of functions, vectorisation capabilities of *MATLAB* application and array pre-allocation were frequently used.

In the first phase of the program code development, 1D absorbed dose distributions based on the standard photon beam dose profile measurements in a water phantom and idealised, artificial dose distributions were used aiming at testing the accuracy, robustness and speed of execution of the code. Tests were performed for calculating the dose difference, distance-to-agreement, histograms and gamma (γ) indices. These results were compared with the results from publications obtained by other authors who either developed their code or used commercial applications.

The measured 1D photon beam dose profiles and 2D dose distribution for clinical IMRT fields calculated in a QC phantom were the basis for the investigation of the properties of the squared gamma (γ^2) index distribution in the next part of the thesis.

In another step, a set of clinical head and neck IMRT fields were used to calculate the relative dose distribution at depth in a uniform QC phantom. For these fields, dose measurements were simulated by assuming that the calculated value represented the expectation value, and by adding a random spatial and dose uncertainty. The simulated measurements were then

compared to the calculated dose using the γ-index, and the distribution of the γ-index failure rate was analysed.

Finally, the previous simulations involving a set of clinical IMRT fields were extended to cover not only one detector, but an entire array of hundreds of detectors, mimicking a measurement in a TPS-calculated IMRT field. As in the previous step, a random uncertainty was added to each dose measurement, but this time all detectors were given the same displacement on each occasion. The relative number of detector points outside the tolerance limit was scored, and the procedure was repeated a statistically acceptable number of times.

Additional numerical data analyses were done in Microsoft Excel and R (RStudio, Version 1.1.423) programming language and software environment was used for pertinent statistical analyses.

4.2 Development of γ-index calculation code and investigation of the γ-index distribution properties for 1D and 2D dose distributions

4.2.1 Introduction

The computer code was developed in *MATLAB* to calculate the 1D and 2D γ-index distribution with either local or global dose normalisation. The input variables for the routines define the reference (*ref*) and evaluated (*eval*) dose distribution data sets, their starting coordinates and distance/pixel dimensions. Furthermore, it accepts the gamma absolute criterion percentage and the DTA criterion, and allows for additional parameters definition: a) the reference value for the global gamma calculation (the default is the maximum dose value in the reference dose distribution); b) the search limit that determines how far the code will search in the distance axes during γ-index computation; c) the number of distance steps factor that is equal to the resolution factor times the search limit.

The output variable of the calculation is an array (1D or 2D) containing the computed γ-index values with the same dimensions as the input dose distribution arrays.

4.2.2 1D dose distribution

The relative values of the absorbed dose D(x) at the spatial coordinate x, a 1D dose profile, in the penumbra region of a 10x10 cm^2, 6 MV photon beam were obtained as an analytical function [19] fit to the measured data:

$$D(x) = \eta \{T + (1-T)(A\, erf[B_1(x_0 - x)] + (1-A) erf[B_2(x_0 - x)])\} + D_1 \qquad (4.1)$$

The parameters η, T, A, x_0, B_1, B_2 and D_1 are the parameters of the fit defined as in [19]. The error function erf(x), shown in Figure 4.1, is defined by:

$$erf(x) = \frac{2}{\sqrt{x}} \int_0^x e^{-t^2} dt \tag{4.2}$$

A cumulative distribution function (CDF) of a normal distribution with the standard deviation σ and mean μ is:

$$\Phi(x) = \frac{1}{2}\left(1 + erf\left(\frac{x-\mu}{\sigma\sqrt{2}}\right)\right) \tag{4.3}$$

and it ranges from a value of 0 at x = -∞ to 1 at x = ∞.

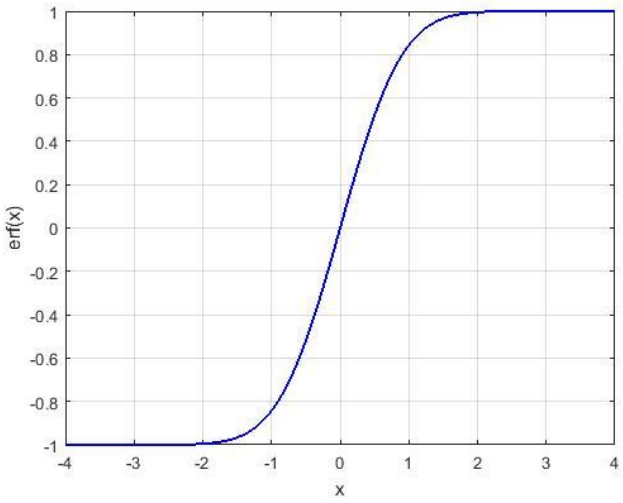

Figure 4.1. The error function erf(x).

The measured data is obtained from the photon beam commissioning data sets for *TrueBeam* (Varian Medical Systems) linear accelerator. The 1D dose profiles were measured with a Semiflex ionization chamber in the MP3 water scanning phantom (both PTW, Freiburg, Germany). From the set of measurements, two representative profiles acquired at depths of 1.5 cm (d_{max}) and 10 cm in water were used for testing the developed code for calculating the dose difference, DTA and γ -index.

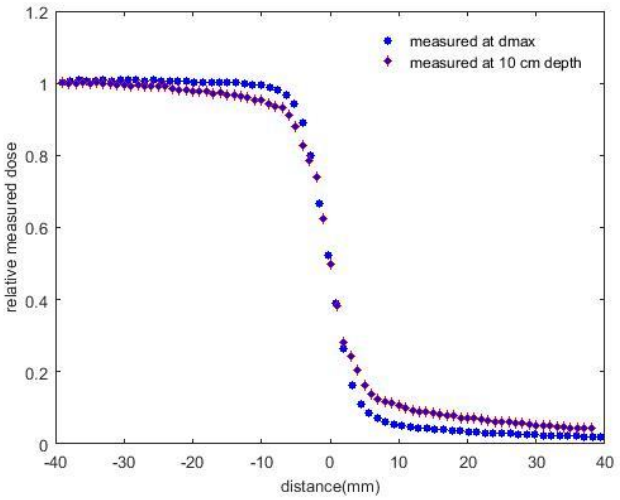

Figure 4.2. Measured normalised profiles of the 10x10 cm^2 6 MV photon beams at two depths in water, d_{max}=1.5 cm and 10 cm.

The reference dose distribution was represented with a function fit (Eq. (4.1)) to the measured data (Figure 4.2) and the evaluated dose distributions were modified by changing the normalisation factor η, collimator edge position shift x_0 and dosimetric shift D_1, one at a time.

The code offers local or global gamma calculation with a choice of normalisation, different level of interpolation of the reference and evaluated dose distribution defined with the resolution parameter, limiting (search) parameter that determines how far the function will search in the distance axes when computing the γ-index, and the percent dose difference and distance-to-agreement criterion. The γ-index array that results from the calculation has the same dimension as input vectors containing the data for the reference and evaluated dose distribution.

4.2.3 2D dose distributions

Testing of the γ-index calculation routines for 2D dose distributions was done by simulating a simple artificial reference (*ref*) and evaluated (*eval*) dose distribution. For simplicity and speed, the original dose distributions were represented by a 128×128 array with 0.1 × 0.1 cm^2 pixel size. The central part of the dose distribution, consisting of 64 × 64 pixels, was prescribed to 100 cGy dose and outside this central part, the dose was set to 0 cGy. The evaluated 2D dose distributions were constructed in the following ways:

1) The central part of the evaluated dose distribution was shifted by $1/\sqrt{2}$ pixels in both x and y direction from the central axis position in the reference dose distribution and the dose was increased to 101 cGy.

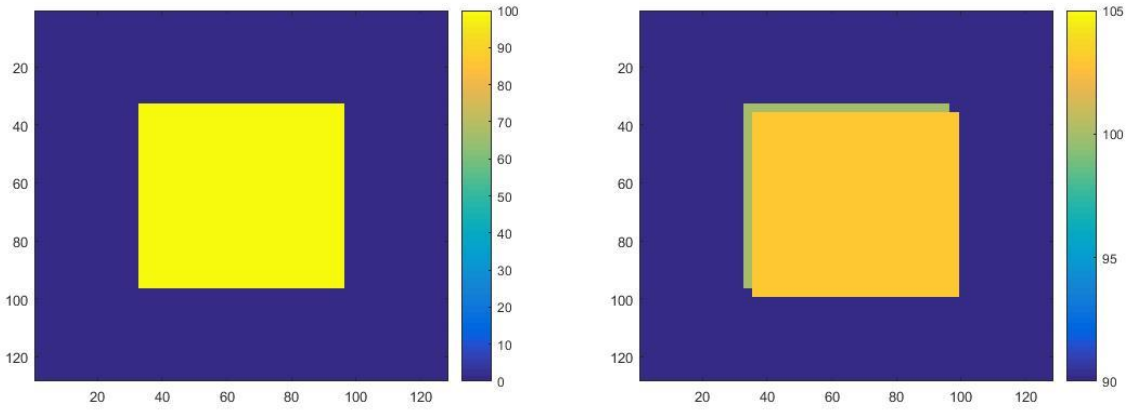

Figure 4.3. The uniform reference 2D dose distribution (left) containing the central part having the dose of 100 cGy. The reference dose distribution with a central part having the dose of 100 cGy and an evaluated dose distribution shifted 1 pixel in x and y direction with the central region having an increased dose of 103 cGy (right). The image of the distributions shown right is scaled to better visualise the difference. The colour bar indicates the dose in cGy.

2) The central part was shifted by 1 pixel in both x and y direction from the central axis position in the reference dose distribution and the dose was increased to 103 cGy.

3) The central part was shifted by 1 pixel in both x and y direction from the central axis position in the reference dose distribution and the dose was increased to 105 cGy.

The code that calculates the γ-index distribution is complemented with the statistical evaluation [59], [61] of the γ-index distribution: a) mean gamma value γ_{mean}; b) median gamma value γ_{med}; c) maximum gamma value γ_{max}; d) percentage of points that have the gamma value less than 1 (P<1, passing rate) and e) 99-th percentile of the gamma value distribution denoted as $\gamma_{1\%}$ and calculated from the gamma dose histogram (it represents 1% of points that have an equal or higher gamma value).

Another 2D distribution [73] was constructed from the 6 MV photon beam dose profiles measured in a scanning water phantom. The field size used was 10×10 cm^2. The ionization chamber (*field*) used for the profile measurement was a Semiflex chamber (PTW, Freiburg). The same type of the ionization chamber positioned in air below the linear accelerator collimator, at the edge of the field, was used to measure the beam output variation and then to normalize the signal of the field chamber. The cross-plane profiles were measured at SSD=100 cm, at the depth of 10 cm. The charge collection time was 0.5 sec per point and the sampling distance was uneven; more measurements were acquired in the penumbra region and less in the flat, central part of the field. Prior to constructing an artificial 2D distribution the 1D profile

was smoothed with a filter based on a local regression using weighted linear least squares and a 1st-degree polynomial model and interpolated using the *interp1* routine to produced equally spaced points of the 1D dose profile. The interpolation step was 0.1 mm.

The final 2D dose distribution was obtained by multiplying the 1D dose profile in one dimension by the same profile used for the perpendicular direction. The final reference 2D distribution was additionally smoothed to reduce noise; the central part of the field had integral uniformity of ~1.3%. The distribution was also normalised so that the dose at the central axis was 100 cGy.

For the evaluated dose distribution this 2D distribution was modified in attempting to highlight the discrepancies using the acceptance limits of 3% dose difference and 3 mm distance difference at the certain distance from the centre of the dose distribution.

In the first (1) quadrant, the reference dose distribution was not modified; the reference and evaluated dose distributions in this quadrant were identical. In the second (2) quadrant, the reference dose was reduced by providing a multiplicative dose offset that is a function of the off-axis distance x (in mm).

$$\Delta D(cGy) = -a\Delta x(mm) \tag{4.4}$$

The slope was chosen in such a way to reach the dose decrease of ~3% at the points defined with x= 2.5 cm. The third (3) quadrant was spatially distorted according to the following equation:

$$\Delta y(mm) = b\Delta x(mm) \tag{4.5}$$

where Δy is the spatial shift of the dose value that is proportional to the distance x (mm) and adjusted in such a way that at x=-2.5 cm the shift of the D values is about 3 mm. Finally, in the fourth (4) quadrant the modified distribution contained both, the spatial and dose distortion introduced individually in quadrants 2 and 3.

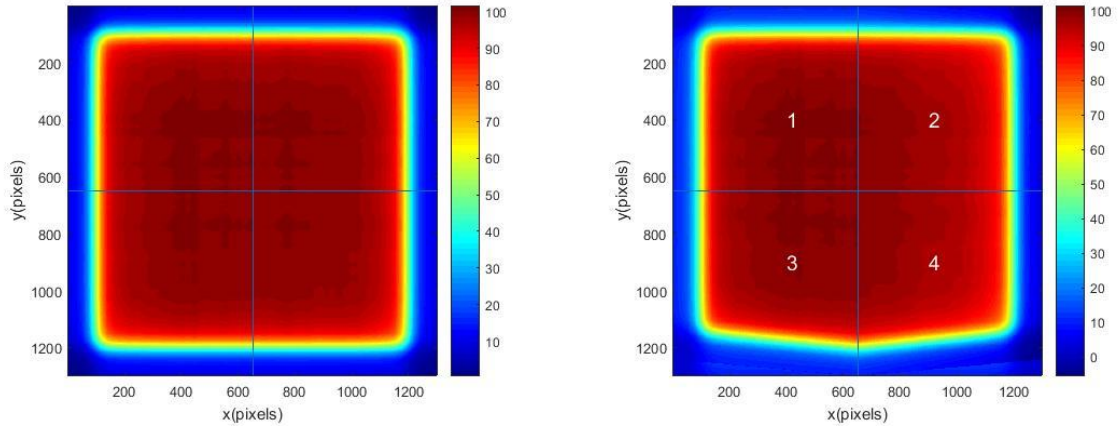

Figure 4.4. The reference (left) and evaluated (right) dose distribution. The pixel size is 0.1 mm and the colour bar indicates the dose in cGy. The introduced dose distribution modifications in individual quadrants of the evaluated distribution are described in the text.

Additionally, supplementary coding allowed for the comparison of the calculated and measured dose distribution in terms of their absolute difference calculated on a pixel by pixel basis. There is an option to display the difference between the positive and the negative range. It helps to find out how one dose distribution differs from another. For the presentation of the dose differences, a limited dose range can be chosen to get a more noticeable overview of the dose differences.

In some instances, the differential or cumulative/integral histograms of different quantities may help to depict the features of these quantities. For instance, the cumulative histogram of the dose difference represents counts of the cumulative number of pixels that have that specified dose difference or more, e.g. 50 % of all pixels have a dose difference of 20 cGy or more and 50 % of all pixels have less than 20 cGy dose difference. So that the data point for 0 Gy dose difference is 100 %.

In contrast, the differential histogram represents only the number of pixels that are within the bin of a specified dose difference, e.g. 10 % of all pixel have the dose difference of 10 cGy.
Similarly, a cumulative and a differential histogram of a γ-index distribution can be displayed. The γ-index value is given on the x-axis, whereas the percentage of the surface of the two-dimensional dose distribution (or volume in case of 3D distribution) is drawn on the y-axis. For the cumulative γ-index histogram, the data point of one particular γ-index shows the sum of all pixels of gamma indices equal and above this specific γ-index.
Therefore, the volume for γ-index equal zero is 100 %. For the differential γ- index histogram, the data point shows a fraction of the surface or volume for a particular γ-index value.

As a final 2D dose distribution example, an EBT3 film irradiated with a 6 MV small photon beam (24 × 24 mm) in a homogenous solid water phantom at the depth of 10 cm and SSD=100 cm (Figure 4.5).

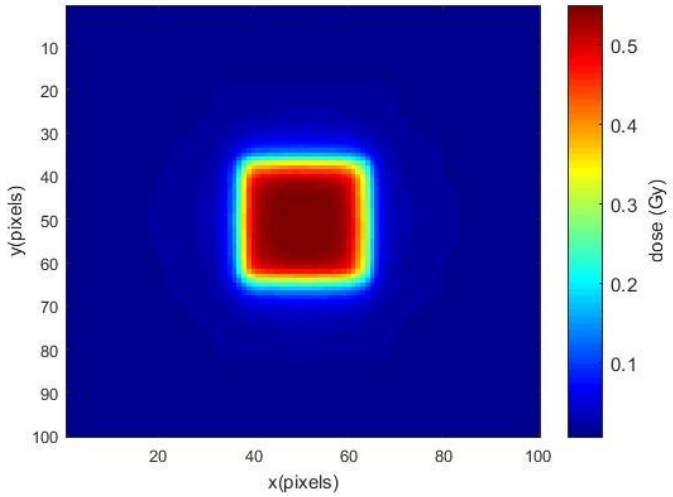

Figure 4.5. Original scanned EBT3 film irradiated with a 6 MV small, 24×24 mm^2, photon beam.

The profile drawn through the scanned image to indicate the approximate FWHM is presented in Figure 4.6:

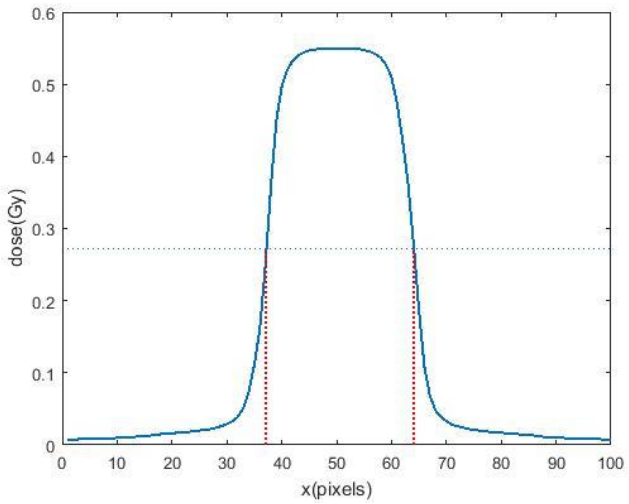

Figure 4.6. Cross-plane 1D profile through the film recorded dose distribution. The red lines denote the approximate field size.

The dose distribution was normalized to 100 cGy and then modified by increasing the part of the distribution that is larger than 95 cGy by 5 cGy. Additionally, the 7^0-counter clock rotation of the distribution is performed. A bilinear interpolation was used. The prepared distributions

were then ready to be resized and cropped to avoid corners that could create artefacts in the analysis.

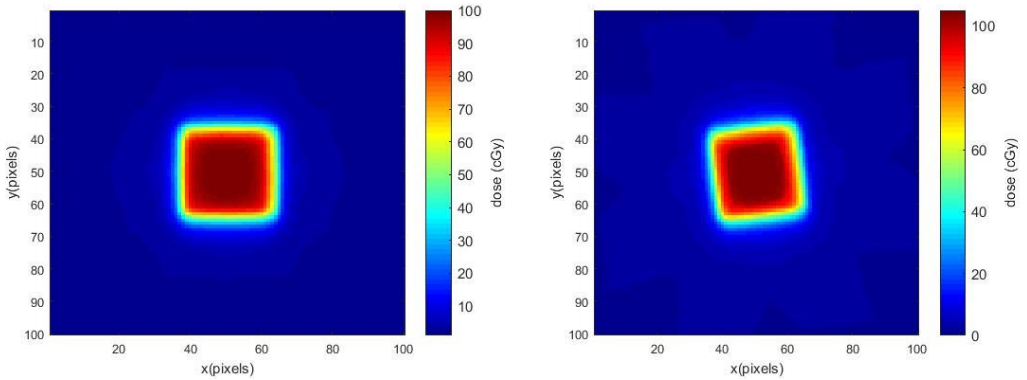

Figure 4.7. Reference and evaluated dose distributions. The evaluated dose distribution was obtained by modifying the central part dose values and counter-clock rotation of the reference distribution as described in the text.

When the distributions are resized to 400 × 400 pixels, their size is effectively reduced to the pixel size of 0.25 mm × 0.25 mm. The distributions cropped to 200 × 200 pixels are shown in Figure 4.8.

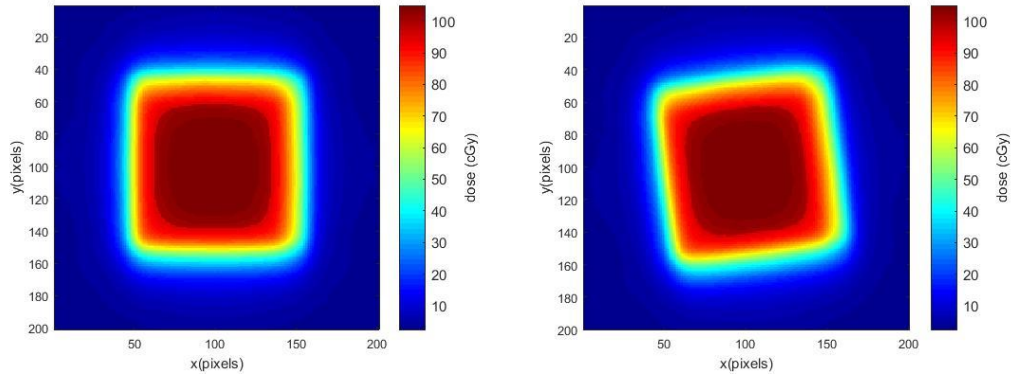

Figure 4.8. Resized and cropped dose distributions prepared for further analysis.

4.3 Properties of the squared γ-index distribution

In this part of the work, again the calculated dose distributions derived from measurements in 1D and 2D for clinical quality control procedures were used. Measurements were simulated based on statistical uncertainties of the absorbed dose measurements and detector positioning. The resulting squared γ-index (γ^2) distribution was investigated and compared with the χ-squared (χ^2) distribution with one degree of freedom (Appendix C).

The χ^2 distribution with k degrees of freedom is the distribution of a random variable that is the sum of the squares of k independent standard normal random variables. Thus, if Z_1, ..., Z_k are standard normal random variables (i.e., each $Z_i \sim N(0,1)$), and if they are independent, then:

$$Z_1^2 + \cdots + Z_k^2 = \chi^2(k) \tag{4.6}$$

If simple random samples (with replacement) y_1, ..., y_k are taken from some $N(\mu,\sigma)$ distribution, and if Y_i denotes the random variable whose values are y_i, then each $(Y_i-\mu)/\sigma$ is standard normal, and $(Y_1-\mu)/\sigma$,…., $(Y_k-\mu)/\sigma$ are independent, thus:

$$\left(\frac{y_1-\mu}{\sigma}\right)^2 + \left(\frac{y_2-\mu}{\sigma}\right)^2 + \cdots + \left(\frac{y_k-\mu}{\sigma}\right)^2 = \chi^2(k) \tag{4.7}$$

Figure 4.9 presents the χ-squared distribution for four different values of the degree of freedom parameter (*k)*.

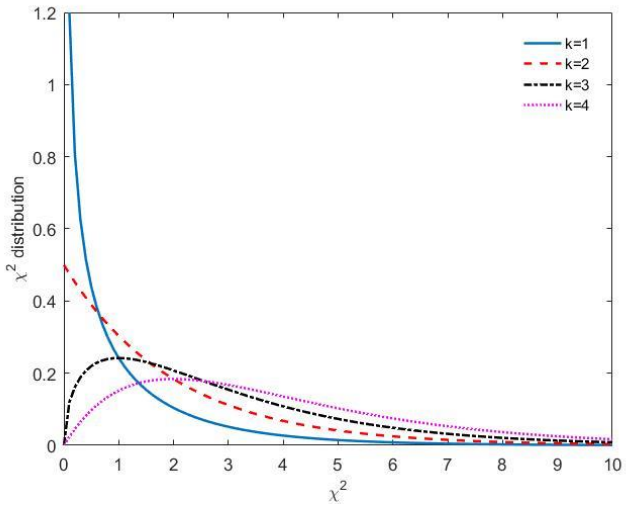

Figure 4.9. χ-squared distribution with k degrees of freedom, k = 1, 2, 3, 4.

4.3.1 1D dose distribution

To investigate the distribution of γ^2 values in clinical situations, firstly a case of the relative 1D dose distribution in a penumbra region of a 10 × 10 cm^2 6 MV photon beam from the *TrueBeam* (Varian Medical Systems) linear accelerator was examined. The 1D dose distributions were measured with an ionization chamber in the water phantom as described in section 4.2.2. From the set of beam profile measurements, two representative profiles acquired at different depths were fitted with the function defined by Eq. (4.1). These fits were further considered as "calculated", true dose distributions (i.e., free of errors) and were used for an investigation of

the relationship of the squared gamma (γ^2) and the chi-square (χ^2) distribution with one degree of freedom.

For simulation purposes, an ideal detector was assumed to be positioned at a point x_m (Figure 4.10) during the measurement of 1D absorbed dose distribution (profile). A measured dose value was simulated by adding a random misplacement (random measurement uncertainty) from that point. The displacement was drawn from the normal distribution, $x_d \sim N(x_m, \sigma_x)$, where the symbol ~ indicates that a random variable x_d has a distribution, N denotes the normal distribution with two parameters, the mean, x_m, and the standard deviation σ_x. The measured dose is then determined at this displaced position and a random dose deviation, drawn again from the normal distribution $D_m \sim N(D_c(x_d), \sigma_D)$. Thus, for each nominal measurement point, a measured value was simulated by taking the calculated dose at a randomly displaced position, and by adding a random dose measurement noise.

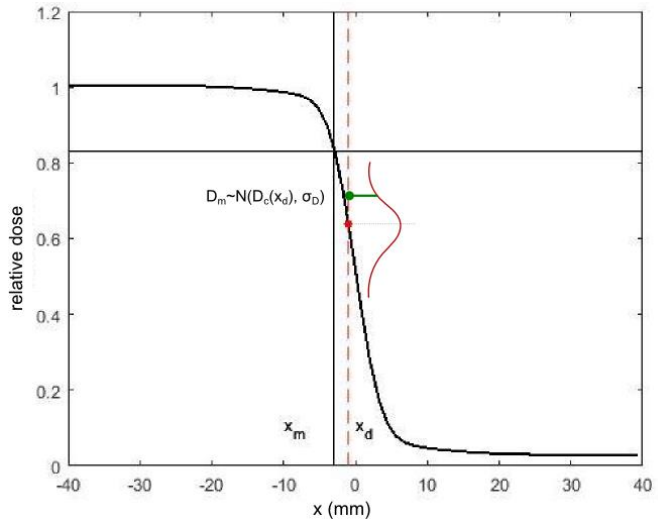

Figure 4.10. Calculated 1D dose distribution used as true penumbra and the fit using Eq. (4.1) for a 10 × 10 cm^2 6 MV photon beam from *TrueBeam* (Varian Medical Systems) linear accelerator.

Both the detector displacement and the measurement uncertainty were drawn from normal distributions (*MATLAB* function *rand*), with standard deviations σ_x and σ_D (σ_x=1 mm/σ_D=1 cGy, σ_x=2 mm /σ_D=2 cGy, σ_x=3 mm /σ_D=3 cGy), respectively. Then, the nearest calculation point was determined according to the gamma evaluation procedure and the smallest γ^2-index was calculated. The acceptance criteria were set to $\Delta D=\sigma_D$ for the dose difference and to $\Delta r=\sigma_x$ for the distance-to-agreement (DTA).

By repeating this simulation, many times (10^4-10^5 times), a distribution of squared gamma (γ^2) values were obtained, which was then compared with the χ-squared (χ^2) distribution with one degree of freedom.

The statistical approach with a novel dose uncertainty model introduced [23] and elaborated through the application of the method for dose verification [24] was utilised. According to that proposal, the dose uncertainty is separated into two components, positional or space-oriented σ_s, and non-space-oriented, σ_{ns} uncertainties. While the first category covers uncertainties caused by spatial displacements and possible misregistration of dose distributions under the comparison, the second category may, for instance, include different dosimetry uncertainties such as uncertainties related to dosimetric input data to TPS.

The uncertainties combined with uncertainty propagation give:

$$\sigma_t = \sqrt{\sigma_s^2 + \sigma_{ns}^2} \tag{4.8}$$

and a confidence interval can then be defined for the measured dose difference.

$$|\Delta D| = |D_d - D_m| \leq k\sigma_t \tag{4.9}$$

or

$$\frac{|\Delta D|}{k\sigma_t} \leq 1$$

The γ-index value is the minimum distance between the measurement and the calculated curve, determined in a normalized space-dose coordinate system and the acceptance criterion is that the $\gamma \leq 1$.Rewriting the general expression for the γ-index (Chapter 3) and accepting the notation given above, with the replacement $\Delta r=\sigma_x$ and $\Delta D=\sigma_D$, the following holds:

$$\gamma^2 = \left(\frac{x_d - x_m}{\sigma_x}\right)^2 + \left(\frac{D_d - D_m}{\sigma_D}\right)^2 \leq 3.841 \tag{4.10}$$

If this inequality is scaled to fit the γ-index method, so that if the criteria, the denominators in Eq. (4.10) are set equal to 1.96 standard deviations, gamma values will be less than, or equal to 1.0 in 95% of the cases.

$$\gamma^2 = \left(\frac{x_d - x_m}{1.96\sigma_x}\right)^2 + \left(\frac{D_d - D_m}{1.96\sigma_D}\right)^2 \leq 1 \tag{4.11}$$

The fraction of values above 3.841 for the acquired γ^2-distribution determines the failure rates. These were calculated in both, a 1D dose distribution case as above, and in a 2D case as given in the section below, and it represents the extension of previously published work [74].

4.3.2 DICOM data sets and processing

Digital Imaging and Communications in Medicine (DICOM) is an international standard for medical digital images and the information related to them. The different components in the radiotherapy treatment chain (e.g. CT, TPS and the linear accelerator) all communicate through DICOM files. Moreover, all the information required at any given step of the treatment process can be obtained from the DICOM files.

DICOM RT is specified for radiotherapy modality and for this thesis there are three classes of DICOM files that are of interest: *DICOM RT image* includes all the images acquired during the treatment and information about their position, plane and orientation; *DICOM RT plan* has all the geometric and dosimetric data relating to treatment plan (treatment beams, dose prescription, patient setup); The 3D dose matrix is stored in a separate *DICOM RT dose* file that also contains information on the coordinates of the dose grid, which typically is more sparse than the CT grid. The file is linked to the DICOM file of the treatment plan it is calculated for.

The DICOM export facility was used to export the plan parameters and *MATLAB* scripts to create input files. The DICOM data were extracted from dose distribution arrays exported from TPS, which was used to simulate QA measurements with a diode (or ionisation chamber) array. In order to do this, the IMRT fields were maintained from the patient treatment plan but transferred to a uniform phantom geometry. Also, the linear accelerator gantry and couch were rotated in the treatment planning system, so that the beam axis was normal to the planes (slices). Then, the plane of interest, located at the measurement depth, was selected. Thus, the extracted 2D dose distribution should be comparable to the diode/ionization chamber array QA measurement.

4.3.3 TPS and detector array in clinical QA

The *Oncentra MasterPlan* (Nucletron B.V., Veenendal, the Netherlands) TPS was used for calculating doses in a phantom, which is a part of patient specific IMRT QA practice in a clinical environment (Radiotherapy Department at Skåne University Hospital, Lund, Sweden). The underlying dose calculation algorithm is based on a collapsed cone (CC) convolution approach [28]. A ray-trace technique is used through the irradiated object to get the total energy released per unit mass (TERMA) at all points of the dose calculation grid. The TERMA is separated into a primary part (collision kerma) and a scatter part. Both parts are transported separately along multiple lines from the interaction point. The energy from each voxel

intersected by a fan line in the irradiated medium is collected and deposited according to the elemental composition of the medium and density variations along the fan line.

The *MapCHECK 2™* detector (Sun Nuclear Corporation) provides a QA test of the linear accelerator's ability to successfully deliver a planned QA dose map (called delivery QA or DQA) in a phantom. The DQA plan is not a measurement of the planned dose map that would have been delivered during the treatment of the patient but a recalculation, on a phantom, of the dose defined by the treatment planning system, TPS, which must be delivered by the linear accelerator.

The *MapCHECK 2™* detector consists of 1527 diode detectors with a uniform detector spacing throughout the array of 7.07 mm, equalling a total octagonal detector array size of 32 × 26 cm. The sampling frequency of this detector is 50 ms and each diode in the array has an active detector area of 0.64 mm^2 and an active detector volume of 0.000019 cm^3 [75]. The *MapCHECK 2™* array has a physical detector depth of 1.20 cm and a water-equivalent depth of 2 cm.

4.3.4 2D dose distributions

The 2D dose distribution case was based on an IMRT field calculated by the *Oncentra MasterPlan* (Nucletron B.V., Veenendal, the Netherlands) TPS with a pixel resolution of 1 mm and linear interpolation between the points of the dose matrix. The size of the dose matrix was 401×401 mm and the voxel size: 1×1×0.52 mm^3.

The calculations were carried out for three 2D dose distributions. A representative dose distribution planes from the stack (401×401×81) of calculated dose distributions at depth of 5 cm in the phantom are depicted in Figure 4.11.

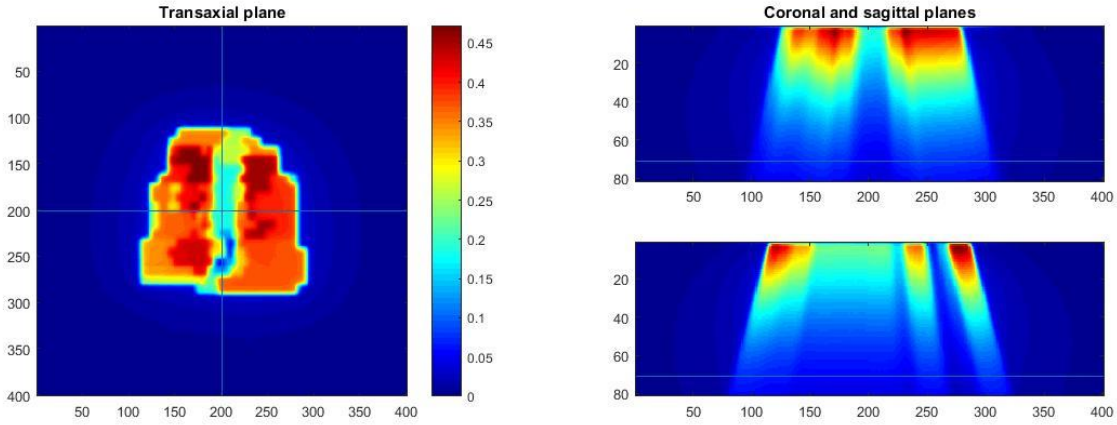

Figure 4.11. Left: 2D dose distribution calculated at the depth of 5 cm in a phantom and used in simulations. Blue lines in the transaxial plane indicate the positions of the coronal and sagittal planes shown in the figure on the right side. Right: Coronal and sagittal planes extracted from the stack of calculated doses. The colour bar indicates the dose in Gy-s.

In this dose distribution, a set of points (3) were chosen for which the simulations were conducted. By repeating this simulation 10^4 times, again a distribution of γ^2 values were obtained and compared with the χ^2 distribution with one degree of freedom.

4.3.5 Failure rates for individual points in 2D dose distributions

The calculation of failure rates in individual points from 2D dose distributions was based on IMRT fields, calculated by the *Oncentra MasterPlan* TPS like described in section 4.3.4. The program code written to investigate the properties of failure rates included the following general steps:

a) reading in the stack (DICOM) data 2D dose distributions calculated by the TPS in a uniform phantom;

b) reading in the dose scaling factor and pixel dimensions;

c) resizing the dose distribution, if necessary and relevant;

d) initiating a simulation loop and starting with mispositioning of the detector coordinates x, y where shifts were randomly taken from the normal distribution;

e) evaluation of the dose value for the mispositioned detector point by using 2D linear interpolation;

f) addition of the random dose measurement uncertainty; a value drawn from the normal distribution;

g) definition of the limited minimum gamma value search region around the mispositioned point;

h) calculation of a set of γ^2-index values inside the search region and finding the minimum value;

i) repeating the simulation required number of times to obtain substantial statistics; and

j) calculating and recording the vector of failure rate values.

4.4 Simulation of a detector-array measurement in IMRT

4.4.1 Introduction

In a previous section, the method is described for investigation of the statistical distribution of the γ^2-index values in 1D and 2D cases. This was done by simulating a measurement situation using a calculated dose distribution (TPS) and by adding a random Gaussian uncertainty to the detector position and dose value. The simulated measurement was then compared with the original calculation, and the gamma-value was calculated according to standard expression, using the dose difference and DTA criteria equal to the simulated uncertainties.

In this part the objective was to investigate if the observed match of the distribution of γ^2 values follows well the χ^2 distribution with one degree of freedom found valid for a single measurement, can be applied to a more clinically relevant situation.

A large number of detectors are typically encountered in practical dose verification, QC procedures with detector arrays (diodes or ionization chambers). These detectors are located at fixed positions with some detector spacing in array geometry able to cover a certain filed size during a measurement.

If the random variable X follows the binomial distribution with parameters n ∈ $\mathbb{N}$ and p ∈ [0, 1], we can write in short notation X ~ B (n, p). The probability of getting exactly k successes in n trials is given by the:

$$P(X = k) = \binom{n}{k} p^k (1-p)^{n-k} \tag{4.12}$$

If the assumption can be done that all detectors in the array are statistically independent, the probability of having exactly k detectors outside the tolerance limit can be obtained by the binomial P(X=k) distribution (4.12) where n is the total number of detectors, and p is the probability of a single detector being outside the tolerance limit.

However, the detectors in the array are not statistically independent regarding the position uncertainty. Since all detectors are mounted in an array, they will all move together with the entire device.

4.4.2 Methods

The previous simulation was extended to cover not only one detector, but an entire array of 100 and 400 detectors, mimicking a measurement in a TPS-calculated IMRT-field (see Figure 4.12).

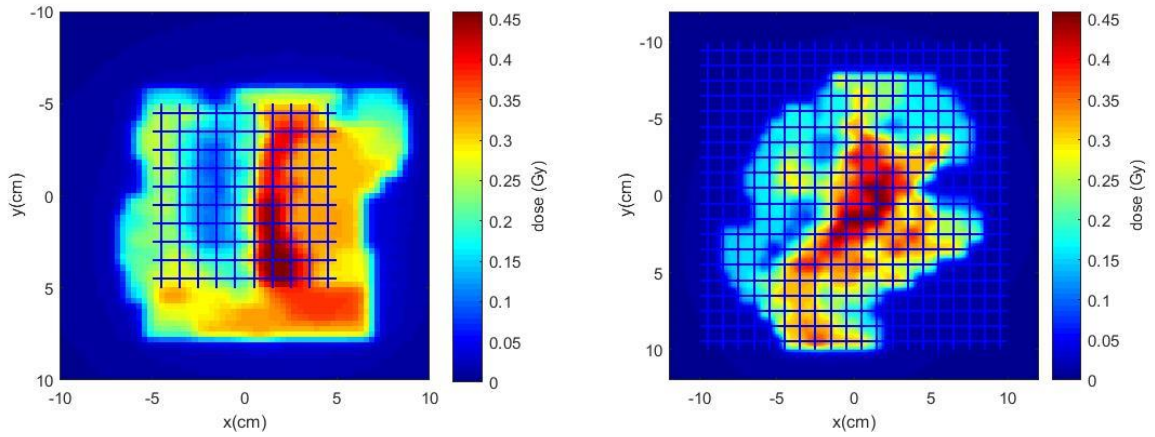

Figure 4.12. The TPS-calculated dose distributions for IMRT-fields, and the positions of the 100 (left) and 400 (right) simulated detectors (blue crosses).

The detectors were distributed at 1 cm in the arrays 10×10 and 20×20. Two sets with three dose distributions calculated at the depth of 5 cm were used in simulations. The pixel sizes of the dose distributions were 1 mm and 3 mm in two dose distribution sets, respectively.

As in the case of a single measurement, again a random uncertainty drawn from the Gaussian distribution was added to each dose measurement, but this time all detectors were given the same random displacement on each occasion. The relative number of detector points outside the tolerance limit of 3.841 (i.e., the failure rate) was scored, and the procedure was repeated 10^4 times. The illustration of the algorithm described above is given in Figure 4.13.

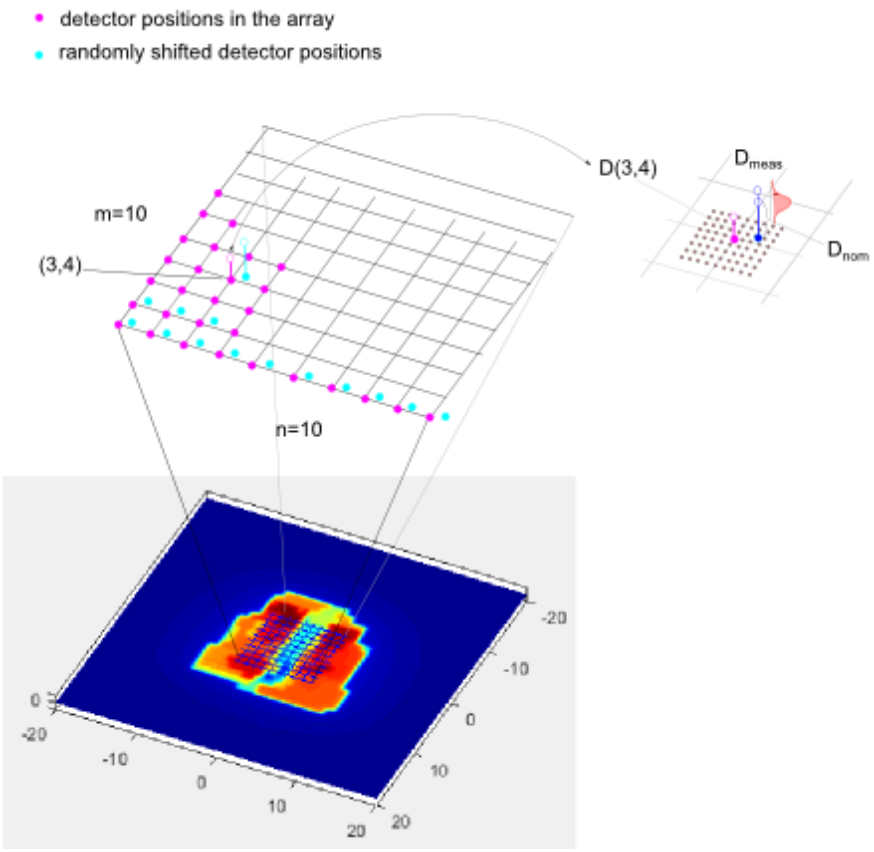

Figure 4.13. Dose distribution of an IMRT field calculated at 5 cm depth in the uniform phantom shown with the grid of detectors superimposed on the field. The detector positions are indicated by purple circles and the detector positions shifted in concert for a random vector are denoted by the cyan circles. The right side of the figure illustrates the fine sub-grid of points spread out around one detector position, a shifted position at which the nominal and measured dose were derived in a process of finding the minimal γ^2 among the sub-grid points.

The initially designed code involved a loop to repeat N simulations of the entire miss-positioned detector array. All detectors (M=100, Figure 4.13) had the same randomly shifted initial positions – their x and y coordinates. The dose measured with a particular randomly shifted array detector was determined by a 2D linear interpolation from the given dose distribution to obtain the nominal dose at shifted detector positions. Subsequently, a random dose measurement uncertainty drawn from the Gaussian distribution, N (0, σ_D), was added to the nominal detector dose, D_{nom}, to obtain the measured dose D_{meas}.

A sub-grid of points around every detector position was defined and its resolution was regulated by the spatial uncertainty $\sigma_{x,y}$ value; it was a small fraction of $\sigma_{x,y}$ to improve the accuracy of the calculation. A variable search limit for a minimum γ^2 value was defined and its influence on the outcome was checked. The doses at the sub-grid points were calculated with a 2D linear interpolation and the minimum γ^2 value was calculated for each detector position in a simulation run. Runs involving the detector array were repeated a large number (10^4) of times.

In an improved version of the program code, the following changes were introduced to increase the speed of the program execution: a) reduction of the number of inherently slow 'for' loops; b) pre-calculation of randomly shifted detector positions for all simulation runs; c) use of effective *meshgrid* function, single-precision variables and parallel 'for' loops where possible and applicable.

4.5 Statistical analysis of the gamma evaluation acceptance criteria

4.5.1 Introduction

In this part of the work, the same statistical approach as introduced in section 4.3.1 with a novel dose uncertainty model [23, 24] was used. The model described in section 4.3.1 assumes that two types of uncertainties, spatial and non-space oriented, are uncorrelated or precisely, that the contribution of the positional displacement to the non-spatial dose uncertainty is negligible. With this assumption, the statistical acceptance criterion is defined as:

$$|\Delta D| \leq k\sigma_t \tag{4.13}$$

where

$$\sigma_t = \sqrt{\sigma_D^2 + G^2\sigma_x^2} \tag{4.14}$$

and where G is the spatial dose gradient, σ is the standard deviation (in dose (D) and spatial position (x), respectively) and k is the confidence factor. This can also be reformulated as:

$$\frac{|\Delta D|}{k\sqrt{\sigma_D^2+G^2\sigma_x^2}} \leq 1 \tag{4.15}$$

Here, it is assumed that the calculated dose value is the expected value and that the dosimetric and spatial uncertainties are normally distributed. Thus, with k=1.96, Eq. (4.15) will be fulfilled in 95% of the cases.

In a parallel, analytical investigation of the gamma evaluation factor, [66] showed, that if second-order derivatives are small (a small curvature of the dose distribution in a near neighbourhood), the γ-index can be approximated by:

$$\gamma = \min(\Gamma) \approx \frac{|\Delta D|}{\sqrt{\Delta D_{max}^2+G^2\Delta x_{max}^2}} \tag{4.16}$$

Thus, through the combination of the first-order approximation in Eq. (4.16) and the uncertainty approach in Eq. (4.15), we may re-interpret the gamma-evaluation acceptance criteria in Eqs. (3.9) and (3.10). By using $\Delta D_{max} = k\sigma_D$, and $\Delta x_{max} = k\sigma_x$ this means (with k=1.96) that the

gamma values will be less than or equal to one in 95% of the cases (i.e., a failure rate of 0.05), given that no systematic errors are affecting the difference between the calculations and measurements.

4.5.2 Clinical IMRT distributions

To examine the validity of the approximation made in Eq. (4.16), we investigated the presence and effect of second-order derivatives (SOD) in the absorbed dose distributions in a uniform (PMMA) phantom, calculated using the treatment planning system *Oncentra Master Plan* (Nucletron B.V., Veenendaal, the Netherlands), for a set of 30 clinical, head and neck IMRT fields. For this analysis, the QA method used at the department, where the treatment plan is recalculated in a QC phantom with all beams at 0^0 gantry angle and normal to the phantom surface.

For each field, the relative absorbed dose distribution (labelled in the further text as F1-F30) was calculated at 5.0 cm depth with a resolution of 85×85 pixels, and a pixel size of 3 mm×3 mm, which was typical for the department's QA practice at the time. The absorbed dose was scored at 361 points arranged in a 19×19 matrix resembling a QC detector array of ionization chambers or semiconductor diodes. At each point, the second-order derivative of the absorbed dose distribution was determined by using the *MATLAB* built–in function '*gradient'*, twice. Only the absolute value of the gradient was used in this analysis. This function, when applied to a 2D function, f (x, y), returns a matrix of partial derivatives in the x and y directions. These are then combined to calculate the absolute value of the gradient and the process is repeated to obtain the absolute value of the SOD of the function, which was used in the analysis.

For each calculation point, a measured data point was simulated by adding a random spatial displacement and a random absorbed dose measurement deviation. Random numbers were drawn from a Gaussian distribution with a standard deviation σ_x, σ_y for the spatial coordinates, and σ_D for the absorbed dose, respectively. The new, simulated data point was then compared to the original absorbed dose distribution and a γ-index value was calculated according to the 2D-version of Eqs. (3.9) and (3.10). By repeating this procedure 10^4 times, the distribution of gamma values was collected, and the fraction of gamma values that did not satisfy Eq. (3.10), i.e., the failure rate, was determined. Simulations were done both without introducing any dose threshold in calculating the gamma values and, in order to bear a resemblance to the clinical approach, with a dose threshold of 15% of the maximum dose recorded in the dose distribution.

The consistency of the set of 30 2D dose distributions was analysed regarding the occurrence and the distribution of second-order derivatives, and for a subset of 10 dose distributions, the influence of the choice of simulation parameters, σ_x, σ_y and σ_D on the resulting distributions of failure rates were further investigated.

The original code was also modified to allow calculating and recording the distribution of γ-index values for individual points in a 19×19 matrix. The recorded points of interest, coordinates x and y of the measured dose distribution and individual gamma values enabled subsequent analysis of the histograms of occurrence of a failure rate and better understanding of the relationship of the simulation parameters and histogram features.

Chapter 5
RESULTS

5.1 Introduction

The first part of this chapter presents the results of the development of an efficient and fast γ-index calculation programme code for 1D and 2D dose distribution comparisons. These programs were checked for consistency and the results for the dose difference, distance-to-agreement (DTA), γ-index values or other statistical parameters were in simple dose comparison cases related to expected results and in some cases with the published results. By varying different input parameters of the calculation, information on the program execution time was obtained. This code offers the choice of the local or global gamma calculation, different level of interpolation of the reference and evaluated dose distribution, limiting parameter that determines how far the function will search in the distance axes when computing the gamma, and the percent dose difference and distance-to-agreement criteria.

The next section deals with the simulation results obtained in 1D and 2D dose distribution cases for squared γ-index distributions proved to have similar properties to the statistical χ^2 distribution with one degree of freedom when gamma acceptance criteria are replaced by the standard deviations of space and dose uncertainties.

A thorough investigation of the gamma evaluation acceptance criteria, conducted by studying the statistical distribution of the γ-index value under error-free conditions for the clinical IMRT fields, showed that there is a spatially non-uniform probability of having a gamma value above unity.

5.2 Gamma index calculation code and investigation of the γ-index distribution properties for 1D and 2D dose distributions

5.2.1 1D dose distributions

In the first example, 1D profiles measured in the penumbra region of a 6 MV photon beam, obtained by the linear accelerator (*TrueBeam*, Varian) at two different depths, d_{max} (1.5 cm) and 10 cm, were used to calculate parameters of analytical functions [19] and further treated as reference dose distributions (Figure 5.1). The non-linear Levenberg-Marquart algorithm was used to calculate the function fit parameters. In both cases, a high adjusted R^2 coefficient of

0.999 and a low root mean square error (max. 0.009) parameters of the fit performance were obtained.

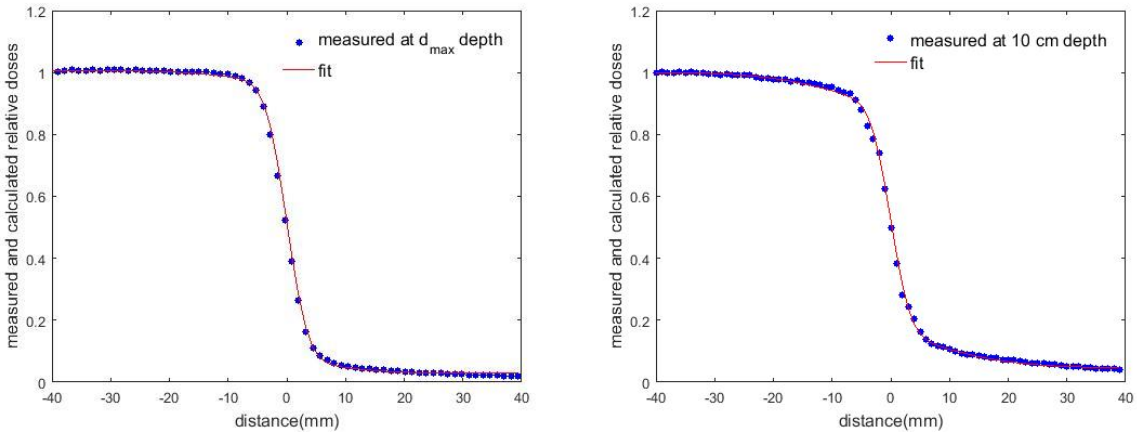

a) b)

Figure 5.1. Profiles of 6 MV photon beams measured at the depth of a) d_{max} and b) 10 cm (blue dots) and functions fitted to experimental data (red line).

Figures 5.2. below depict the 1D reference and evaluated dose distributions with three different modifications, dose difference, distance-to-agreement and the calculated γ-index. The calculated (fitted) function in Figures 5.1. a and b are used as the reference dose distribution.

The left column (Figures 5.2 a,b,c) contains the dose distribution comparisons for the 6 MV photon beam profile obtained by a fit to the data measured at the depth of d_{max} in water and modelled with Eq. (4.1), whereas the right one (Figures 5.2 d,e,f) shows those obtained in the same way but for the beam profile obtained at the depth of 10 cm. The x-axis range in figures is limited to a narrower penumbra band of ±20 mm.

In all cases, a global gamma was used with the normalisation at the maximum value in the reference distribution. The resolution grid was determined by the chosen DTA criterion divided by the resolution factor (e.g. 3 mm/100) and the search limit was extended to 3. It determines how far the code will search in spatial coordinate. In all presented cases, the dose difference and distance-to-agreement criteria were 3% and 3 mm, respectively. To speed up the program execution, the reference data and coordinates, and evaluated coordinates were, before gamma calculation, converted to single precision.

Figure 5.2a illustrates the reference (6 MV, at d_{max} depth) and evaluated dose distribution shifted by +2.5 mm, the dose difference that rises at the penumbra region, distance-to-agreement and the calculated γ-index. The dose difference is shown multiplied by a factor of

10 for better visualisation. Figure 5.2b shows the reference and evaluated dose distribution in which an additional 2% dose normalisation difference (parameter η that modifies the profile) is introduced and a +2.5 mm spatial shift is kept. Finally, the last figure in the left column (Figure 5.2c) shows the same distributions as in the previous two cases (Figure 5.2 a,b), but now for the spatial shift of +2.5 mm, 2% dose normalisation difference and dosimetric offsets of 2.5% concerning the original parameter in the reference distribution. The shape and features of the dose distributions, dose difference and γ-index in Figures 5.2 d,e,f are essentially replicates of those in Figures 5.2 a,b,c in terms of the parameter (e.g. spatial shift, dose normalisation and dosimetric offset) modifications for the evaluated distributions, but now for the beam profile calculated from the data measured at the depth of 10 cm.

In Figure 5.2a, the maximum value of gamma is about 0.8 and it corresponds to the maximum value of the dose difference; the DTA is as expected 2.5 mm since the evaluated distribution was shifted for that amount concerning the reference distribution. The gamma value in the whole range is below 1 which means it passes the acceptance test. When the evaluated distribution is modified so that a normalisation difference is introduced, a narrow region in gamma values distribution appears where it comes closer to the value of 1. When all function parameter modifications are introduced in the evaluated dose distribution, the maximum gamma value exceeds 1.1 in the region where the flat part of the profile turns into the penumbra region. The increase in the DTA in the first part of the curve is noticeable when the evaluated dose distribution contains all three modification; similar behaviour of the γ-index, amplified compared to the dose comparisons for the reference profile at d_{max} is illustrated on the right side of Figure 5.2 c.

6MV photon beam profile at d_{max} **6MV photon beam profile at depth of 10cm**

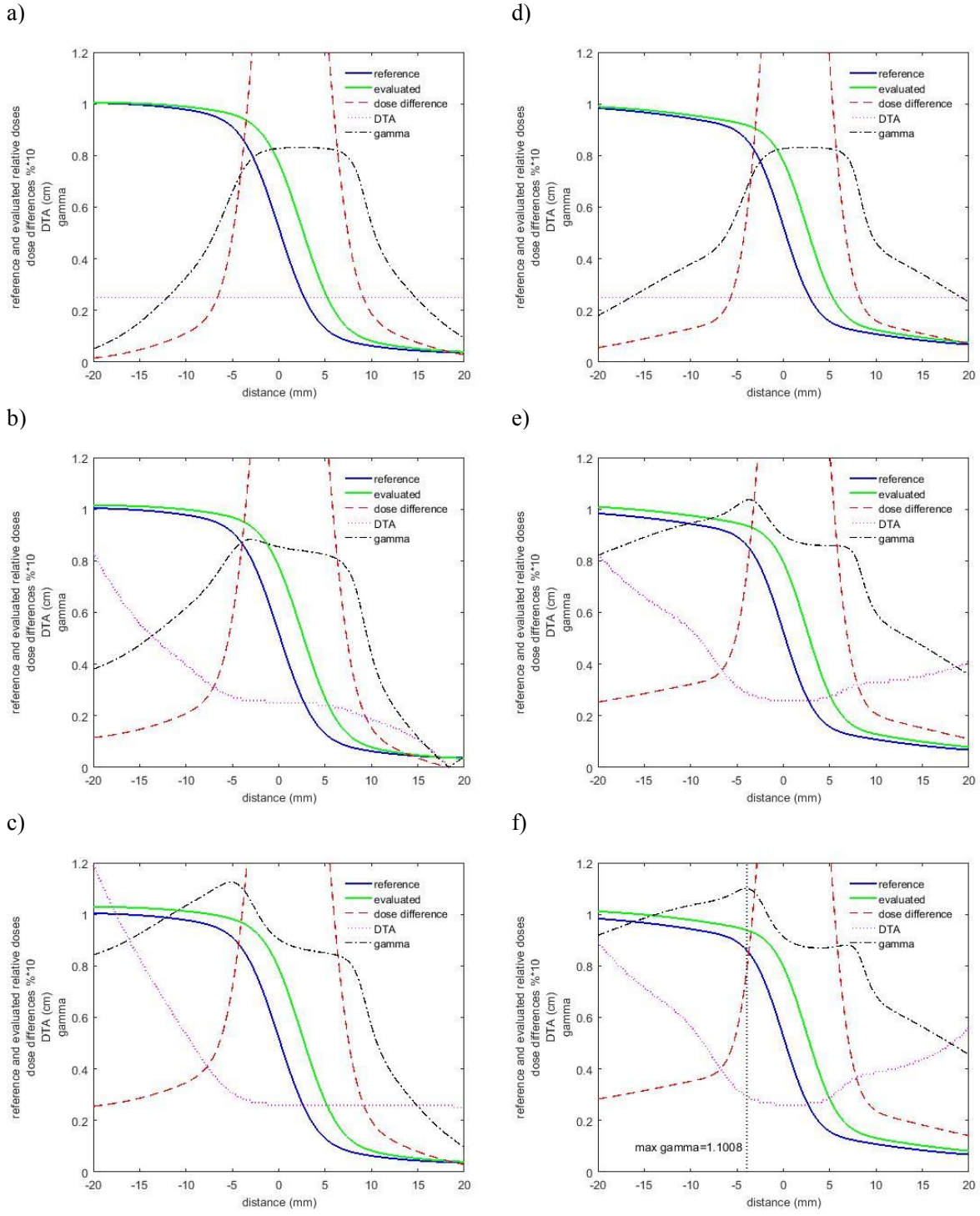

Figure 5.2. Left column: reference and evaluated dose distributions in the penumbra region of a 6MV photon beam at d_{max}, dose difference, distance-to-agreement and γ-index distributions. The evaluated distribution is shifted by 2.5 mm from the reference distribution (Figure 5.2a); evaluated distribution shifted by 2.5 mm and ~2% dose normalisation difference introduced (Figure 5.2b) and evaluated distribution shifted by 2.5 mm, ~2% dose normalisation and dosimetric offset of 2% introduced (Figure 5.2c). Right column: same distributions and modifications as in the left column but for the penumbra region of a photon beam profile at the depth of 10 cm.

5.2.2 2D dose distributions

Programs were afterwards developed to investigate the γ-index properties for 2D dose distributions by simulating a simple artificial reference (*ref*) and evaluated (*eval*) distributions: a) a uniform square dose distribution superimposed centrally on a zero dose background that was compared to the shifted dose distribution with an elevated dose in the central region; b) 2D dose distribution constructed from the measured dose profile at depth compared to evaluated dose distribution obtained by the dose and spatial modification in four quadrants and c) 2D dose distribution constructed from the scanned EBT3 radiochromic film irradiated with a 6 MV small photon beam in a homogenous solid water phantom at the depth of 10 cm (Chapter 4).

In the first set of comparisons, the uniform dose of 100 cGy in the central part of the reference distribution and evaluated dose distribution was shifted by $1/\sqrt{2}$ pixels in both x and y direction from the central axis position in reference dose distribution and the dose was 101 cGy. The results of calculations for increased resolution factor that multiplied with a DTA limit presents the number of steps in spatial coordinates, is given in Table 5.1.

Table 5.1 2D gamma statistical evaluation results of the uniform dose comparisons in which the spatial shift was $\mathbf{1/\sqrt{2}}$ pixels in x and y direction and the dose difference between the reference and evaluated distribution was 1 cGy (change from 100 cGy to 101 cGy). The resolution parameter was increased from 1 (no interpolation) to 50 and dose difference and DTA criteria 3%/3 mm, global gamma.

Resolution	γ_{mean}	γ_{max}	$\gamma_{1\%}$	$P_{\gamma<1}(\%)$	Time (s)
50	**0.333**	**0.476**	**0.411**	**100**	**75.3**
20	0.333	0.486	0.417	100	14.5
10	0.334	0.540	0.448	100	6.3
1	1.028	1.453	1.054	98.4	2.3

The parameters in Table 5.1 were calculated in the limited central region of the γ-index array (50% of the maximum observed dose value) since otherwise, the calculation of the parameter such as the γ_{mean} would not have a proper meaning.

Table 5.2 compares the results for three different dose differences in the evaluated dose distribution, whereas Table 5.3 gives the results for the same metrics as in Tables 5.1. and 5.2 but for three sets of dose difference and DTA criteria: 3%/3 mm, 2%/2 mm and 1%/1 mm (the choice of criteria is limited to only three pairs of values, although different combinations are applied in practice).

Table 5.2 2D γ-index statistical evaluation results similar to the results in Table 5.1 but this time for the same spatial shift of 1 pixel in x and y direction in all cases and the dose difference between the reference and evaluated distribution of 1,3 and 5 cGy. The resolution parameter was 50.

Dose difference (cGy)	γ_{mean}	γ_{max}	$\gamma_{1\%}$	$P_{\gamma<1}(\%)$	Time (s)
1	0.338	0.585	0.476	100	99.8
3	1.002	1.110	1.056	75.0	93.5
5	1.668	1.735	1.701	75.0	112.2

Table 5.3 2D γ-index calculation results similar to the results in Tables 5.1 and 5.2 but for three sets of dose difference and DTA criteria: 3%/3 mm, 2%/2 mm and 1%/1 mm.

Dose difference /DTA	γ_{mean}	γ_{max}	$\gamma_{1\%}$	$P_{\gamma<1}(\%)$	Time (s)
3%/3 mm	0.338	0.585	0.476	100	99.8
2%/2 mm	0.506	0.866	0.707	100	84.6
1%/1 mm	1.013	1.732	1.414	74.2	92.8

Another 2D reference dose distribution constructed from the 6 MV photon beam dose profile measured in a scanning water phantom for the field size of 10×10 cm^2 was utilised in the next γ-index analysis.

Figure 5.3 shows the reference and evaluated dose distributions, their absolute dose difference distribution and the integral dose difference histograms. Clearly, for the first quadrant, the dose difference is equal to 0 Gy. In the second quadrant, the difference introduced through modifying the reference distribution as described in Chapter 4 appears constant, however, this is just visualised as such due to the coarse colour map resolution. In quadrants 3 and 4, the differences in the steep dose gradient become visible; the maximum difference in quadrant 3 is 44 cGy, and in quadrant 4 increases to 49 cGy. The visible difference region forms a triangular pattern that reflects the spatial shift versus x position.

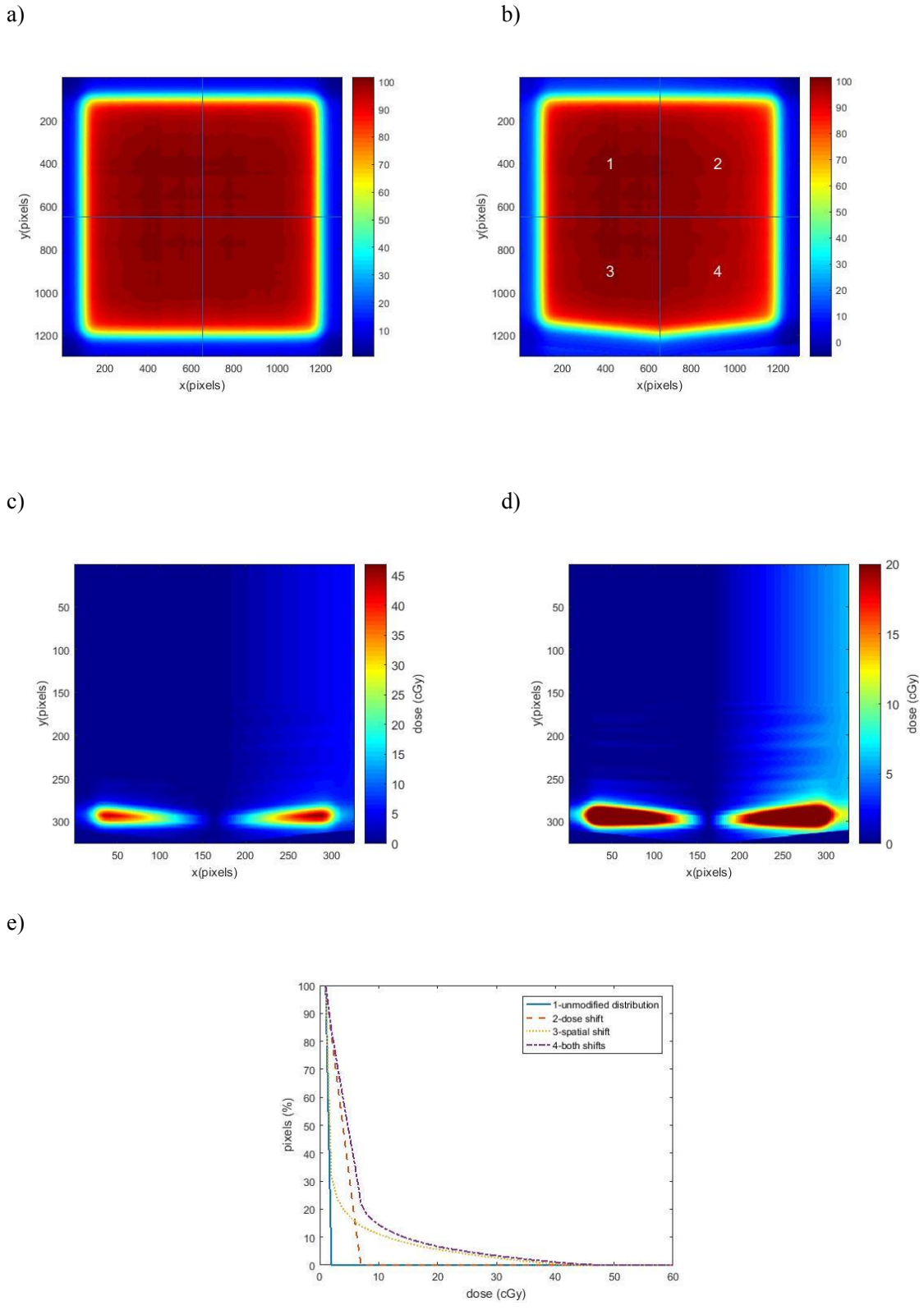

Figure 5.3. Reference dose distribution (a), evaluated dose distribution (b), absolute dose difference of the reference and evaluated dose distribution (c), same as in (c) but for the reduced dose range (d), and the dose difference integral histogram (e). The reference and evaluated dose distributions in figures a) and b) were resized to 326×326 pixels prior to further calculation.

The γ-index array calculated for the area (294×294 pixels) cropped from the originally constructed evaluated distribution (Figure 5.3.b) is depicted in Figure 5.4a. γ-index calculations run for a range of resolution factors showed that calculation time increased from 154 s (resolution factor 10) to 3882 s (resolution 50).

a) b)

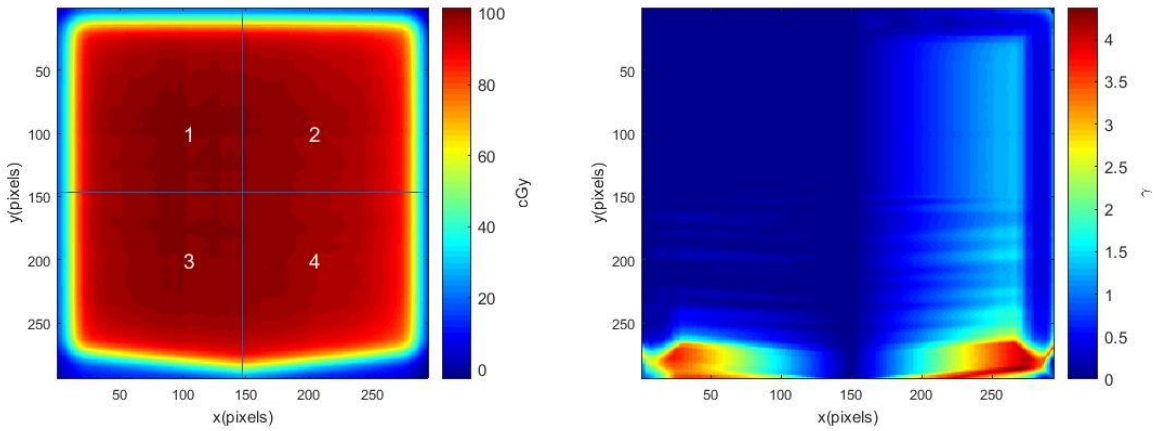

c)

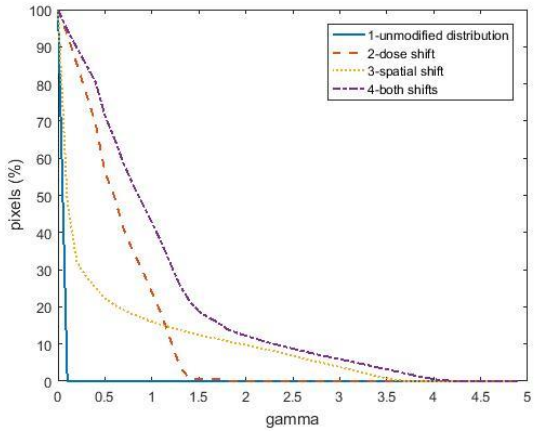

Figure 5.4. Evaluated cropped dose distribution used in γ-index array calculations (a). γ-index array calculated with the resolution factor 10 and the search limit of 10 (b). The cumulative γ-index histograms for each quadrant of the γ-index array (c).

The first quadrant exhibits γ-index values equal to zero since no modification of the reference dose distribution was introduced to produce the evaluated dose distribution. In the second quadrant, the dose difference increases in the positive x-direction. In the high dose region, the γ-index increases up to a maximum of ~1.5. In the steep dose gradient regions of the quadrant, the γ-index approaches zero. The value in this region depends on the subtlety of the calculation

grid- resolution factor; for a small grid size, the dose difference will not affect the dose comparison. In the low dose region, a γ-index can become larger than 1 because the reference dose is still not equal to zero and the maximal dose shift makes evaluated distribution equal to zero. In the third quadrant, the γ-index is larger than 1 only for a small area, for which the spatial shift is responsible since it pulls up the steep dose gradient of the bottom field edge. In the high dose region, the spatial shift does not account for a high γ-index, here the γ-index is almost zero for the whole region. In fourth quadrant, γ-index values increase in the high dose region in the positive x-direction. It is the result of the combination of the dose shift and spatial shift. At the right edge of the field, the γ-index is equal to zero. The dose difference does not affect the dose difference comparison as described for quadrant 2 and as the spatial shift is in y-direction the γ-index in this region is equal to zero. The area of the steep dose gradient region at the bottom edge of the field, where the gradient is shifted to the top, is larger than in quadrant 3. The maximum reaches a value of 4.

For a final 2D dose distribution example, an EBT3 film irradiated with a 6 MV small photon beam (24 × 24 mm) in a homogenous solid water phantom at the depth of 10 cm and SSD=100 cm (Figure 4.5), the dose difference (not absolute but rather reference-evaluated) is depicted in the figure below:

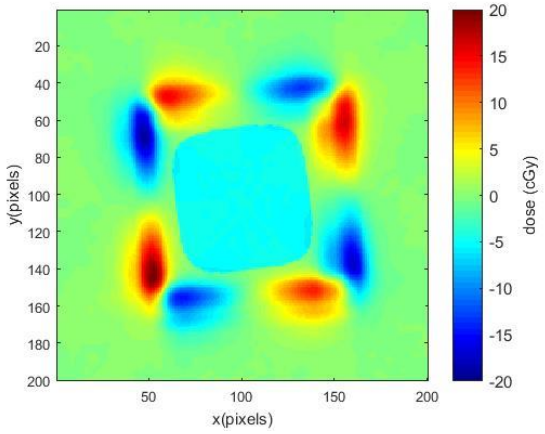

Figure 5.5. Dose distribution difference.

The dose difference shows within the central beam area, as expected, the difference of about 5 cGy due to the increased dose in the evaluated distribution, and there are larger interchanging positive and negative differences at the beam edges due to the rotation of the evaluated distribution.

Finally, some calculated γ-index distributions for different sets of criteria of the dose difference and DTA are shown. The colour scale is the same for all cases: a) 0.5 mm/1% (normalization: global), b) 0.5 mm/1% (local), c) 1 mm/2% and d) 2 mm/3% (both global). The resolution in these calculations was 10. For the calculations with global normalization the γ_{max} value reduces from 5.089 (a) to 1.689 (d), while the γ_{mean} value dropped from 1.121 to 0.357 in cases (a) and (d), respectively. In the case of local normalization, the γ_{max} and γ_{mean} values are 5.536 and 1.545, respectively. Clearly, spots with high gamma values due to the definition of local normalization appear, beside the rotated central part, also at the distribution periphery.

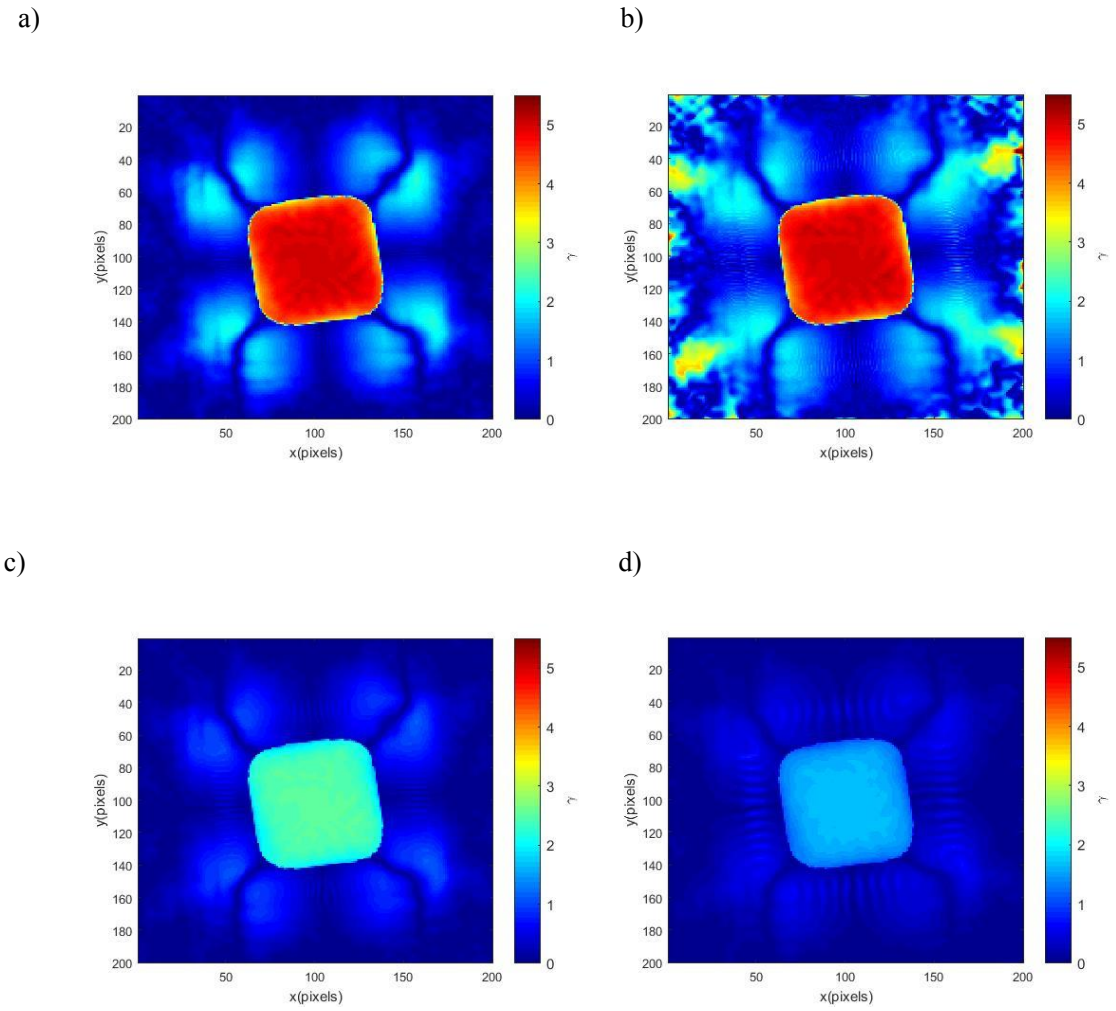

Figure 5.6. The γ-index arrays for three different criteria described in the text.

The regions of low γ-index value at the periphery of the distributions are common to all cases. Other parts that have low γ-index values are stripes emerging from beam corners that coincide with low dose difference values seen in Figure 5.5.

5.3 Simulation results: properties of the squared gamma distribution

5.3.1 1D dose distributions

Two 1D dose distributions (profiles) for 6 MV photon beams, measured at the depth of maximum dose and at 10 cm depth in a water phantom, fitted with the theoretical curves [19] depicted in Figure 5.1 were used in this investigation. The parameters of the function fit as described in Chapter 4 were used to calculate the continuous function D(x) that was considered as the calculated dose distribution in further investigations; D denotes the dose and x the spatial coordinate. According to the χ^2 distribution with one degree of freedom, 5% of the values should be greater than 3.841, given that there is no true deviation (Figure 5.7).

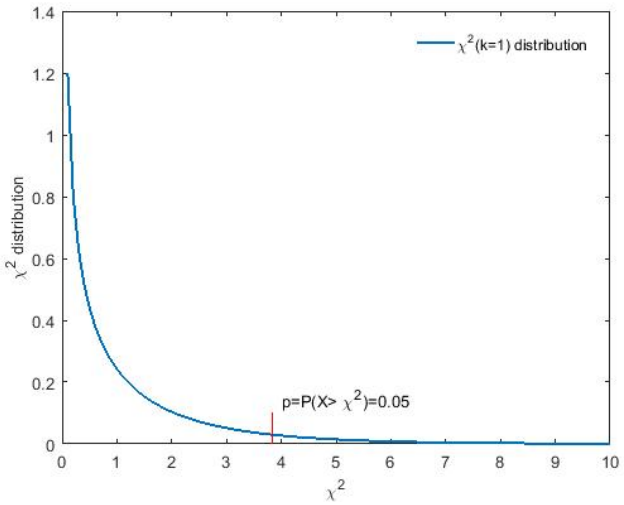

Figure 5.7. χ^2- probability density distribution with one degree of freedom.

Figure 5.8 shows good agreement for 1D dose distribution (6 MV photon beam profile at d_{max}), using a sets of simulation parameters: σ_D=1 cGy and σ_x=1 mm (5.8a), σ_D=2 cGy and σ_x=2 mm (5.8b), and σ_D=3 cGy and σ_x=3 mm (5.8c), where γ^2-distribution follows very well the χ^2-distribution with one degree of freedom.

a)

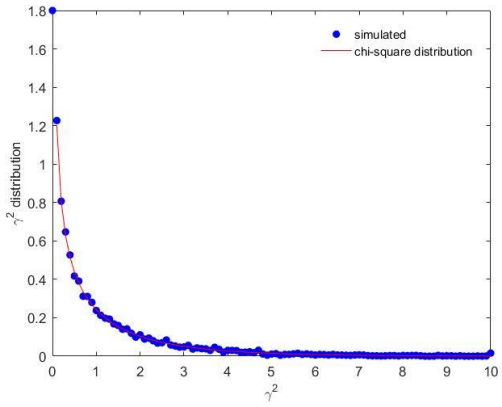

b)

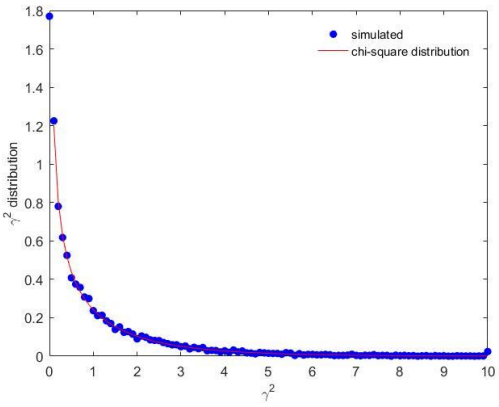

c)

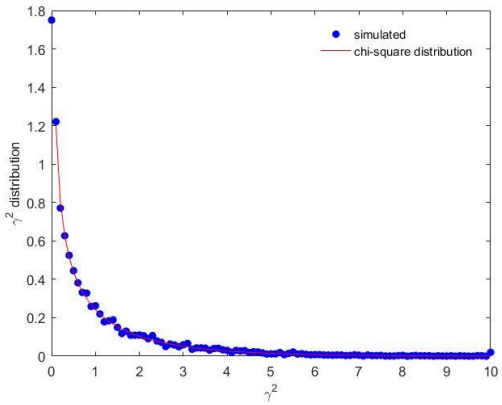

Figure 5.8. Distribution of gamma values in 1D for different set of simulation parameters: σ_D=1 cGy and σ_x=1 mm (a), σ_D=2 cGy and σ_x=2 mm (b), and σ_D=3 cGy and σ_x=3 mm (c).

The γ^2-distributions simulated for other points along x-axis between -1.6 cm to 1.4 cm for the profiles determined at d_{max} and 10 cm depth, respectively, noticeably follow similar results i.e., that the rate of failure stays close to 5% (Figure 5.9) along with all positions x-axis regardless of the shape of the dose distribution and the absorbed dose gradient.

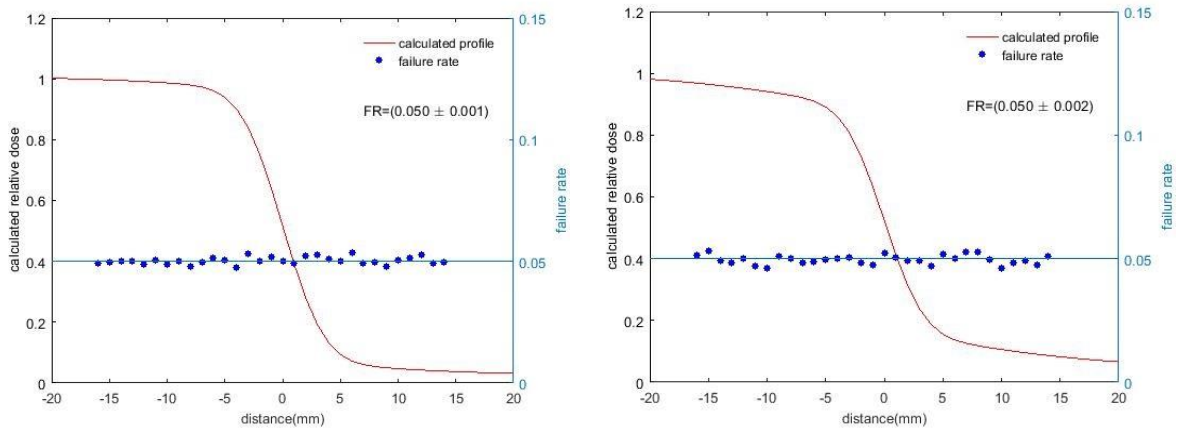

a) b)

Figure 5.9. Failure rate obtained by simulations at points along the x axis in the range from -1.6 cm to 1.4 cm for the profiles determined at a) d_{max} and b) 10 cm depth.

Summary of failure rate results for simulations at points along x-axis for different dose difference and DTA criteria, 1 cGy/ 1mm, 2 cGy/2 mm and 3 cGy/3 mm are presented in Table 5.4. All failure rate values are close to 5%.

Table 5.4 Summary of failure rate results for simulations at points along x-axis for different dose difference and DTA criteria, 1%/ 1mm, 2%/2 mm and 3%/3 mm.

	Dose difference (%)/ DTA (mm) criteria		
1D dose distribution at:	1 cGy/1 mm	2 cGy/2 mm	3cGy/3 mm
d_{max}	0.050±0.001	0.050±0.002	0.049±0.002
10 cm	0.050±0.002	0.049±0.003	0.050±0.002

5.3.2 2D dose distribution

The 2D dose distribution case was based on an IMRT field used in the treatment of a head and neck tumour localisation calculated by the *Oncentra Master Plan* treatment planning system. IMRT fields were maintained from the patient treatment plans but transferred to a phantom geometry. The 2D dose distribution at the depth of 5 cm was chosen from the stack of calculated planes.

In Figure 5.10, the γ^2-distribution (blue circles) is shown for the position (x,y) marked with a black cross. The γ^2-distribution follows very well the χ^2-distribution (red curve).

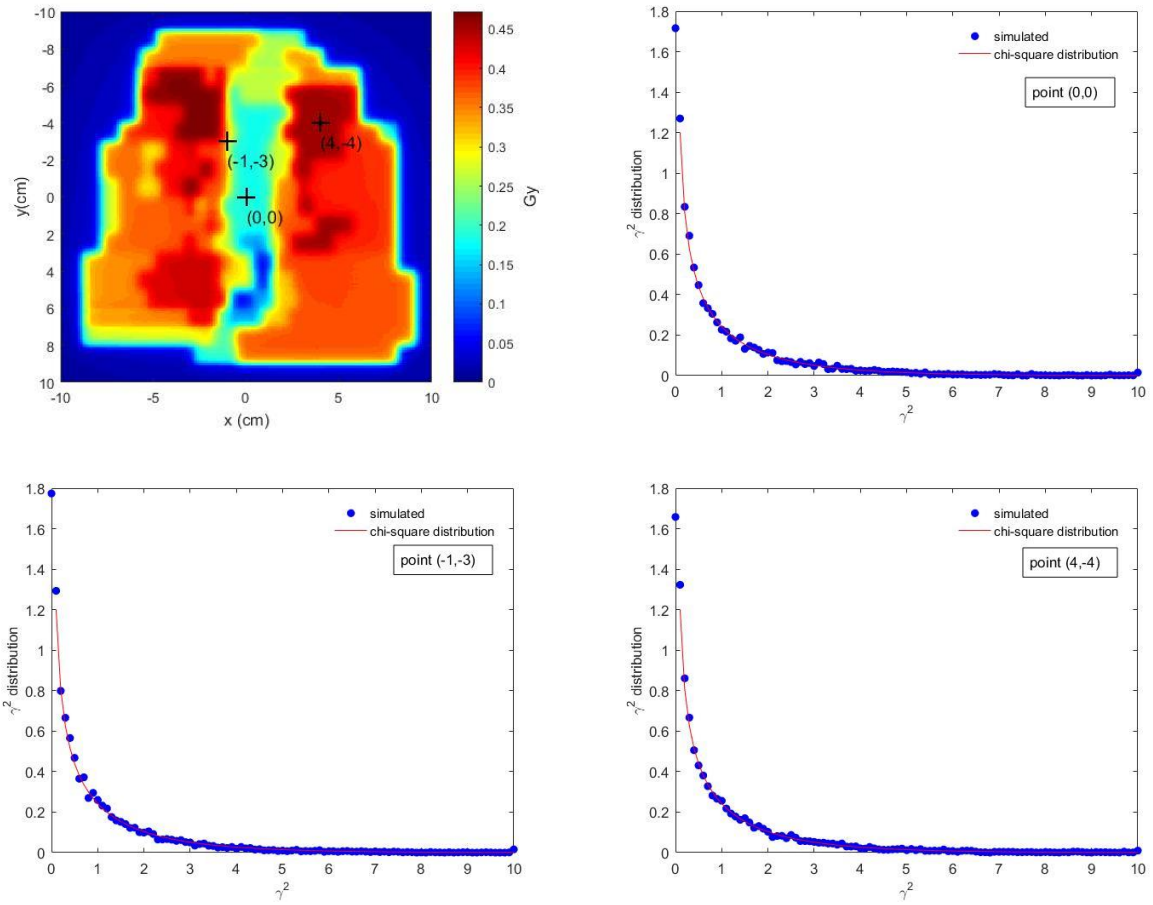

Figure 5.10. Left: 2D dose distribution based on an IMRT field calculated at 5 cm depth; black crosses mark the selected points in which the failure rates were calculated. Right: The distribution of γ^2 values versus γ^2 calculated at the point (0,0) in 2D dose distribution. Down: The distribution of γ^2 values versus γ^2 calculated at the points (-1, -3) left and (4, -4) right, in 2D dose distribution.

The original 2D dose distribution (401×401 pixels, 1 mm pixel size) was resized (scaled) using a range of scale factors and the simulations were repeated to calculate failure rates for these resized distributions for points indicated in Figure 5.10. For the scale factor greater than 1 the output, resized distribution, has larger matrices than the input. For instance, a scale factor of 0.1 resizes the original 2D distribution into a 41×41 pixels distribution. A bi-cubic interpolation was used in resizing dose distributions.

Figure 5.11 shows the fraction of values above 3.841, the failure rate, for the acquired γ^2-distribution as a function of a scale factor for three positions indicated by crosses in Figure 5.10. It shows that the failure rate does not always stay at 5% for points different from (0,0), the point located under the block. The point (-1, -3) is in the high dose gradient region, whereas the point (4, -4) is in the high dose region. In case of 3 cGy/3 mm criteria, the failure rate stays at about 5% for points (0,0) and (4, -4), and ~3% for the point in the high dose gradient region, for all

scale factors even below 1. Similar behaviour is visible for the 2 cGy/2 mm criteria. Nevertheless, for tighter criteria of 1%/1 mm the deviation from 5% towards higher failure rates appear for the point in the high dose gradient region.

This was an indication that the approximation is not good enough for points where the dose gradient is high. Therefore, the investigations were expanded to examine the second derivative at these points because the second derivative was presumably making the approximation break down.

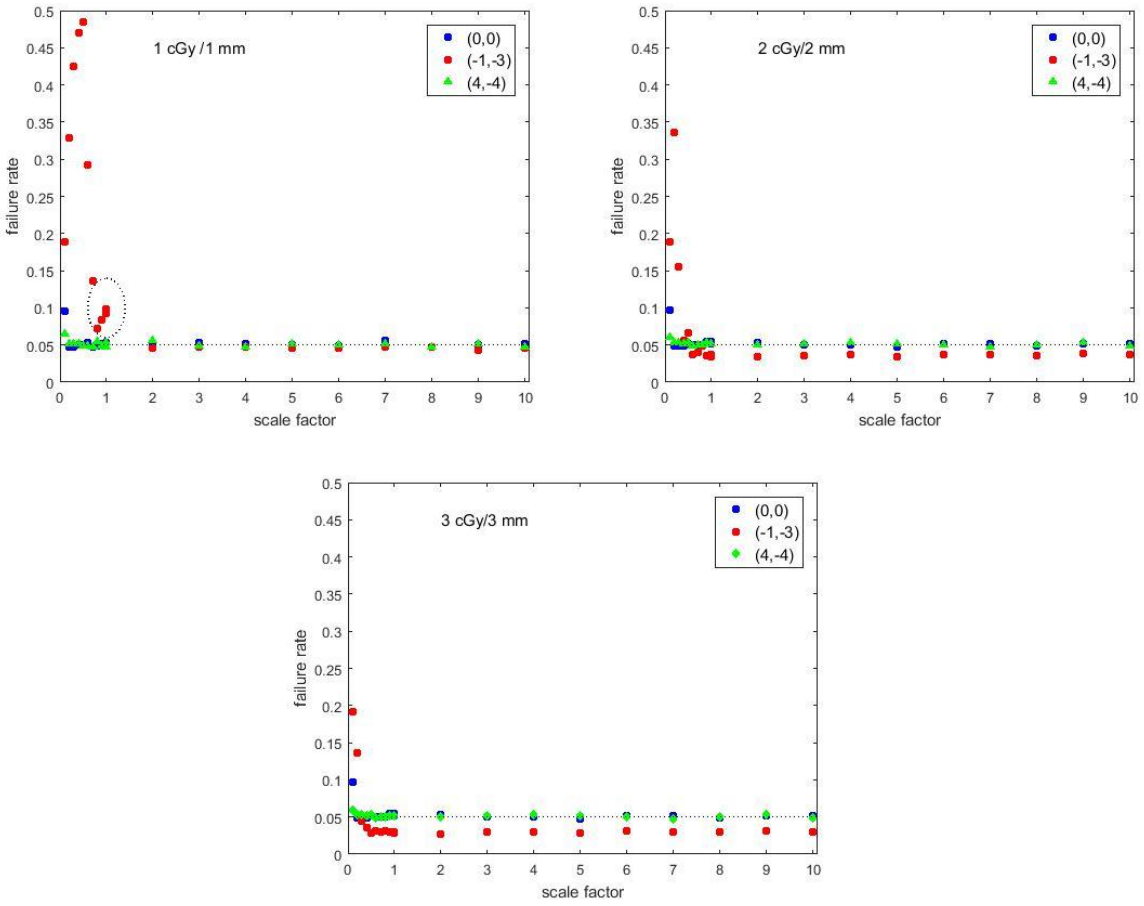

Figure 5.11. Failure rates obtained by simulations as a function of scale factor for points at position (0,0), (4, -4) and (-1, -3) and for three different values of acceptance criteria σ_D (1,2,3 cGy) for the dose difference and to $\sigma_{x,y}$ (1,2,3 mm) for DTA.

5.4 Results - simulation of a detector-array measurement in IMRT

The simulations for a detector array were done for 100 detectors and 400 detectors. Two different groups of dose distributions with the spatial resolution 1 mm (denoted as D1, D2 and D3) and 3 mm (F1, F2, F3) were used.

The dose distributions, calculated at the depth of 5 cm in a phantom, were used in simulations and the simulated detectors were distributed at a 1 cm distance, in an array of 10×10 or 20×20.

The simulation parameters were: 1, 2, 3 % uncertainty in the dose distribution (*sigdos*) and 1,2,3 mm for the spatial uncertainty (*sigpos*) combined into three pairs 1%/1 mm, 2%/2 mm and 3%/3 mm.

Figure 5.12 shows the failure rate probability distributions as functions of the failure rate obtained from the detector array simulations utilizing the F1 dose distribution calculated at the depth of 5 cm in the uniform phantom. The pixel size of the dose distribution is 3 mm × 3 mm. In this simulation case, the detector array had 100 detectors separated 1 cm and the spatial uncertainties $\sigma_{x,y}$ and dose uncertainties σ_D were 1, 2 and 3 mm, and 1, 2 and 3%, respectively. The failure rate probability distribution (y-axis) was obtained from the raw failure rate values calculated in 10^4 simulations as the number of observations per histogram bin divided by the total number of observations. The binomial probability distribution with parameters n=100 (detectors) and p=0.05 is added to the graph for comparison.

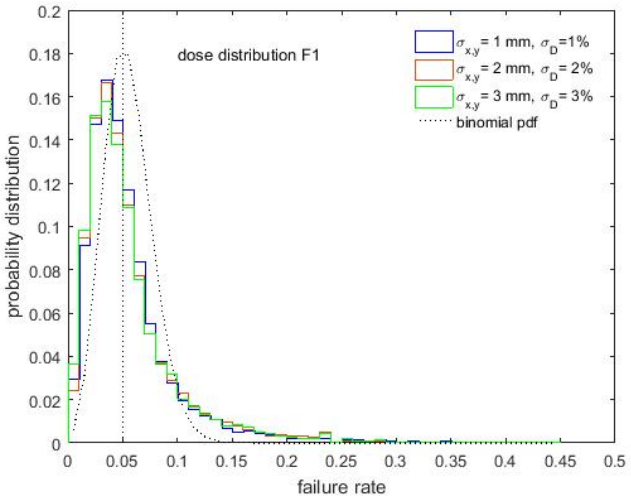

Figure 5.12. Failure rate probability distribution vs failure rate for the F1 dose distribution for three pairs of simulation parameters (1%/1 mm, 2%/2 mm and 3%/3 mm). The binomial distribution is added for comparison.

The results for other the two dose distributions (F2, F3) are shown in Figure 5.13. Clearly, for all three dose distributions, the probability distribution function preserves the shape with minimal differences, but the peak centroid position is shifted towards the lower failure rate value of about 4% rather than 5%, expected from the binomial distribution (n=100 and p=0.05).

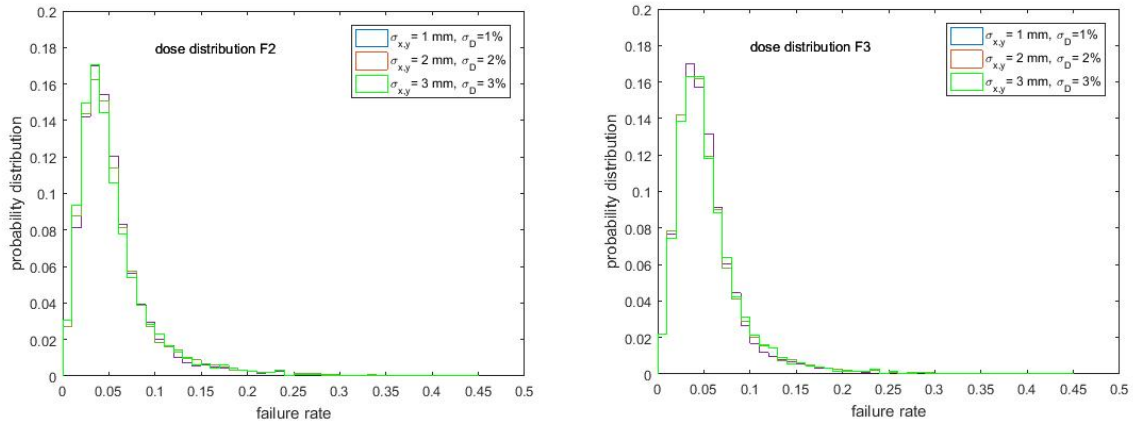

Figure 5.13. Failure rate probability distribution as a function of the failure rate for the F2 and F3 dose distributions and three pairs of simulation parameters: 1%/1 mm, 2%/2 mm and 3%/3 mm.

Figure 5.14 illustrates the simulation results obtained for a single set of simulation parameters (1%/ 1 mm) for three dose distributions (F1, F2, F3).

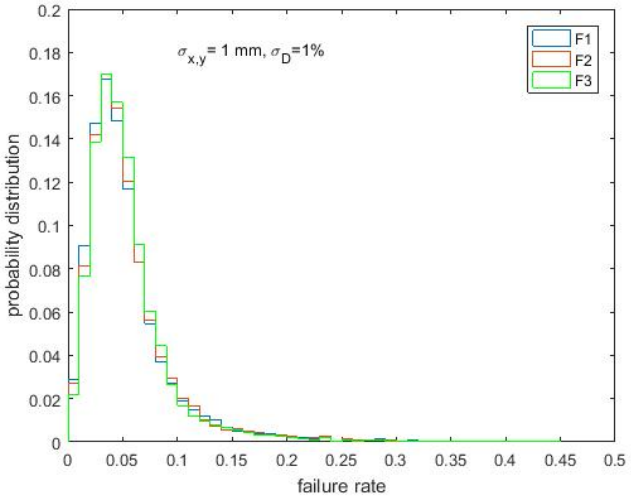

Figure 5.14. Failure rate probability distribution vs failure rate for three dose distributions (F1, F2, F3) and a single set of simulation parameters (1%/ 1 mm).

Another set of simulations was done for 3 dose distributions having the spatial resolution of 1 mm; distributions are denoted by D1, D2 and D3. Since very similar results were obtained, only one result for the dose distribution D1 is shown (Figure 5.15).

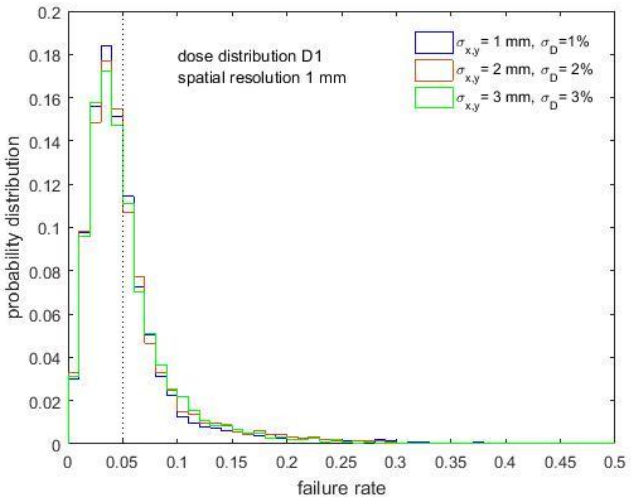

Figure 5.15. The results as in Figure 5.12 but for the dose distributions having higher spatial resolution (1 mm).

The next figure (Figure 5.16) shows the results of simulations conducted using three pairs of simulation parameters: 1%/1 mm, 2%/2 mm and 3%/3 mm, for D1 dose distribution and with the spatial resolution of 1 mm like the one for which the results are shown in Figure 5.15. The number of detectors has been increased to 400.

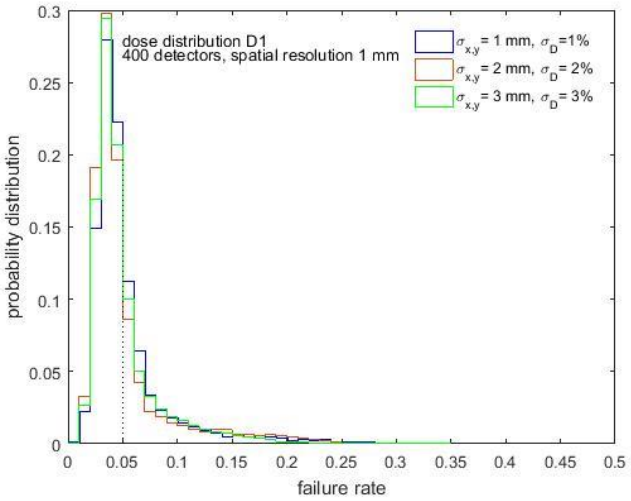

Figure 5.16. Failure rate probability distribution vs failure rate for D1 dose distribution for three pairs of simulation parameters (1%/1 mm, 2%/2 mm and 3%/3 mm) and for 400 detectors.

As expected, because the individual detector points are not statistically independent, there is a discrepancy between the simulated probability distributions and the theoretical binomial distribution. Therefore, the theoretical cumulative dose distribution cannot be used to accurately relate the tolerance levels and observed failure rates. Instead, an empirical cumulative distribution function (ECDF) is constructed from the simulation results. The ECDF calculated

for the dose distribution F1 and simulation parameter values of 1% and 1 mm is given in Figure 5.17. Then, by calculating the inverse ECDF for a desired probability, a corresponding maximal failure rate tolerance level can be obtained. For instance, the probability is 5% (1-0.95) that the failure rate exceeds 14%.

This can be interpreted as a maximum expected failure rate, if the deviations are only due to random variability. If the observed failure rate is larger than this value, the deviations would probably not be only due to random variability, at a significance level of α=0.05.

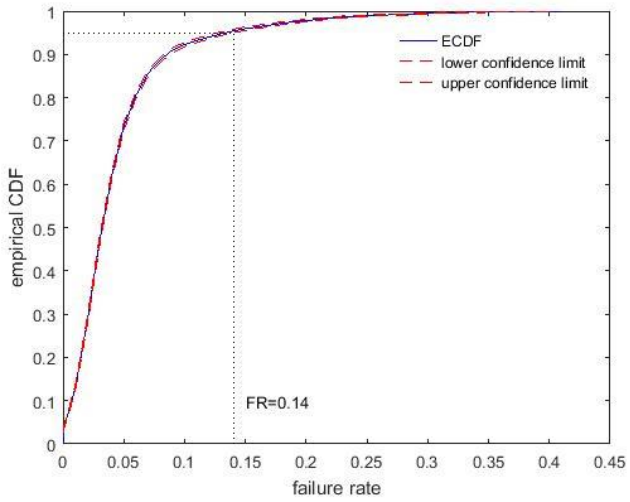

Figure 5.17. Empirical cumulative distribution function (ECDF) constructed for the dose distribution F1 and the parameter values of 1% and 1 mm.

An example of the ECDF calculated by averaging curves obtained for three dose distributions and simulations of a detector array with 400 detectors and parameters 1%/ 1 mm is shown in the Figure 5.18. In this case, the probability is 5% that the failure rate exceeds ~13%. The function uncertainties indicated are the standard deviations of the mean values. This allows to estimate the uncertainty of the derived failure rate. The variability of the ECDF should be checked for larger number of ECDFs to evaluate the accuracy and robustness of the proposed scheme.

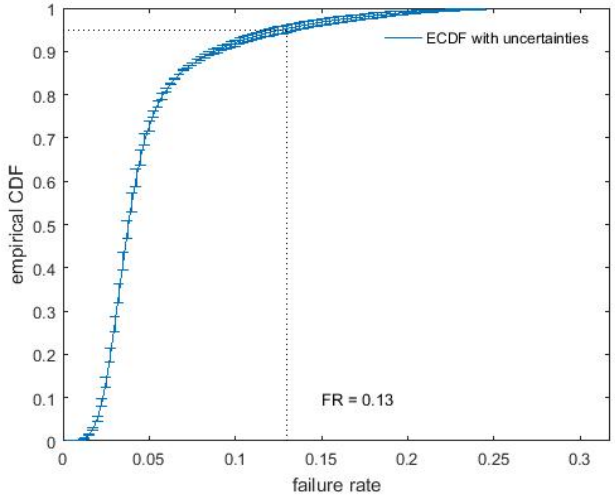

Figure 5.18. The average empirical cumulative distribution function (ECDF) with uncertainties calculated from the simulation data for the dose distributions F1, F2, and F3, 400 detectors and simulation parameters 1%/ 1 mm.

5.5 Clinical IMRT distributions

Thirty (30) clinical, head and neck (H&N), IMRT fields, in further text denoted by F1-F30, were created on the CT images of the uniform phantom. The absorbed dose distributions for each IMRT field was calculated using TPS at the position of a detector.

As an example, the absorbed dose distribution of one of the IMRT fields (F1) is shown in Figure 5.19.a. The corresponding absolute value of the second-order derivative (Gy/cm^2) is shown in Figure 5.19.b. The near-edge effects are illustrated with an enlarged corner area.

A typical histogram of the dose distribution values recorded at 5 cm depth is depicted in Figure 5.19.c and distribution of the second-order derivative for the same dose distribution is given in Figure 5.19.d.

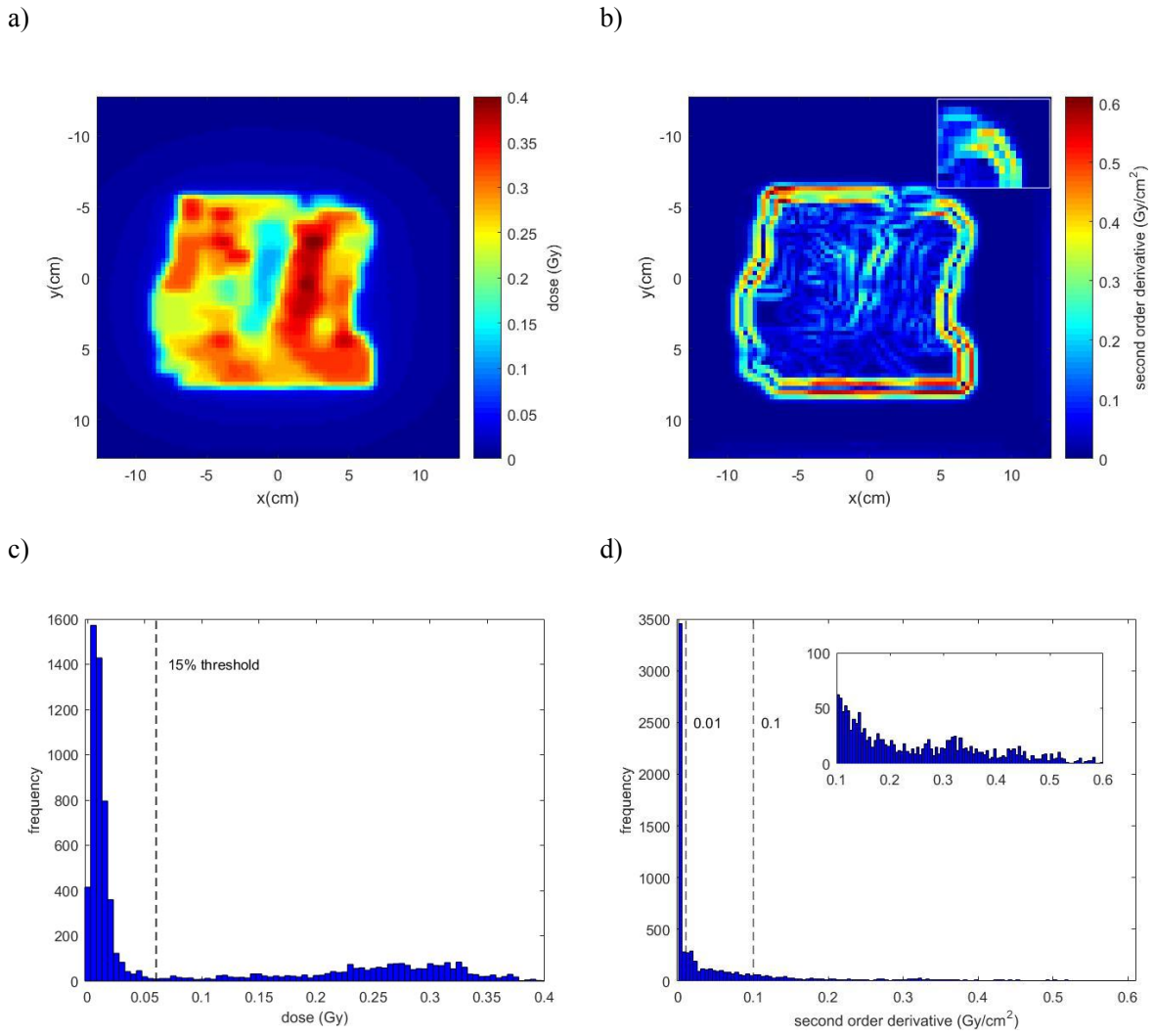

Figure 5.19. (a) Absorbed dose distribution at 5 cm depth calculated using the TPS for a clinical IMRT study, (b) the map of the corresponding second derivative values of the dose distribution shown in (a) with an enlarged map area in the upper right corner; (c) The dose-frequency histogram versus dose; vertical line indicates the threshold value of 15% of the maximum dose observed in the dose distribution, and (d) frequency distribution of second-derivative values; vertical lines indicate the limits of second-order derivative value bins used in further quantitative analyses.

For this particular case (dose distribution F1), the spatial distribution of a large number of gamma values as a function of the measured coordinates x and y for the whole 19 × 19 matrix of simulated detector positions were calculated for several $\sigma_{x,y}$ values ($\sigma_{x,y}$ denotes that the same σ was used in both spatial dimensions). The resultant distributions for $\sigma_{x,y}$=1, 3 and 6 mm and σ_D=1% are shown in Figure 5.20. No dose threshold was applied.

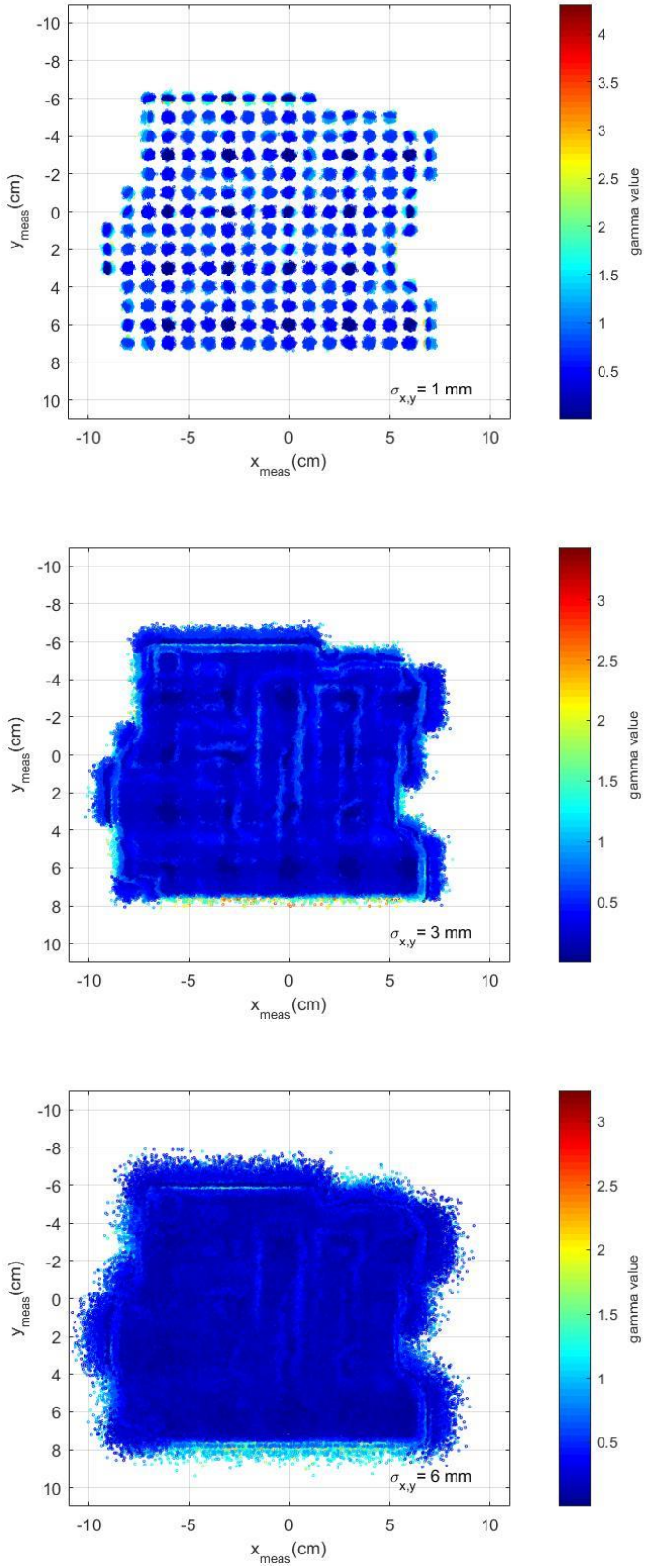

Figure 5.20. Spatial distributions for γ-index values calculated per point for the whole 19 × 19 matrix of simulated detector positions, shown as a function of the measured coordinates x and y. The calculations were carried out for 1, 3 and 6mm spatial uncertainty (from up to down).

For the same case, using the simulation parameters $\sigma_{x,y}$=3 mm and σ_D=1% chosen for standard deviations of the spatial coordinates and absorbed dose, respectively, the failure rate frequency distribution, separated into three components corresponding to low (<0.01), medium (>0.01, <0.1), and large (>0.1) values of the second derivative of the absorbed dose distribution, without a dose threshold applied during the simulation, is shown in Figure 5.21a. As expected, given that the approximation in Eq. (4.15) is valid, there is a distinct peak at 0.05. This corresponds to the failure rate that should be expected with the given acceptance criteria. For higher SOD-values, however, the peak is less distinct, and there is also evidence for higher failure rates. The relation between high SOD-values and the occurrence of higher failure rates is also illustrated by Figure 5.21b, which shows the failure rate values for the different measurement points, where the occurrence of high failure rates, marked in red colour, correlates with the calculated high values of the second derivative as depicted in the Figure 5.19b

a)

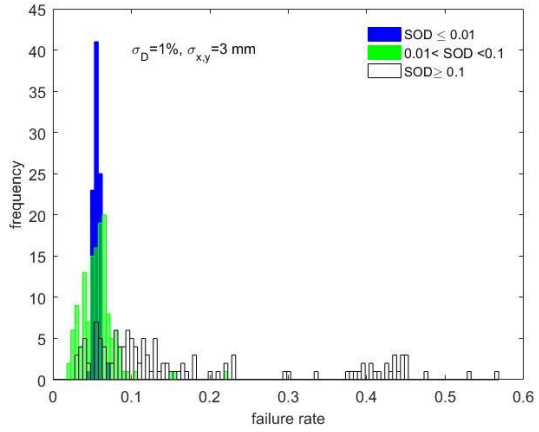

b)

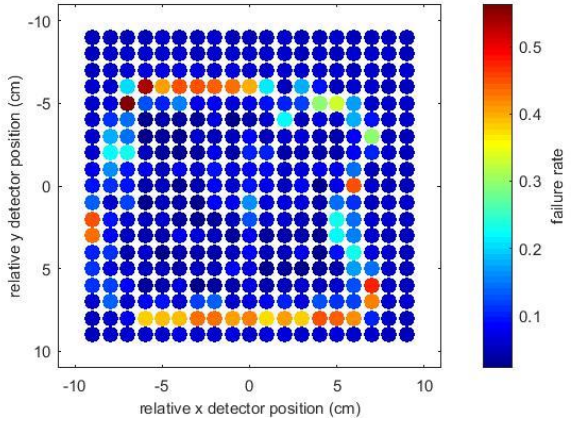

c)

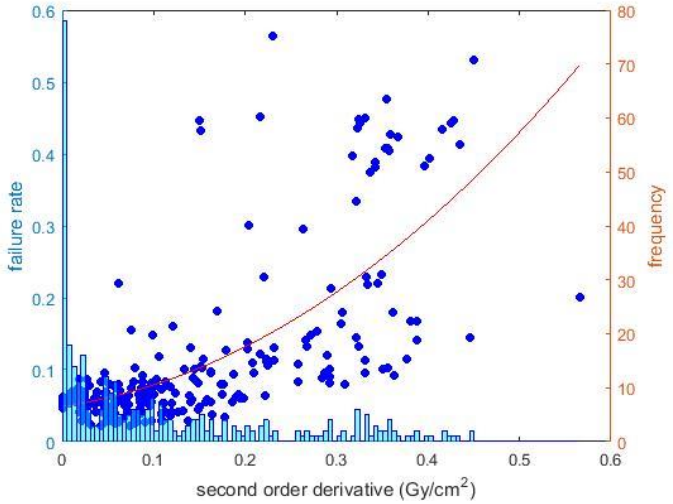

Figure 5.21. a) Failure rate frequency distribution for the F1 distribution separated into three components corresponding to different values of the second derivative of the dose distribution. (b) 2D distribution of failure rate values for the different simulated measurement points (matrix 19 × 19) in the F1 distribution. (c) Combined scatter graph of failure rates vs SOD and failure rate frequency histogram.

Figure 5.21c shows a simulation result of the calculated failure rates as a function of SOD for simulation parameters for standard deviations of the spatial coordinates, $\sigma_{x,y}$=3 mm, and absorbed dose σ_D=1%. The left y-axis is related to the calculated failure rate marked with blue circles and the right one shows the frequency of observed failure rate values. A red line is added to the graph just for visualising the trend of failure rates vs SOD.

The presented case (dose distribution F1) is representative of all tested fields (n=30). About 60% of the points in the dose distributions had relative values below the dose threshold of 15% of the maximum dose recorded in the dose distribution. The second-order derivative was less than 0.01 in more than 50% of the points, and less than 0.1 in about 80% of the points.

The k-sample Anderson-Darling test is a nonparametric statistical method that tests the hypothesis that the populations from which two or more groups of data were drawn are identical. Every group should be an independent random sample from a population.

The k-sample Anderson-Darling test showed that the hypothesis that independent distribution samples (sample size=381) of second-order derivatives calculated for all 30 distributions (images) were drawn from a common parent distribution could not be rejected at the level of significance of 0.05. This was a rationale to randomly select 10 dose distributions for further detailed processing.

A very consistent pattern of the calculated failure rates as a function of SOD for all 30 dose distributions is depicted in Figure 5.22a. For a subset of 10 dose distributions, the calculated failure rates vs the second derivative with a dose threshold of 15%, as shown in Figure 5.22b, gives a very similar result compared to the non-threshold failure rates. The reduced number of points in the low second derivative value range in the graph results from the fact that this is also the range that corresponds to the low-dose points (i.e., below the threshold) in the dose distribution.

a)

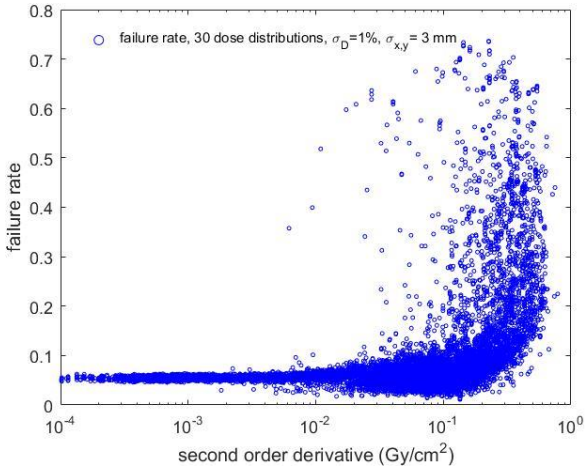

b)

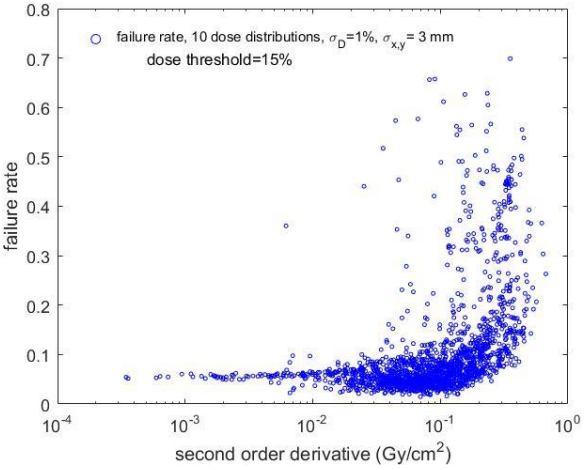

Figure 5.22. (a) Failure rates as functions of second derivatives calculated for 30 images with the simulation parameters of σ_D=1% for the random absorbed dose measurement deviation and 3 mm random spatial displacement. (b) A random subset (n=10) of dose distributions simulated with the same parameters as for Figure 5.21a, but with a 15% dose threshold applied.

For the subset of 10 absorbed dose distributions, taken from the parent set (n=30) of distributions, simulations were carried out for a range of random spatial displacement values

from 1 to 9 mm and random absorbed dose measurement deviation of 1%, 2% and 3%. As an example, the failure rate versus the second-order derivative, calculated for $\sigma_{x,y}$=1, 3, 6 and 9 mm, σ_D=1%, and a 15% dose threshold, is shown in Figure 5.23a. For further analysis, the obtained failure rate distributions were divided into three bins with different values of the second derivative, below 0.01, between 0.01 and 0.1, and above 0.1, as indicated by the vertical lines in Figure 5.23a. The failure rate frequency distributions in the range of SOD-values between 0.01 and 0.1, and for four values of $\sigma_{x,y}$ (1, 3, 6 and 9 mm), are depicted in Figure 5.23b. The vertical dashed line indicates the position of the 0.05 failure rate.

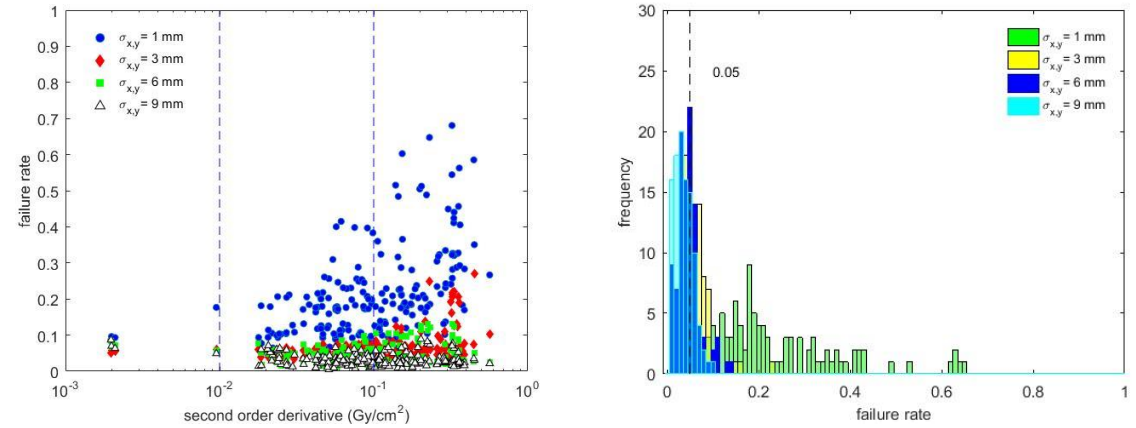

a) b)

Figure 5.23. (a) Failure rate versus secondary derivative calculated for dose distribution F1 and for four values of positional uncertainty (1, 3, 6 and 9 mm) and dose uncertainty of σ_D=1%. Vertical lines limit bins of secondary derivative values; (b) Frequency distributions of the failure rates constructed for the central bin of second derivatives (values 0.01–0.1) depicted in Figure 5.23a.

Figures 5.24a and 5.24b show the median of the failure rate frequency distribution, as a function of the spatial uncertainty used in the simulations, for the two bins having SOD-values between 0.01 and 0.1, and over 0.1. The remaining bin, with SOD-values below 0.01 does not contain any important information when the 15% threshold is applied in simulations.

a)

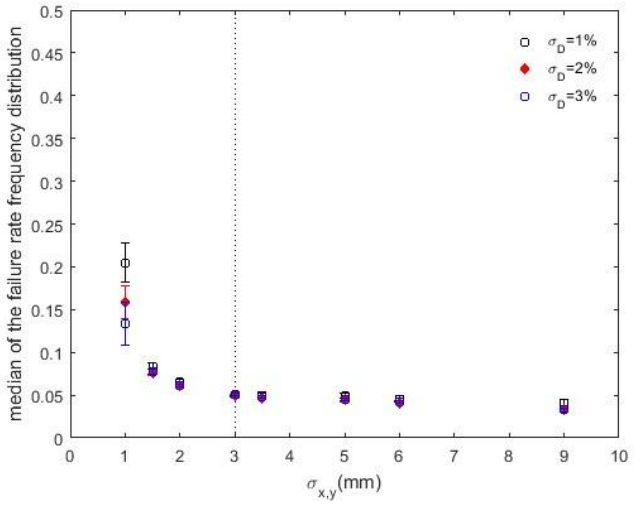

b)

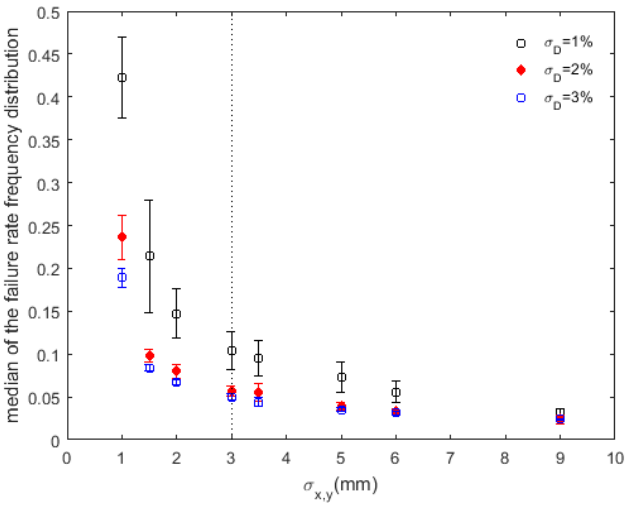

Figure 5.24. Median values of failure rate distributions calculated for the range of standard deviations for the spatial coordinates (1-9 mm) and absorbed dose (1-3%) for the two bins of SOD values between 0.01 and 0.1 (a), and above 0.1 (b).

From Figure 5.24a it is apparent that the median value for spatial uncertainties above 3 mm (i.e., equal to or above the spatial resolution of the calculated dose matrix) is very close to 0.05, and that the dose uncertainty in the range of 1-3% has practically no influence on the median of the distribution. A similar pattern is shown in Figure 5.24b for the higher SOD values, except for the lowest value of the dose uncertainty, σ_D=1%.

In a validation data set of additional 5 clinical, head and neck IMRT fields, taken from the parent set (n=30) of dose distributions, simulations were carried out for a limited range of random spatial uncertainties, 1, 2, 3, 5 and 9 mm, and random absorbed dose measurement

deviation of 1%, 2% and 3%. Again, 10^4 simulations were performed to obtain the failure rates vs SOD results. The median values of the failure rate frequency distributions, as a function of the spatial uncertainty used in the simulations, for the two bins having SOD-values between 0.01 and 0.1 (Table 5.5), and over 0.1 (Table 5.6) were calculated.

Table 5.5 Median values of failure rate distributions calculated for the initial set of IMRT fields and the validation set for a range of SOD values between 0.01 and 0.1 [Gycm^{-2}] and the limited set of the spatial coordinate standard deviations, $\sigma_{x,y}$ =1,2,3,5 and 9 mm and random absorbed dose measurement deviation of 1%, 2% and 3%.

	0.01<SOD<0.1 [Gycm^{-2}]					
	σ_D=1%		σ_D=2%		σ_D=3%	
$\sigma_{x,y}$ (mm)	Initial set (n=10)	Validation set (n=5)	Initial set (n=10)	Validation set (n=5)	Initial set (n=10)	Validation set (n=5)
1	0.205±0.023	0.194±0.011	0.158±0.019	0.159±0.026	0.134±0.025	0.138±0.036
2	0.065±0.004	0.067±0.001	0.061±0.002	0.063±0.002	0.061±0.001	0.063±0.002
3	0.051±0.003	0.055±0.003	0.049±0.002	0.054±0.002	0.051±0.002	0.055±0.001
5	0.049±0.004	0.052±0.004	0.045±0.002	0.050±0.003	0.045±0.002	0.050±0.002
9	0.040±0.005	0.049±0.006	0.033±0.003	0.042±0.004	0.032±0.002	0.040±0.004

Table 5.6 Median values of failure rate distributions calculated for the initial set of IMRT fields and the validation set for a range of SOD values larger than 0.1 [Gycm^{-2}] and the limited set of the spatial coordinate standard deviations, $\sigma_{x,y}$ =1,2,3,5 and 9 mm and random absorbed dose measurement deviations of 1%, 2% and 3%.

	0.1<SOD [Gycm^{-2}]					
	σ_D=1%		σ_D=2%		σ_D=3%	
$\sigma_{x,y}$ (mm)	Initial set FR (n=10)	Validation set FR (n=5)	Initial set FR (n=10)	Validation set FR (n=5)	Initial set FR (n=10)	Validation set FR (n=5)
1	0.423±0.047	0.531±0.043	0.236±0.026	0.309±0.030	0.189±0.011	0.232±0.016
2	0.147±0.029	0.238±0.047	0.080±0.008	0.106±0.016	0.067±0.003	0.074±0.008
3	0.104±0.022	0.174±0.035	0.057±0.006	0.077±0.010	0.050±0.004	0.059±0.006
5	0.073±0.018	0.103±0.021	0.039±0.004	0.051±0.007	0.035±0.002	0.042±0.004
9	0.031±0.005	0.048±0.008	0.024±0.005	0.033±0.004	0.024±0.001	0.030±0.002

Whereas the results in Table 5.5 show good agreement between the median FR values in the initial and the validation set for the whole range of absorbed dose measurement and spatial standard deviations when the SOD values are limited to the range 0.01- 0.1 Gycm^{-2}, in the higher SOD value range (>0.1) (Table 5.6) this is lost due to much larger spread of individual FR results and skewness of the distribution. Nevertheless, regardless of generally higher median values, the global trend of FRs is preserved and it does not alter the conclusions drawn from the results presented in Figure 5.24.

An interesting feature of the distribution of γ-index values calculated in these simulations for an individual detector position can be observed from the constructed frequency histogram

distribution. The analysis has been done for a few detector points and the distributions of γ-index values were created in 10^4 simulations. The characteristics of the γ-index value frequency histogram stem mainly from the interplay of variables such as the shape of the dose distribution including the present dose gradients, spatial resolution of the dose distribution, dose difference and DTA applied and the level of the interpolation of the dose distribution utilized in searching the minimum γ-index values. However, the pattern of distinct peaks that can be observed in histograms can be related to the sample size (finite resolution) used in calculating the minimum γ-index values. For a sample size (1 mm) used in simulations above using the dose distributions with the spatial resolution of 3 mm and the $\sigma_{x,y}$=1 mm and σ_D=2% from the definition of the γ-index:

$$\gamma^2 = \left(\frac{x_d - x_m}{1.96\sigma_x}\right)^2 + \left(\frac{y_d - y_m}{1.96\sigma_y}\right)^2 + \left(\frac{D_d - D_m}{1.96\sigma_D}\right)^2 \quad (5.1)$$

The position of the first peak at ≈0.510 is determined by the term $\sqrt{(1\text{ mm})^2/(1.96\cdot 1\text{ mm})^2}$ as indicated in Figure 5.25a. The next visible peaks such as in the Figure 5.25b, corresponds to the values of $\sqrt{(1\text{ mm})^2/(1.96\cdot 2\text{ mm})^2}\approx 0.255$ and to the $\sqrt{(1\text{ mm})^2/(1.96\cdot 2\text{ mm})^2+(3\text{ mm}^2/(1.96\cdot 2)}\approx 0.807$. The same reasoning can be applied to get the peaks in Figure 5.25c, noting that the standard deviation of the spatial coordinates is 3 mm.

The values in between two peaks come from the dose difference contribution, and as the gamma value increases at some value, determined by the spatial step suddenly the dose and spatial difference start contributing to the gamma histogram bin and the peak appears. Similarly, the peaks can be associated with spatial γ-index properties.

a)

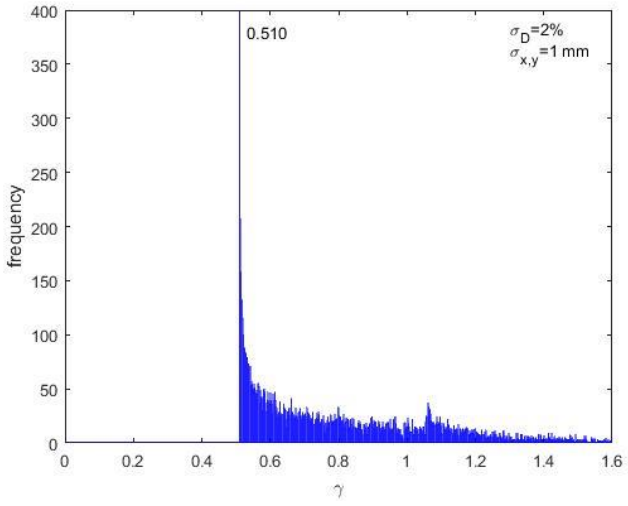

b)

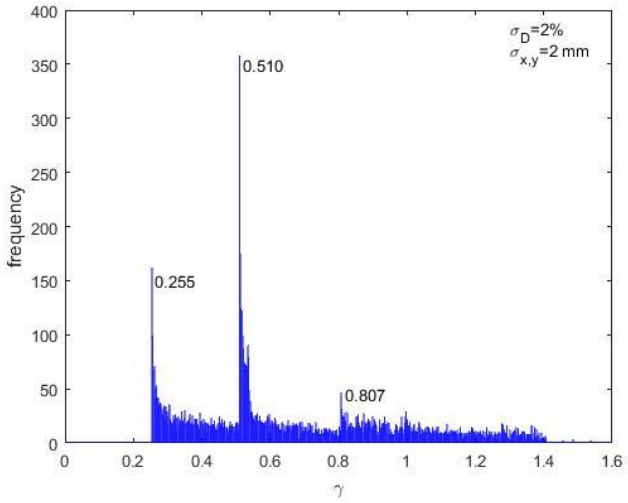

c)

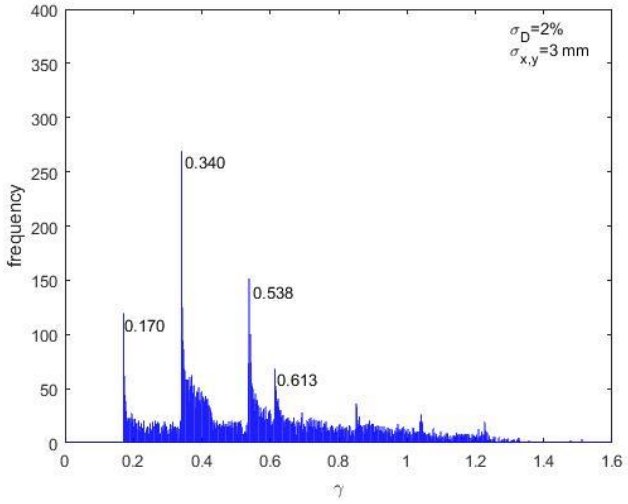

Figure 5.25. γ-index frequency histograms for a single point in a dose distribution obtained in simulation in which the dose difference and distance-to-agreement were replaced by the standard deviations of the spatial coordinates and dose for three pair of values (σ_D=2% combined with $\sigma_{x,y}$=1,2 and 3 mm).

Chapter 6
DISCUSSION

6.1 Introduction

The objective of external beam radiotherapy is to deliver a high absorbed dose to the tumour volume while sparing the normal tissue and nearby organs. Besides, the other important components in radiotherapy treatment planning process, accurate dosimetry and design of the patient treatment plan are essential to assuring the goals of radiotherapy can be reached.

After the period of matured use of 3D conformal radiotherapy, the advent of IMRT and VMAT dose delivery with MLC equipped linear accelerators, producing the complex shapes of dose distributions, urged for better understanding of dosimetry tools and their limitations in measuring these distributions to guarantee the quality of the IMRT/VMAT implementation. The complexity of technology increases potential uncertainties and inaccurate and poor delivery reproducibility can have clinical implications [76].

Patient specific QA of IMRT/VMAT is critically important and facilitates its successful and reliable clinical implementation. The methodology includes several dosimetric tasks that are performed before the treatment of each patient. By checking the accuracy of dose calculation, treatment plan transfer and the delivery, patient specific QA assures ultimately the correct delivery of the prescribed dose to patients. Several documents prepared by professional societies recommend patient specific QA as part of the whole IMRT/VMAT process [45-47], [77, 78].

The absorbed dose distribution complexity and decoupling of the beam geometry and the dose delivered to the target mean that the QA of IMRT dose distributions should preferably be more focused on the composite delivered dose rather than on the QA of beam segments. Furthermore, the dose should be checked at multiple points. Since this type of radiotherapy includes high dose gradient regions that are tailored to target volumes while avoiding healthy tissue, both the absolute and relative dose gradient positions need to be verified with QA measures.

While the acceptance criteria for the radiotherapy treatment unit and treatment planning systems are established and well understood, the patient specific IMRT QA acceptance criteria in different institutions vary considerably. This is a consequence of the different dose delivery systems, treatment planning system algorithms and their practical implementation as well as the measurement equipment used in conducting QA programme [38].

Different sources cause errors in IMRT/VMAT planning and delivery. In the first category, the TPS errors, the most important factors that can lead to erroneous treatment planning are the ways how MLC leaf end and tongue and groove effect are modelled, the transmission of the collimator and MLCs, small beam output factors and off-axis dose profiles. The choice of the dose calculation grid size can cause errors and artefacts, as well as the heterogeneity correction models utilised in dose calculation algorithms.

The uncertainties of the dose delivery system also affect delivery accuracy. This comprises potential MLC leaf position errors, the motion of leaves, and characteristics such as the beam flatness, symmetry, dose rate and beam segments with a small number of MU-s.

The QA patient specific measurements, analysis tools and sometimes inadequate understanding of their characteristics may lead to additional uncertainties in QA results and poor interpretation.

In the further discussion, the focus is on the radiotherapy treatment verification that can be reduced to the dose comparison process aiming at determining whether the reference and evaluated dose distributions agree to within some clinically significant limits. Extensive research in this field has been conducted within the past almost 30 years [16, 17], [19, 20], [55, 56], [58], [65], [79]. Early dose distribution comparison metric proposals included the simple dose difference test, distance-to-agreement (DTA) and the composite dose difference and DTA test [55, 56]. The limitations of these metrics were instantly recognised, and researchers explored options for improvements.

In 1998, the gamma index analysis was proposed [19] and with different variations and revisions of formalism [20], [22], [58] and modifications aiming at improved calculation speed [59], [61-64] stayed until now the most commonly used dose comparison metric [60], [67].

A gamma index analysis results in the fraction of evaluation points having γ-index less than 1, a γ-index passing rate. In a clinical setting, were fast decision making and actions are crucial, the use of decision thresholds based on the γ-index passing rate is essential. The main advantage of the γ-index passing rate is that it compresses a verification measurement into a single number. However, being a single number is at the same time the disadvantage since it does not indicate the dose comparison spatial information, i.e., where the failure happens and what might be the clinical significance of that failure. Furthermore, γ-index is an absolute metric and it gives no indication on the sign of the dose or distance variation that caused the failure point in a dose comparison process. For instance, higher evaluated (measured) doses than the reference

(planned) dose at some point in PTV for more than the dose difference criterion, would be clinically acceptable. The reverse applies to organs at risk where lower delivered dose than the planned below the criterion, would realize the radiotherapy goal.

Two more advantageous properties of gamma analysis are that, if performed under controlled conditions, it can be effectively used in dose audit studies for advanced radiotherapy techniques [80] and second, can be used in retrospective studies to observe the trends of patient QA over the time [81].

The key properties of an ideal dose comparison metric were described by Childress et al [65]. They include, but are not limited to: a) physical meaning and ease of understanding; b) biological significance; c) computation time needed to calculate the metric; d) dose distribution (plane/volume) size and dose range independence; e) measuring technique independence; f) comparability between the institutions and g) consistency over time. Obviously, the gamma analysis does not possess all of the above properties and until a better metric possibly based on both statistical and clinical relevance is found, recommendations for harmonised reporting of the conducted gamma analyses [60], [67] should bring improved consistency when comparing QA or clinical study results.

The subject of this thesis has focussed on the investigation of the gamma evaluation acceptance criteria, by studying the statistical distribution of the γ-index value under error-free conditions, in an attempt to single out statistically significant deviations in the general situation.

In the first part of the thesis, the calculation tools for a common gamma analysis in 1D and 2D dose distribution cases were developed and tested.

Next, the measured 1D absorbed dose distributions fitted with an appropriate smooth curve and 2D absorbed dose distribution for clinical IMRT fields calculated in a QC phantom were prepared for use in simulations. A random Gaussian uncertainty was added to the dose value and the detector position to these calculated dose distributions to simulate the measurements. The simulated measurement was then compared with the original calculation, and the γ-index value was calculated using dose difference and distance-to-agreement criteria equal to the simulated uncertainties. The resulting distribution of squared gamma γ^2 values was explored.

Also, extending the previous simulations, an entire array of detectors, mimicking a measurement in a TPS-calculated IMRT field, was simulated to check if the results valid for a single measurement can be applied to a clinically significant situation.

Further, a set of clinical head and neck IMRT fields were used to calculate the relative dose distribution at depth in a QC phantom. Again, the gamma evaluation tool was used to relate the simulated measurements at many detector positions to the calculated dose. The distribution of the resulting γ-index was analysed for different levels of positional and dose uncertainties.

6.2 Development of γ-index calculation code and investigation of the γ-index distribution properties

In the introduction to this research, fast and efficient computational tools were developed and evaluated for standard dose distribution comparisons with gamma analysis methods in 1D and 2D dose distribution cases. The developments in *MATLAB* involved handling of different type of 1D, 2D and 3D data; either artificially produced distributions or DICOM dose distributions from clinical practice. The dose comparisons included 1D dose profile distribution comparisons and the clinical 2D dose distributions comparison. These computer programs allow to search the whole evaluated dose distribution or to limit the search to a user-defined search radius. A local or global γ-index can be chosen as well as the setting of the dose difference and distance-to-agreement criteria and different level of interpolation.

Firstly, a 1D dose distribution case was analysed. A mathematically derived reference profile representing the penumbral region of 6 MV, 10 cm × 10 cm field, at two different depths, d_{max} and 10 cm, was generated from a superposition of error functions [19] and allowance for adjusting the positional shift, dosimetric offset and distribution normalisation factor. The profile has two distinct regions, a low-gradient region (the flat portion) and a high-gradient region (the penumbral region).

Evaluated dose distribution was created from the reference dose distribution by introducing, one at a time, a positional shift, dose normalisation changes and dosimetric offset modification. In all testing cases a global gamma was used with the normalisation at the maximum value of the reference distribution, the resolution grid was determined by the chosen DTA criterion divided by the resolution factor (e.g. 3 mm/10) and the search limit was extended to 3.

As confirmed by our calculations, for both 6 MV photon beam profiles (obtained by a fit to the data measured at the depth of d_{max} in water and the depth of 10 cm), γ-index pass the acceptance test ($\gamma < 1$) in the case of a slightly laterally shifted evaluated dose distribution, which is consistent with the composite evaluation. Figures 5.2 (a and d, the first row) show practically symmetric distributions of the dose difference and the γ-index values that reaches a plateau at

about 0.8, indicating that gamma analysis test passes for all points in the investigated region. The DTA values in Figures 5.2. a, d, are constant, 0.25, as expected. With the normalisation difference introduced to evaluated distribution, the gamma index becomes asymmetrical and in case of the profile at 10 cm depth becomes larger than 1. The DTA gets larger (up to 0.8 cm) in the left portion of the profile. When the third modification, the dose offset is introduced, similar global shapes for γ-index and DTA distributions at both, d_{max} and 10 cm depths are obtained (Figure 5.2 c and f, last row). The maximum gamma value is 1.101 for the comparison of profiles at 10 cm depth; all three dose modifications being introduced. The DTA distributions exhibit the "u" shape with constant values of ~ 0.25 cm in the penumbra region where the DTA is essentially determined by the spatial shift. All observed results are consistent with expectations and previously published results.

In the 2D case, three sets of dose distributions were investigated. For the first one, the reference dose distribution was simulated with a uniform central section (100 cGy) superimposed on a zero background and the evaluated dose distribution was modified by increasing the central section of the reference distribution by 1, 3 or 5 cGy and a spatial shift of the distribution by either$1/\sqrt{2}$ or 1 pixel in x and y-direction.

In this set of comparisons and for statistical analysis, the code was set up to calculate global γ-index values, the mean (γ_{mean}), max (γ_{max}) value, 99th γ-percentile ($\gamma_{1\%}$) and the passing rate ($P_{\gamma<1}(\%)$). Increasing the resolution factor in calculating the parameters led to a convergence of these values; above the resolution factor of 50, the results did not change. The γ_{mean} and γ_{max} converged to 0.333 and 0.476, respectively. The gamma passing rate was 100% since the combined effect of a small spatial shift and the dose difference did not overcome the loose criteria of 3%/3 mm.

Decreasing the dose difference from 5 cGy to 1 cGy decreased the γ_{mean}, γ_{max}, and $\gamma_{1\%}$ parameters and $P_{\gamma<1}(\%)$ reached 100%. For the fixed spatial shift and dose difference of 1 cGy the parameters γ_{mean}, γ_{max}, and $\gamma_{1\%}$ dropped with increasing the dose difference and DTA criteria. The gamma passing rate was 100 % with 2%/2 mm and 3%/3 mm criteria. The results obtained were consistent with the expected properties of the gamma analysis.

It was found that the results of gamma statistical evaluation have a little dependence on increasing the resolution parameter; the pass rate is always 100%, except for a resolution parameter 1 (no interpolation), where we have higher values for γ_{mean}, γ_{max}, and $\gamma_{1\%}$, and smaller pass rate. Keeping the same spatial offset and resolution parameter as in last calculation, but

now for three different dose differences (1%, 3% and 5 %) in the evaluated dose distribution, high gamma failures rate for higher dose difference between two distributions were obtained.

For the second sets of dose distributions, a 2D dose distribution was constructed from the 6 MV photon beam dose profiles measured with a scanning water phantom to represent the reference dose distribution. In constructing the evaluated dose distribution, the reference distribution was modified to highlight the discrepancies using the criteria of 3% dose difference and 3 mm distance difference at a certain distance from the centre of the dose distribution. It was modified differently in three out of four quadrants to check the influence of the spatial only, the dose only, and both shifts in concert, on the parameters of interest such as the dose difference and γ-index distribution.

The dose difference in the first quadrant has a constant value of zero, because this quadrant is unmodified, while the second one (dose shift) appears constant; however, this is just due to the coarse colour map resolution. In quadrant 3 (space shift), near the beam edge, because of the steep dose gradient, the dose differences become large, even with only a relatively small spatial shift between the two dose distributions. This marked dose difference feature is typical for small spatial offsets in steep dose gradient regions. A similar result, as in quadrant 3, appears in quadrant 4 (dose and spatial shift) where again in steep dose gradients the spatial offset causes very large dose differences.

As pointed out in Chapter 4, supplementary coding allowed for the comparison of the calculated and measured dose distribution in terms of their absolute difference calculated on a pixel by pixel basis. We used it for the presentation of the dose differences (Figure 5.3c). Additionally, cumulative/integral histograms of different quantities may be also helpful in depicting the features of these quantities (Figure 5.3e).

In the test case with an EBT3 film irradiated with a small (24 × 24 mm) 6 MV photon beam in a solid water phantom at the depth of 10 cm, a fundamental difference between the global and local dose normalisation in gamma analysis was satisfactorily illustrated. Unless a dose distribution is partitioned into some meaningful regions, based on the dose and dose gradient criterion, and treated separately, local gamma normalisation using uniform local dose difference in all regions is not a good dose distribution comparison metric.

Therefore, from all the conducted tests, it can be concluded that the developed programs for gamma analysis work properly and present a good computational basis for further investigations.

6.3 Properties of the squared γ-index distribution

To investigates the distribution of γ^2 in clinical situations, simulations were performed for different realistic cases in 1D and 2D. For the 1D case, two dose distributions, 6 MV photon beam profile data measured at the depth of maximum dose and 10 cm depth in a water phantom during the commissioning of the linear accelerator (*TrueBeam*, Varian Medical Systems), were fitted with the theoretical curve [19] in the same way as it was done in evaluating the γ-index calculation code. Then, applying the methodology described in section 4.3.1, the calculated γ^2-values were compared with the χ^2 distribution to test the statistical significance of the measured deviation. The χ^2 distribution is, as discussed in Chapter 3, closely related to the quadratic forms of normally distributed variables. The square of a standard normal random variable is a χ^2 random variable. If X_1 is a χ^2 random variable with n_1 degrees of freedom and X_2 another χ^2 random variable with n_2 degrees of freedom and if X_1 and X_2 are independent, then their sum has a χ^2 distribution with $n_1 + n_2$ degrees of freedom; it can be generalised to a sum of more than two independent χ^2 random variables. Combining these two properties, it follows that the sum of squares of n independent standard normal random variables is a χ^2 random variable with n degrees of freedom.

If we assume that the positioning of a detector is normally distributed and the spatial coordinates are independent of each other, as well as that the detected dose is also considered to be normally distributed and independent from the positioning of the detector, according to the definition, the squared γ-index (γ^2) should follow a χ^2 distribution with two degrees of freedom. On the other hand, since the absorbed dose and detector position are not entirely independent variables (and the relationship between them is unknown), this is no longer the case. While an approximate solution to this situation can be obtained by using more refined mathematics [26], a simpler approach using reduced degrees of freedom was tested in this work.

The sophisticated probabilistic gamma index method [26], relying on the properties of quadratic forms, relates the experimental uncertainties with the dose comparison test results. The probability of failing the gamma index test at some dose point of interest, larger than a predefined level, can be obtained. Having a good knowledge of experimental or another type of uncertainties in the reference and evaluated dose distributions, a more decisive answer can be obtained. On another side, having this dose comparison tool one can design studies to check if the determined uncertainties may influence the sensitivity of the test.

Results have shown good agreement for 1D dose distribution (6 MV photon beams at d_{max} and 10 cm depth). For the simulation parameters: 1, 2 and 3 cGy uncertainties in the dose distribution and 1, 2 and 3 mm for the spatial uncertainty combined into three pairs 1 cGy/1 mm, 2 cGy/2 mm and 3 cGy/3 mm of acceptance criteria, γ^2-distribution follows very well the χ^2 distribution with one degree of freedom. Importantly, the rate of failure stayed close to 5% along all positions of the x-axis regardless of the shape of the dose distribution and the absorbed dose gradient. These results are very useful, as they make it straightforward to implement a statistical interpretation of the gamma evaluation index into current gamma-evaluation procedures, without modification [74].

In the case of 2D distribution, again γ^2-distributions followed very well the χ^2distribution with one degree of freedom but this time only for the points in low dose gradient (points with coordinates (0,0) and (4,4), Figure 5.10 *(left)*). This is due to known disadvantage of the gamma index method, that it does not recognize the dose gradient.

It was an indication that the approximation is not good enough for points where the dose gradient is high. Therefore, we expanded our research to examine the second derivative at these points, because that is the apparent factor that makes the approximation break down.

Further extension of the previous investigations, where it was demonstrated that the resulting distribution of γ^2-values follows the χ^2distribution with one degree of freedom, consisted of a detector array that may hold several hundreds of detectors. It was investigated how this outcome, valid for a single measurement, can be applied to a more clinically pertinent situation. For those reasons, simulations were done for detector arrays with 100 and 400 detectors with two groups of dose distributions with the spatial resolution of 1 mm and 3 mm.

The dose distributions, IMRT field used in the treatment of a head and neck tumour localisation, calculated at the depth of 5 cm were used in simulations. The spacing of the detectors was 1 cm for the 10×10 or 20×20 array detectors. The simulation parameters were: 1, 2, 3 % uncertainty in the dose distribution and 1,2,3 mm for the spatial uncertainty combined into three pairs 1%/1 mm, 2%/2 mm and 3%/3 mm. Theoretically, if all detectors in the array were statistically independent, the probability of having exactly k detectors outside the tolerance limit can be obtained by the binomial distribution. However, from the detector array simulations, it was evident that the failure rate distribution could not be predicted by the theoretical binomial distribution. The reason is that the positions of the individual detectors are not statistically independent, as they all move together with the entire detector device. Therefore, an alternative

scheme was proposed to provide failure rate probabilities from the empirical cumulative distribution function (ECDF), as calculated from the simulation results. From the preliminary studies, it was indicated that the simulated ECDFs were practically invariant with respect to dose and spatial uncertainties, as well as the number of detectors. However, further studies are needed to investigate the variability for a larger number of ECDFs, to evaluate the accuracy and robustness of the proposed scheme.

6.4 Statistical analysis of the gamma evaluation acceptance criteria

In the following section of the thesis (sections 4.5 and 5.5), we have addressed the yet unresolved issue regarding the choice of appropriate acceptance criteria for the gamma evaluation method for comparing dose distributions. This consideration is based on the previous investigations [23, 24], [66]. In the first one, the authors assumed that the non-spatial uncertainties,$\sigma_{ns}(r)$, of the dose uncertainty are independent of the spatial uncertainties, $\sigma_s(r)$, although non-spatial uncertainty may be affected by the spatial shift because the uncertainty is a function of the position. Investigations were done with 1D dose distribution simulations. At any point, the dose uncertainty depends on several dose values and gradients from multiple beams/ beam segments rather than from the whole dose profile. The uncertainty for the overall profile was determined from available information on dose values and gradients for each small contribution, a small segment. In their work, for simple 1D dose distribution simulations, the authors showed that the offset of 3 mm contributes to the non-spatial uncertainty less than 0.2% to a maximum dose. Some additional schemes for dose comparison technique were also derived in the publication. In the first one, the tolerance is chosen as a maximum value from a set of pairs $[k\sigma_{ns}(r), k\sigma_s(r)]$, where k is a constant for a confidence level and in contrast to the composite analysis in which the dose difference and DTA criteria apply over the complete dose distribution, here the tolerance varies from point to point due to the spatial dependence. The next scheme is like χ-index test [22]. However, in this second scheme the dose uncertainty in each beam segment is considered, while the χ-index test uses a complete dose distribution. In this scheme, the relative dose difference standard deviation and spatial displacement Δr are determined by the user and are independent of the geometrical complexity. The third scheme, a linear combination of the dosimetric and gradient dose deviations form a possible maximum dose difference between the reference and evaluated dose distribution.

Employing a mathematical framework, the standard expression for calculating the γ-index was reformulated as a set of coupled differential equations [66]. The equations can be solved to an

arbitrary order. The zeroth, first-order and semi second-order solutions were developed and tested. The derivatives of the dose distribution at grid points were calculated by the central finite differences and the function values and gradients between the grid points by interpolation. Finally, the coupled partial differential equations to an arbitrary order in the Taylor series expansion provided the distance at a minimum point to the surface distance and dose value at the solution point by a series expansion or interpolation. The failure rates calculated within the developed framework for presented IMRT and proton pencil beam scanning dose distributions showed that the first-order numerical methods were accurate to within 1% and were the best choice for the distributions known to have small second-order derivatives.

Based on those assumptions it was speculated in this work that by studying the statistical distribution of the gamma value under error-free conditions, it should be possible to determine which gamma evaluation acceptance criteria should be used to single out statistically significant deviations in the general situation.

Therefore, a set of 30 clinical head-and-neck IMRT fields, calculated with the department's TPS in a uniform QC phantom was used as an input to simulate the dose measurements, by taking the calculated values as expectation values to which a random measurement uncertainty was added. The gamma evaluation tool was then used to compare the simulated measurements to the calculated dose, and the distribution of the resulting γ-index values for a large number of simulations was analysed for different levels of positional and dose uncertainties.

As confirmed by the present investigation, a fixed set of gamma evaluation criteria can be used to single out statistically significant deviations at the expected failure rate (i.e., 0.05), as long as the second-order derivative of the absorbed dose distribution is low. This is the case for more than 50% of the points of the clinical IMRT fields that we have investigated in this study. For other points, however, the second-order derivative is larger, resulting in failure rates that are substantially higher than 0.05. This means, that if the gamma analysis were to be used with fixed criteria based on the standard deviations of positioning and dose measurement uncertainties, there would be false failures at points in regions with large values of the second-order derivative. It should be noted that this is an issue inherent in the gamma-evaluation method, regardless of the approximation in Eq. (4.16). For the range of criteria that are chosen for the spatial and dosimetric agreement in the gamma analysis, the probability of having a gamma-value above unity is not uniform across a dose distribution in the presence of large values of the second-order derivative, even if there are only random deviations in position and dose measurement.

However, for cases where the spatial uncertainty is equal to or larger than the spatial resolution of the dose matrix, the width of the failure rate distribution becomes much smaller, and its median value close to the expected value of 0.05, except for the lowest value of the dose uncertainty (1%). For larger, more reasonable dose uncertainties the median value of the failure rate distribution again seems to approach 0.05. Thus, if these limitations are recognised, the results of this investigation can be used to set statistically meaningful acceptance criteria for the gamma evaluation method.

Chapter 7
CONCLUSION

The gamma analysis (γ-index) as an evaluation method is the most used method for the verification of advanced IMRT/VMAT techniques. For the comparison of a given reference dose distribution point and any one of the evaluated (e.g. calculated) dose distribution points, a generalized Euclidian distance in the (k+1) – D spatial-dose space can be calculated in single quantity normalized by the dose difference and spatial tolerance criteria. A clear advantage of the gamma analysis as a simple dimensionless metric, is that it condenses to a single value-the gamma passing rate. At the same time, beside the computational burden, an obvious shortcoming is that it does not provide information on where the failing points in the distribution are. Since it does not carry the information about the sign of the dose due to which a certain point failed, nor if the failure was due to discrepancies in distances, its clinical value cannot be readily judged. The past attempts to overcome the limitations of gamma analysis can be categorised into the variants that were trying to limit the dose distribution resolution dependence, setting more rational criteria of acceptance, reducing gamma index calculation time, or correlating the dose distribution comparison mismatches to the patient anatomy or radiobiological model.

Several studies on the clinical relevance of the gamma passing rate have shown a weak or moderate correlation between the selected clinical parameters and IMRT QA gamma passing rate was observed. Larger values of some clinical parameters were associated with higher IMRT QA passing rate. It was concluded that the gamma passing rate was not sensitive to clinically relevant patient dose errors.

In this work we investigated the statistical distribution of the gamma index value under error-free conditions to study the relation between the gamma evaluation failure rate and statistically significant deviations in the general situation.

These investigations started with the development of the flexible and efficient computer code for standard gamma index evaluation for 1D and 2D clinical dose distributions. The programs were tested with representative quality assurance (QA) dose measurements and clinical 2D dose distributions available from the perpendicular field-by-field (PFF) IMRT field QA measurements. The results for the characteristic statistical gamma parameters were according to the expectations.

Using the 1D beam profile functions and treatment planning system calculated dose distribution, and by adding a random Gaussian uncertainty to the dose value and the detector position, a measurement was simulated. This simulated measurement was then compared with the original calculation, and the γ-index value was calculated according to the definition, using dose difference and distance-to-agreement criteria equal to the simulated uncertainties. The resulting distribution of squared γ-index values followed very well the chi-squared distribution with one degree of freedom in 1D and 2D cases. It makes it straightforward to implement a statistical interpretation of the gamma evaluation index into current gamma evaluation procedures.

To study the statistical distribution of the gamma value under error-free conditions, a set of clinical head-and-neck IMRT fields calculated with the treatment planning system (TPS) in a QC phantom, was used as an input to simulate the dose measurements. The calculated values were expectation values to which a random measurement uncertainty was added. The gamma evaluation tool was then used to compare the simulated measurements to the calculated dose, and the distribution of the resulting gamma index values for a large number of simulations was analysed for different levels of positional and dose uncertainties. As long as there are no large second order derivatives in the absorbed dose distributions, the gamma value can be expected to behave according to the statistical approach in which the positional or space oriented and non-space-oriented uncertainties are normally distributed and uncorrelated, or specifically, that the contribution of the positional displacement to the non-spatial dose uncertainty is negligible.

Simulated dose measurements derived from clinical head-and-neck IMRT absorbed dose distributions, calculated with the TPS and evaluated by the γ-index analysis tool, showed that the probability of having a gamma-value above unity is not spatially uniform. The gamma evaluation produced relatively more false positives in dose distribution regions with larger values of the second order derivative. This means that the statistical significance of the gamma failure criterion (i.e., $\gamma>1$) is not uniquely related to a given set of spatial and dose tolerance values. It is speculated that this shortcoming may be partly responsible for the limited ability of the gamma evaluation method to detect errors in clinically relevant situations.

The simulation results valid for a single measurement in 1D and 2D dose distributions were extended to test their applicability to a clinically more relevant case, an array of a large number of detectors commonly used in radiotherapy QA measurements. The simulated failure rate distributions would follow a binomial probability distribution if the detectors in the array were statistically independent and the properties of the theoretical distribution could be used for

setting the maximum expected failure rate, given that deviations are only due to the randomness. As the individual detector points are not statistically independent, there is a discrepancy between the simulated probability distributions and the theoretical binomial distribution: a peak centroid shift towards lower values and higher probabilities of higher failure rates compared to a theoretical distribution. Therefore, the theoretical cumulative dose distribution cannot be used to accurately relate the tolerance levels and observed failure rates. Instead, an empirical cumulative distribution function (ECDF) was proposed to be constructed from the simulation results. By calculating the inverse ECDF for a desired probability, a corresponding maximal failure rate tolerance level is obtained. A more thorough evaluation of the proposed method shall be conducted including larger number of test dose distributions and common random detector displacements and random doses in scoring the failure rate. This will enable a proper evaluation of the robustness of the method and an estimate of the uncertainty of the gamma tolerance levels.

BIBLIOGRAPHY

[1] Intensity Modulated Radiation Therapy Collaborative Working Group, "Intensity-modulated radiotherapy: current status and issues of interest," *Int J Radiat Oncol Biol Phys,* vol. 51, pp. 880-914, 2001.

[2] Li XA, Wang JZ, Jursinic PA, Lawton CA, Wang D, "Dosimetric advantages of IMRT simultaneous integrated boost for high-risk prostate cancer," *Int J Radiat Oncol Biol Phys,* vol. 61, pp. 1251-7, 2005.

[3] Brahme A, Roos J E, Lax I, "Solution of an integral equation encountered in radiation therapy," *Phys Med Biol,* vol. 27, pp. 1221-9, 1982.

[4] Bortfeld T, "IMRT: A review and preview," *Phys Med Biol,* vol. 51, pp. R363-R379, 2006.

[5] Fenoglietto P, et al., "Persistently better treatment planning results of intensity-modulated (IMRT) over conformal radiotherapy (3D-CRT) in prostate cancer patients with significant variation of clinical target volume and/or organs-at-risk," *Radiother Oncol,* vol. 88, pp. 77-87, 2008.

[6] Gomez D, Cahlon O, Mechalakos J, Lee N, "An investigation of intensity-modulated radiation therapy versus conventional two-dimensional and 3D-conformal radiation therapy for early stage larynx cancer.," *Radiat Oncol,* vol. 5, p. 74, 2010.

[7] Mackie TR, et al., "Tomotherapy: a new concept for the delivery of conformal radiotherapy," *Med Phys,* vol. 20, pp. 1709-19, 1993.

[8] Yu CX, Tang G, "Intensity-modulated arc therapy: principles, technologies and clinical implementation," *Phys Med Biol,* vol. 56, pp. R31-R54, 2011.

[9] Teoh M, Clark CH, Wood K, Whitaker S, Nisbet A, "Volumetric modulated arc therapy: a review of current literature and clinical use in practice," *The British journal of radiology,* vol. 84, pp. 967-96, 2011.

[10] Otto K, "Volumetric modulated arc therapy: IMRT in a single gantry arc," *Med Phys,* vol. 35, pp. 310-7, 2008.

[11] Yu CX, "Intensity-modulated arc therapy with dynamic multileaf collimation: an alternative to tomotherapy," *Phys Med Biol,* vol. 40, pp. 1435-49, 1995.

[12] Kutcher GJ, et al., "Comprehensive QA for radiation oncology: Report of AAPM Radiation Therapy Committee Task Group 40," *Med Phys,* vol. 21, pp. 581-618, 1994.

[13] Klein EE, et al., "Task Group 142 report: Quality assurance of medical accelerators," *Med Phys,* vol. 36, pp. 4197-212, 2009.

[14] Low DA, Moran JM, Dempsey JF, Dong L, Oldham M, "Dosimetry tools and techniques for IMRT," *Med Phys,* vol. 38, pp. 1313-38, 2011.

[15] Nelms BE, Zhen H, Tomé WA, "Per-beam, planar IMRT QA passing rates do not predict clinically relevant patient dose errors," *Med Phys,* vol. 38(2), pp. 1037-44, 2011.

[16] Jursinic PA, Nelms BE, "A 2-D diode array and analysis software for verification of intensity modulated radiation therapy delivery," *Med Phys,* vol. 30, pp. 870-9, 2003.

[17] Létourneau D, Gulam M, Yan D, Oldham M, Wong JW, "Evaluation of a 2D diode array for IMRT quality assurance," *Radiother Oncol,* vol. 70, pp. 199-206, 2004.

[18] Poppe B, et al., "Two-dimensional ionization chamber arrays for IMRT plan verification," *Med Phys,* vol. 33, pp. 1005-15, 2006.

[19] Low DA, Harms WB, Mutic S, Purdy JA, "A technique for the quantitative evaluation of dose distributions," *Med Phys,* vol. 25, pp. 656-61, 1998.

[20] Low DA, Dempsey JF, "Evaluation of the gamma dose distribution comparison method," *Med Phys,* vol. 30, pp. 2354-64, 2003.

[21] Basran PS, Woo MK, "An analysis of tolerance levels in IMRT quality assurance procedures," *Med Phys,* vol. 35, pp. 2300-7, 2008.

[22] Bakai A, Alber M, Nusslin F, "A revision of the gamma-evaluation concept for the comparison of dose distributions," *Phys Med Biol,* vol. 48, pp. 3543-53, 2003.

[23] Jin H, Chung H, Liu C, Palta J, Suh TS, Kim S, "A novel dose uncertainty model and its application for dose verification," *Med Phys,* vol. 32, pp. 1747-56, 2005.

[24] Jin H, Palta J, Suh TS, Kim S, "A generalized a priori dose uncertainty model of IMRT delivery," *Med Phys,* vol. 35, pp. 982-96, 2008.

[25] Jin H, Palta JR, Kim YH, Kim S, "Application of a novel dose-uncertainty model for dose-uncertainty analysis in prostate intensity- modulated radiotherapy," *Int J Radiat Oncol Biol Phys,* vol. 78, pp. 920-8, 2010.

[26] Henríquez FC, Castrillón SC, "A probability approach to the study on uncertainty effects on gamma index evaluations in radiation therapy," *Comput Math Methods Med,* vol. 2011, pp. 861-9, 2011.

[27] INTERNATIONAL ATOMIC ENERGY AGENCY, "Implementation of the International Code of Practice on Dosimetry in Radiotherapy (TRS 398): Review of Testing Results, IAEA-TECDOC-CD-1455," IAEA, Vienna, 2010.

[28] Ahnesjö A, Aspradakis MM, "Dose calculations for external photon beams in radiotherapy," *Phys Med Biol,* vol. 44, pp. 99-155, 1999.

[29] Johnsson SA, Ceberg CP, Knöös T, Nilsson P, "On beam quality and stopping power ratios for high-energy x-rays," *Phys Med Biol,* vol. 45(10), pp. 2733-45, 2000.

[30] Zhu TC, et al., "In-air output ratio, sc, for megavoltage photon beams," *Medical physics,* vol. 36, pp. 5261-91, 2009.

[31] Chang DS, Lasley FD, Das IJ, Mendonca MS, Dynlacht JR, Production and Properties of Radiation. In: Basic Radiotherapy Physics and Biology, Cham: Springer, 2014.

[32] Webb S, "Optimization of conformal radiotherapy dose distributions by simulated annealing," *Phys Med Biol,* vol. 34, pp. 1349-70, 1989.

[33] Bortfeld T, Bürkelbach J, Boesecke R, Schlegel W, "Methods of image reconstruction from projections applied to conformation radiotherapy," *Phys Med Biol,* vol. 35, pp. 1423-34, 1990.

[34] Convery DJ, Rosenbloom ME, "The generation of intensity-modulated fields for conformal radiotherapy by dynamic collimation," *Phys Med Biol,* vol. 37, pp. 1359-74, 1992.

[35] Van Dyk J, The Modern Technology of Radiation Oncology, chapter Beam shaping and intensity modulation in modern technology of radiation oncology, Madison, WI: Medical physics publishing, 1999.

[36] Merritt M, Zhang Y, Radhe H, Radhe M, "A Successive Linear Programming Approach to IMRT Optimization Problem," Computational and Applied Mathematics (CAAM) technical reports, 2002.

[37] Li JS, Lin T, Chen L, Price RA Jr, Ma CM, "Uncertainties in IMRT dosimetry," *Med Phys,* vol. 37, pp. 2491-500, 2010.

[38] Ibbott GS, Followill DS, Molineu HA, Lowenstein JR, Alvarez PE, Roll JE, "Challenges in Credentialing Institutions and Participants in Advanced Technology Multi-Institutional Clinical Trials," *Int J Radiat Oncol Biol Phys,* vol. 71(1 Suppl), pp. S71-S75, 2008.

[39] Buonamici FB, Compagnucci A, Marrazzo L, Russo S, Bucciolini M, "An intercomparison between film dosimetry and diode matrix for IMRT quality assurance," *Med Phys,* vol. 34, pp. 1372-9, 2007.

[40] Carol M, et al., "Initial clinical experience with the Peacock intensity modulation of a 3-D conformal radiation therapy system," *Stereotact Funct Neurosurg,* vol. 66, pp. 30-4, 1996.

[41] Ling CC, et al., "Conformal radiation treatment of prostate cancer using inversely-planned intensity-modulated photon beams produced with dynamic multileaf collimation.," *Int J Radiat Oncol Biol Phys,* vol. 35, pp. 721-30, 1996.

[42] Wang X, Spirou S, LoSasso T, Stein J, Chui CS, Mohan R, "Dosimetric verification of intensity-modulated fields," *Med Phys,* vol. 23, pp. 317-27, 1996.

[43] Chui CS, Spirou S, LoSasso T, "Testing of dynamic multileaf collimation," *Med Phys,* vol. 23, pp. 635-41, 1996.

[44] Mijnheer B, Clinical 3D Dosimetry in Modern Radiation Therapy, CRC Press, 2017.

[45] Hartford AC, et al., "American college of radiology (acr) and american society for radiation oncology (astro) practice guideline for intensity-modulated radiation therapy (imrt).," *Am J Clin Oncol,* vol. 35, pp. 612-7, 2012.

[46] Ezzell GA, et al., “IMRT commissioning: multiple institution planning and dosimetry comparisons, a report from AAPM Task Group 119,” *Med Phys,* vol. 36, pp. 5359-73, 2009.

[47] Ezzel GA, et al., “Guidance document on delivery, treatment planning, and clinical implementation of IMRT: Report of the IMRT subcommittee of the AAPM radiation therapy committee,” *Med Phys,* vol. 30, pp. 2089- 115, 2003.

[48] Nelms BE, Simon JA, “A survey on planar IMRT QA analysis,” *J Appl Clin Med Phys,* vol. 8, pp. 76-90, 2007.

[49] Alber M, Broggi S, De Wagter C, et al, “GUIDELINES FOR THE VERIFICATION OF IMRT,” in *ESTRO booklet, 7*, Brussels, 2008.

[50] Pawlicki T, et al., “Moving from IMRT QA measurements toward independent computer calculations using control charts,” *Radiother Oncol,* vol. 89, pp. 330-7, 2008.

[51] Sun B, et al., “Evaluation of the efficiency and effectiveness of independent dose calculation followed by machine log file analysis against conventional measurement based IMRT QA,” *J Appl Clin Med Phys,* vol. 13, pp. 140-54, 2012.

[52] van Elmpt W, McDermott L, Nijsten S, Wendling M, Lambin P, Mijnheer B, “A literature review of electronic portal imaging for radiotherapy dosimetry,” *Radiother Oncol,* vol. 88, pp. 289-309, 2008.

[53] Gum F, Scherer J, Bogner L, Solleder M, Rhein B, Bock M, “Preliminary study on the use of an inhomogeneous anthropomorphic Fricke gel phantom and 3D magnetic resonance dosimetry for verification of IMRT treatment plans,” *Phys Med Biol,* vol. 47, pp. N67-N77, 2002.

[54] Gorjiara T, et al., “Investigation of radiological properties and water equivalency of PRESAGE_ dosimeters,” *Med Phys,* vol. 38, pp. 2265-74, 2011.

[55] Van Dyk J, Barnett RB, Cygler JE, Shragge PC, “Commissioning and quality assurance of treatment planning computers,” *Int J Radiat Oncol Biol Phys,* vol. 26, pp. 261-73, 1993.

[56] Harms WB Sr, Low DA, Wong JW, Purdy JA, “A software tool for the quantitative evaluation of 3D dose calculation algorithms,” *Med Phys,* vol. 25, pp. 1830-6, 1998.

[57] Spezi E, Lewis DG, “Gamma histograms for radiotherapy plan evaluation,” *Radiother Oncol,* vol. 79, pp. 224-30, 2006.

[58] Depuydt T, Van Esch A, Huyskens DP, “A quantitative evaluation of IMRT dose distributions: refinement and clinical assessment of the gamma evaluation,” *Radiother Oncol,* vol. 62, pp. 309-19, 2002.

[59] Wendling M, et al., “A fast algorithm for gamma evaluation in 3D,” *Med Phys,* vol. 34, pp. 1647-54, 2007.

[60] Hussein M, Clark CH, Nisbet A, “Challenges in calculation of the gamma index in radiotherapy - Towards good practice,” *Phys Med,* vol. 36, pp. 1-11, 2017.

[61] Stock M, Kroupa B, Georg D, “Interpretation and evaluation of the gamma index and the gamma index angle for the verification of IMRT hybrid plans,” *Phys Med Biol,* vol. 50, pp. 399-411, 2005.

[62] Ju T, Simpson T, Deasy JO, Low DA, “Geometric interpretation of the γ dose distribution comparison technique: Interpolation-free calculation,” *Medical Physics,* vol. 35, pp. 879-87, 2008.

[63] Chen M, Lu W, Chen Q, Ruchala K, Olivera G, “Efficient gamma index calculation using fast Euclidean distance transform,” *Phys Med Biol,* vol. 54, pp. 2037-47, 2009.

[64] Gu X, Jia X, Jiang SB , “GPU-based fast gamma index calculation,” *Phys Med Biol,* vol. 56(5, pp. 1431-41, 2011.

[65] Childress NL, Rosen II, “The design and testing of novel clinical parameters for dose comparison,” *Int J Radiat Oncol Biol Phys,* vol. 56, pp. 1464-79, 2003.

[66] Clasie BM, Sharp GC, Seco J, Flanz JB, Kooy HM, “Numerical solutions of the γ-index in two and three dimensions,” *Phys Med Biol,* vol. 57, pp. 6981-97, 2012.

[67] Diamantopoulos S, Platoni K, Patatoukas G, Karaiskos P, Kouloulias V, Efstathopoulos E, “Treatment plan verification:A review on the comparison of dose distributions,” *Phys Med,* vol. 67, pp. 107-15, 2019.

[68] Miften M, et al., “Tolerance limits and methodologies for IMRT measurement-based verification QA: Recommendations of AAPM Task Group No. 218,” *Med Phys,* vol. 45, pp. e53-e83, 2018.

[69] Yan G, Liu C, Simon TA, Peng LC, Fox C, Li JG, “On the sensitivity of patient specific IMRT QA to MLC positioning errors,” *J Appl Clin Med Phys,* vol. 10(1), pp. 120-8, 2009.

[70] Steers JM, Fraass BA, “IMRT QA: Selecting gamma criteria based on error detection sensitivity,” *Med Phys,* vol. 43(4), p. 1982, 2016.

[71] Bresciani S, et al. , “Tomotherapy treatment plan quality assurance: the impact of applied criteria on passing rate in gamma index method.,” *Med Phys,* vol. 40(12), p. 121711, 2013.

[72] Song JH, et al., “Gamma analysis dependence on specified low-dose thresholds for VMAT QA,” *J Appl Clin Med Phys,* vol. 16(6), pp. 263-72, 2015.

[73] Jiang SB, Sharp GC, Neicu T, Berbeco RI, Flampouri S, Bortfeld T, “On dose distribution comparison,” *Phys Med Biol,* vol. 51(4), pp. 759-76, 2006.

[74] Ceberg C, “A note on the interpretation of the gamma evaluation index,” in *7th International Conference on 3D Radiation Dosimetry (IC3DDose). IOP Publishing, 2013, Vol. 444, p. 012082*, 2013.

[75] *MapCHECK 2 , Reference Guide (Document 1177011, Rev D). Sun Nuclear Corporation,* 2009.

[76] Thwaites D, “Accuracy required and achievable in radiotherapy dosimetry: have modern technology and techniques changed our views?,” in *J Phys Conf Ser; 444:12006*, 2013.

[77] Moran JM, et al., “Safety considerations for IMRT: executive summary,” *Med Phys,* vol. 38(9), pp. 5067-72, 2011.

[78] Mans A, et al., “The NCS code of practice for the quality assurance and control for volumetric modulated arc therapy,” *Phys Med Biol,* vol. 61(19), pp. 7221-35, 2016.

[79] Shiu AS, et al., “Verification data for electron beam dose algorithms,” *Med Phys,* vol. 19(3), pp. 623-36, 1992.

[80] Hussein M, et al., “A methodology for dosimetry audit of rotational radiotherapy using a commercial detector array,” *Radiother Oncol,* vol. 108, p. 78–85, 2013.

[81] Childress NL, White RA, Bloch C, Salehpour M, Dong L, Rosen II., "Retrospective analysis of 2D patient specific IMRT verifications," *Med Phys,* vol. 32, p. 838, 2005.

[82] Nelms BE, Zhen H, Tomé WA, "Per-beam, planar IMRT QA passing rates do not predict clinically relevant patient dose errors," *Med Phys,* vol. 38(2), pp. 1037-44, 2011.

APPENDIX A
The dosimetric quantities of interest in the thesis

Photon fluence and photon fluence rate

The photon fluence (Φ) is defined as the number of particles (dN) incident on a sphere of cross-sectional area (dA):

$$\Phi = dN/dA \quad (1)$$

The unit of photon fluence is cm^{-2}.

The photon fluence rate is defined as the photon fluence per unit time:

$$\varphi = d\Phi/dt \quad (2)$$

The unit of photon fluence rate is $cm^{-2} \cdot s^{-1}$.

Absorbed dose

Absorbed dose D, or dose, is defined as the expectation value of the absorbed energy (dε) per unit of mass of a medium (dm):

$$D = d\varepsilon/dm \quad (3)$$

The unit of dose is the gray (Gy).

Percent Depth Dose (PDD)

As the photon beam propagates through a water medium, the dose deposition varies with depth (z) and depends also on the field size (A), distance from the source (f) and beam energy. Therefore, measurements of the central axis dose distribution for different field sizes provide a good beam characterization method. Percent Depth Dose (PDD) is a quantity used for beam characterization and is obtained by measuring the absorbed dose at any depth z along the central axis of the beam and then usually normalised to the absorbed dose at a reference depth z_{max}, thus:

$$PDD(z, A, f, E) = \frac{z}{z_{max}} \; x \; 100\% \quad (4)$$

In practice, PDD is measured for different nominal beam energies and different rectangular field sizes during linear accelerator commissioning. The commissioning data are then used as a benchmark for future QA measurements.

Tissue phantom ratio-$TPR_{20,10}$

For high energy photons produced by clinical accelerators the beam quality Q is specified by the tissue phantom ratio $TPR_{20,10}$. $TPR_{20,10}$ is defined as the ratio of doses on the beam central axis at depths of 20 cm and 10 cm in water obtained with a constant source to detector distance of 100 cm and a field size of 10 × 10 cm^2 at the position of the detector. The $TPR_{20,10}$ is a measure of the effective attenuation coefficient describing the approximately exponential decrease of a photon depth dose curve beyond the depth of maximum dose z_{max}, and, importantly, it is independent of electron contamination of the incident photon beam. A higher $TPR_{20,10}$ is associated with a more penetrating beam.

The $TPR_{20,10}$ can be related to the measured $PDD_{20,10}$ using the following relationship:

$$TPR_{20,10} = 1.2661PDD_{20,10} - 0.0595$$

where $PDD_{20,10}$ is the ratio of PDDs at depths of 20 cm and 10 cm for a field of 10 × 10 cm^2 defined at the water phantom surface with an SSD of 100 cm. This empirical relationship was obtained from a sample of almost 700 linear accelerators.

APPENDIX B
The nomenclature used in thesis

The nomenclature used in this thesis is summarized in Table B.1.

All equations in Table B.1 are described in Chapter 3. In discussions of the dose comparison techniques, it assumes that there are two dose distributions that might have been determined in one (1D), two (2D) or three (3D) dimensions, termed a *reference* (e.g. measured) and an *evaluated* (e.g. calculated) dose distribution [19]. The *reference* distribution is typically the one against which the *evaluated* distribution is being compared. When practical in the thesis, the general terms, *reference* and *evaluated* are replaced with the actual, measured and calculated.

Table B1 Nomenclature used in this thesis

Symbol	Equation	Description
$D_e(\vec{r}_e)$	N/A	Evaluated dose D_e at position $\vec{r}_e$
$D_r(\vec{r}_r)$	N/A	Reference dose D_r at position $\vec{r}_r$
ΔD	N/A	Dose difference criterion. Can either be local or global. Normally 3% of the maximum dose
Δr	N/A	Distance-to-agreement (DTA) criterion. Normally 3 mm
$r(\vec{r}_r, \vec{r}_e)$	$r(\vec{r}_r, \vec{r}_e) = \lvert\vec{r}_e - \vec{r}_r\rvert$	Spatial distance between the reference and evaluated dose points
$\delta(\vec{r}_r, \vec{r}_e)$	$\delta(\vec{r}_r, \vec{r}_e) = \lvert D_e(\vec{r}_e) - D_r(\vec{r}_r)\rvert$	Difference between the evaluated dose D_e at position $\vec{r}_e$ and reference dose D_r at position $\vec{r}_r$
$\Gamma(\vec{r}_r, \vec{r}_e)$	$\Gamma(\vec{r}_r, \vec{r}_e) = \sqrt{\frac{r(\vec{r}_r, \vec{r}_e)^2}{\Delta r^2} + \frac{\delta(\vec{r}_r, \vec{r}_e)^2}{\Delta D^2}}$	Generalized Γ function, computed for all evaluated positions $\vec{r}_e$ and reference positions $\vec{r}_r$
$\gamma(\vec{r}_r)$	$\gamma(\vec{r}_r) = \min\{\Gamma(\vec{r}_r, \vec{r}_e)\} \forall \{\vec{r}_e\}$	γ function, the minimum generalized Γ function in the set of evaluated points

APPENDIX C

Probability distributions and their key properties relevant for simulation studies

This appendix describes the basic properties of binomial, normal and chi-square probability distributions.

Binomial distribution

Let an experiment has only two possible outcomes: either success or failure and suppose that experiment is repeated several times and the repetitions are independent of each other. The total number of experiments where the success outcomes is a random variable whose distribution is called binomial distribution. It has two parameters: the number n of repetitions of the experiment and the probability p of success of an individual experiment.

If X is a discrete random variable, $n \in N$, $p \in (0,1)$ and the support of x equal to:

$$R_X = \{0,1, 2, \ldots, n\} \tag{1}$$

then X has a binomial distribution with parameters n and p if its probability mass function is:

$$p_X(x) = \binom{n}{x} p^x (1-p)^{n-x} \quad \text{if } x \in R \tag{2}$$

$$0 \qquad \text{if } x \notin R \tag{3}$$

where $\binom{n}{x}$ is a binomial coefficient.

The binomial distribution is closely related to the Bernoulli distribution. Then, if a random variable X has a binomial distribution with parameters n and p, with n=1, X has Bernoulli distribution with parameter p if its probability mass function is:

$$p_X(x) = \begin{cases} p & \text{if } x = 0 \\ 1\text{-p} & \text{if } x = 0 \\ 0 & \text{if } x \notin R_X \end{cases} \tag{4}$$

Bernoulli random variable is a random variable having a Bernoulli distribution. The expectation is: E[X]=p, Var[X]=p (1- p). The distribution function of a Bernoulli random variable X is then defined as:

$$F_X(x) = \begin{cases} 0 & \text{if } x < 0 \\ 1\text{-p} & \text{if } 0 \le x < 1 \\ 0 & \text{if } x \ge 1 \end{cases} \quad (5)$$

Normal distribution

Suppose that X is a continuous normal variable that is defined for the whole set of real numbers, R_X=R, then X has a standard normal distribution if its probability density function (pdf) is:

$$f_X(x) = \frac{1}{\sqrt{2\pi}} e^{-\frac{1}{2}x^2} \quad (6)$$

The expectation of a standard normal random variable X is E[X] = 0 and the variance of X is V[X] = 1, which can be easily proved by using the definition of the expectation and variance.

If X is a random variable, its distribution function F_X: R→[0,1] such that:
$F_X(x) = P(X<x)$, ∀x∈R, where P(X<x) is the probability that X is less than or equal to x.
The previous case is a special case of zero mean and unit variance. In the general case, where X is a continuous random variable and the support is the set of real numbers, R_X=R, μ ∈ R, σ ∈ R_{++}, the variable X has a normal distribution with the mean μ and variance σ^2 if and only if its probability density function is:

$$f_X(x) = \frac{1}{\sqrt{2\pi}} \frac{1}{\sigma} e^{-\frac{1(x-\mu)^2}{2 \quad \sigma^2}} \quad (7)$$

which is often indicated by X~N (μ, σ^2).
If X has a normal distribution with the mean μ and variance σ^2, then X= μ+σZ, where Z is a random variable that has a standard normal distribution. The expectation of a normal random variable X is E[X] = μ and the variance of X is V[X] = σ^2.

Chi-square (χ^2) distribution

A random variable X has a χ^2 distribution if it can be written as a sum of squares:

$$X=Y_1^2+Y_2^2+\ldots Y_n^2 \quad (8)$$

where Y_1, …. Y_n are mutually independent standard normal random variable.

Let us first define X as a continuous random variable. Let its support be the set of positive real numbers R_X= [0,∞) and n∈Ny. Then X has χ^2 distribution with n degrees of freedom if and only if its probability density function is defined as:

$$f_X(x) = \begin{cases} cx^{n/2-1}\, exp(-\frac{1}{2}x) & \text{if x} \in R \\ 0 & \text{if x} \notin \text{R} \end{cases} \quad (9)$$

where c is a constant, $c=1/2^{n/2}\Gamma(n/2)$ and Γ is the Gamma function. We write $X\sim\chi^2(n)$ that a random variable X is distributed according to the χ^2 distribution with n degrees of freedom.

The expectation and variance of a χ^2 random variable is, respectively:

$$E[X] = n,\ Var\,[X] = 2n \quad (10)$$

which can be easily proved applying the definitions of the expectation and variance.
The distribution function of a χ^2 random variable is:

$$F_X(x) = \frac{\gamma(n/2,x/2)}{\Gamma(n/2)} \quad (11)$$

where $\gamma(z,y)$ is the lower incomplete Gamma function with the definition:

$$\gamma(z,y) = \int_{-\infty}^{y} s^{z-1}\, exp(-s)ds \quad (12)$$

A few essential properties of the χ^2 variables and distribution are important for investigations conducted in this thesis.

If we have two χ^2 random independent variables, X_1 and X_2 with n_1 and n_2 degrees of freedom then their sum has a χ^2 distribution with n_1+n_2 degrees of freedom:

$$X_1\sim\chi^2(n_1),\ X_2\sim\chi^2(n_2) \Rightarrow X_1+X_2 \sim X_1\sim\chi^2(n_1+n_2) \quad (13)$$

and this property can be generalized to more than two χ^2 random variables, $\sum X_i \sim \chi^2(\sum n_i)$. If Z is the standard normal random variable and X is its square, $X=Z^2$, then X is a χ^2 random variable with 1 degree of freedom. Clearly, combining these two facts it can be concluded that the sum of squares of n independent standard normal random variables is a χ^2 random variable with n degrees of freedom.

APPENDIX D

Example: *Matlab* code for γ-index failure rate calculation for clinical IMRT dose distributions

gammasim_grad2_thresh.m:

```
function[failrate,elapsedtime]=gammasim_grad2_thresh(h,S,x,y,sigdos,sigpos)

tic();

global failrate gradxy elapsedtime Gdistr;

% Number of simulation histories: h
% Matrix size scale factor: S
% Nominal detector point: x, y
% Standard deviations for dose and positioning: sigdos, sigpos
% Included option for automatic writing to excel file
% Image set-30 images obtained from Oncentra MasterPlan (TPS)


% Calculated dose distribution from Oncentra MasterPlan (cm)

filnamn='C:\..\IMAGES F1-F30\F1.dcm';

%

data=dicomread(filnamn); % read the dicom file and save it to the variable data

head=dicominfo(filnamn); % option for a header

PixelSpacingX=head.PixelSpacing(1);

PixelSpacingY=head.PixelSpacing(2);



% images have the resolution of 3 mm
% for each image (labelled F1-F30), the relative absorbed dose distribution % was calculated at 5.0 cm depth


ber0=double(rot90(data(:,:,1,21))).*head.DoseGridScaling;

ber=imresize(ber0,S);  %B = imresize(A, scale) returns image B that is scale (could be larger or smaller than 1) times the size of A.

bS=size(ber);

bxs=PixelSpacingX/10/S; %x-scale

bys=PixelSpacingY/10/S; %y-scale

bxo=bS(1)/2+0.5; %x-offset
```

```
byo=bS(2)/2+0.5; %y-offset
bxv=([1:bS(1)]-bxo).*bxs; %x-vector
byv=([1:bS(2)]-byo).*bys; %y-vector
%
max1=max(ber,[],2); %if A is a matrix, then max(A,[],2) is a column vector containing the maximum value of each row.
max11=max(max1);
bMax =0.15*max11; %limiting value for matrix ber
%
[G1x,G1y]=gradient(ber,bxs,bys);
G1=sqrt(G1x.*G1x+G1y.*G1y);
[G2x,G2y]=gradient(G1,bxs,bys);
grad=sqrt(G2x.*G2x+G2y.*G2y);
%
gradxy=interp2(bxv,byv',grad,x,y,'*linear');
% x,y are coordinates of the point for which we calculate the distribution of gamma
% Gamma evaluation criteria
k0=1.96;
DTAkrit=k0*sigpos;
Dkrit=k0*sigdos;

j1=int16(x/bxs+bxo); % intArray = int16(array) converts the elements of an
% array into signed 16-bit (2-byte) integers of class int16.

k1=int16(y/bys+byo);
Dtps=ber(k1,j1);
if (Dtps > bMax)
```

```
% Simulation
  xrand=random('norm',0,sigpos,h,1);
  yrand=random('norm',0,sigpos,h,1);

for i=1:h
    % Mispositioning of detector point
    [xmeas,ymeas]=meshgrid(x+xrand(i),y+yrand(i));
%
    % Measurement simulation
          Dnom=interp2(bxv,byv',ber,xmeas,ymeas,'*linear');
    % bilinear interpolation
    % to find the dose at the point of interest- mispositioned detector
    % point

    Dmeas=Dnom+random('norm',0,sigdos);

    % smear the dose determined
    % to find the random dose

    G(i)=99;

    jmin=int16((xmeas-3*sigpos)/bxs+bxo);
    jmax=int16((xmeas+3*sigpos)/bxs+bxo);
    kmin=int16((ymeas-3*sigpos)/bys+byo);
    kmax=int16((ymeas+3*sigpos)/bys+byo);
    if jmin < 1
       jmin=1;
    end
     if jmax > 85
```

```
      jmax=85;
    end
    if kmin < 1
      kmin=1;
   end
    if kmax > 85
      kmax=85;
    end

   for j=jmin:jmax
      for k=kmin:kmax
         xtps=(double(j)-bxo)*bxs;
         ytps=(double(k)-byo)*bys;
         Dtps=ber(k,j);
         gam=sqrt(((Dtps-Dmeas)/Dkrit)^2+((xtps-x)/DTAkrit)^2+((ytps-y)/DTAkrit)^2);
         G(i)=min(gam,G(i));
      end
   end
end
Gdistr=G;
Gfail=G(G>1);
toc;
elapsedtime=toc;
failrate=length(Gfail)/length(G);
else
elapsedtime=toc;
failrate=99;
end
```

functiongradgrad_thresh.m:

```
function fungrad = functiongrad2_thresh(x,y)
global failrate elapsedtime gradxy Gdistr;

% gammasim gradgrad2_tresh(h,S,x,y,sigdos,sigpos)

k= 0;
for i=1:19
   for j=1:19
      k = k + 1;
      gammasim_gradgrad_thresh_(10000,1,-10.0+i,-10.0+j,0.01,0.1)
      frgrad(k,1) = -10.0+i;
      frgrad(k,2) = -10.0+j;
      frgrad(k,3) = failrate;
      frgrad(k,4) = gradxy;
   end
end
xlswrite('C:\..\IMAGES F1-F30\F1_001_01_tresh_15.xls', frgrad);
```

LIST OF FIGURES

LIST OF TABLES

BIOGRAPHY

Svjetlana Šunjić is a clinical medical physicist born in Sarajevo. She graduated Physics at the University of Sarajevo, Faculty of Science and Mathematics. Since 1998 she has been employed as a clinical medical physicist at the Institute of Oncology, Clinical Centre of Sarajevo University. From 2009 to 2016, she was a head of the Unit for Radiotherapy Physics, Department of Medical Physics and Radiation Safety, Clinical Centre of Sarajevo University. From 2016 until present, she has been working as a clinical medical physicist at Department for Radiation Protection and Medical Physics, Clinical Centre of Sarajevo University. From 2012, she has been involved in the teaching at the Faculty of Health Studies, University of Sarajevo, as a professional associate. Her professional and research interests are in dosimetry of photon and electron beams and treatment plan verification methods in external beam radiotherapy.

List of selected published works

Original scientific articles:

- **Svjetlana Sunjic**, Crister Ceberg, Tomislav Bokulic. Statistical analysis of the gamma evaluation acceptance criteria: A simulation study of 2D dose distributions under error free conditions", Physica Medica 52 (2018) 42–47.
- Adnan Beganović, Irmina Sefić-Pašić, Amra Skopljak-Beganović, Spomenka Kristić, **Svjetlana Šunjić**, Amra Mekić, Maja Gazdić-Šantić, Advan Drljević, Davorin Samek, Doses to skin during dynamic perfusion computed tomography of the liver, *Radiation Protection Dosimetry*, Volume 153, Issue 1, January 2013, Pages 106–111, https://doi.org/10.1093/rpd/ncs100

Professional articles:

- Hiba Bašić, **Svjetlana Šunjić**, Mirela Kalamujic. Radiotherapy with accelerated heavy particles-hadrons. Medical Journal-2008-14(3):107-110 (original article)
- Nermina Obralić, **Svjetlana Šunjić**, Mustafa J. Radiation Oncology and Computer Technology. Acta Inform Med. 2008; 16(3): 168-171 (review article)
- Nermina Obralić, **Svjetlana Šunjić**. Comparison of conventional and three-dimensional conformal irradiation of prostate cancer. Medical Journal- 2009-15(3):100-104 (original article)

Published scientific conference contribution or abstract:

- Hiba Bašić, Advan Drljević, Senad Vranić, **Svjetlana Šunjić**. Determination of the target volume by computed tomography in irradiation of breast cancer. Radiological Congress of Bosnia and Herzegovina with international participation, 2nd. Congress Book, Tuzla; B&H Association of Radiologists, 2003: 4 (abstract)

- Hiba Bašić, Advan Drljević, Senad Vranić, **Svjetlana Šunjić**. Reduction of lung complications after the breast cancer irradiation by treatment planning based on Computerised tomography. 2nd Congress of Respiratory Society in Bosnia and Herzegovina, 2nd. Congress Book, Sarajevo; Respiratory Society in Bosnia and Herzegovina, 2005: 154 (abstract)
- **Svjetlana Šunjić**, Advan Drljević, Senada Halilovic. Establishment of a QA Programme at Institute of Oncology Sarajevo. Abstract book: 2ND AISCMP *Meeting*, Opatija, 2006 (lecture, abstract)
- **Svjetlana Šunjić**, Advan Drljević. Report on status of medical physicist in Bosnia and Herzegovina. Abstract book: Medical Phyisics conference: *Workshop on Medical Physics in Eastern Europe,* Regensburg, 2006 (lecture, abstract)
- Advan Drljević**, Svjetlana Šunjić**, Senada Halilovic, Branka Metlić, Adnan Beganović, Amra Skopljak Beganović. Establishment of the first Medical Physics & Radiation Safety Department in Bosnia & Herzegovina. Abstract book; *ÖGMP Annual Meeting and 3rd AISCMP Meeting*, Graz, 2008 (poster, abstract)